Archive

LWR CORE THERMAL-HYDRAULIC ANALYSIS--ASSESSMENT AND COMPARISON OF THE RANGE OF APPLICABILITY OF THE CODES COBRA IIIC/MIT AND COBRA IV-I

by

J.E. Kelly, J. Loomis, L. Wolf

Energy Laboratory Report No. MIT-EL 78-026
September 1978

LWR CORE THERMAL-HYDRAULIC ANALYSIS--ASSESSMENT AND COMPARISON OF THE RANGE OF APPLICABILITY OF THE CODES COBRA IIIC/MIT AND COBRA IV-I

by

J.E. Kelly, J. Loomis, L. Wolf

Energy Laboratory

and

Department of Nuclear Engineering

Massachusetts Institute of Technology
Cambridge, Massachusetts 02139

Final Report for Research Project

Sponsored by

Long Island Lighting Company
Northeast Utilities Service Company
Public Service Electric & Gas Company
Yankee Atomic Electric Company

under the

MIT Energy Laboratory Electric Utility Program

Energy Laboratory Report No. MIT-EL 78-026

September, 1978

ABSTRACT

This report summarizes the result of studies concerning the range of applicability of two subchannel codes for a variety of thermal-hydraulic analyses. The subchannel codes used include COBRA IIIC/MIT and the newly developed code, COBRA IV-I which is considered the benchmark code for the purpose of this report. Hence, through the comparisons of the two codes, the applicability of COBRA IIIC/MIT is assessed with respect to COBRA IV-I.

A variety of LWR thermal-hydraulic analyses are examined. Results of both codes for steady-state and transient analyses are compared. The types of analysis include BWR bundle-wide analysis, a simulated rod ejection and loss of flow transients for a PWR. The system parameters were changed drastically to reach extreme coolant conditions, thereby establishing upper limits.

In addition to these cases, both codes are compared to experimental data including measured coolant exit temperatures in a core, interbundle mixing for inlet flow upset cases and two-subchannel flow blockage measurements.

The comparisons showed that, overall, COBRA IIIC/MIT predicts most thermal-hydraulic parameters quite satisfactorily. However, the clad temperature predictions differ from those calculated by COBRA IV-I and appear to be in error. These incorrect predictions are caused by the discontinuity in the heat transfer coefficient at the start of boiling. Hence, if the heat transfer package is corrected, then COBRA IIIC/MIT should be just as applicable as the implicit option of COBRA IV-I.

ACKNOWLEDGEMENTS

This report centers mainly around the Master Thesis of the first author, John Kelly. His devotion to this research and his tireless efforts to debug COBRA IIIC/MIT and to overcome seemingly endless complications are herewith gratefully acknowledged. John's friendly and helpful manner as well as his well-organized way of doing research made it possible for Jim Loomis to grow naturally into an area previously unknown to him. Within this atmosphere, Jim was enabled to contribute important parts to this research in a brief period of time and to become himself a specialist in operating COBRA IIIC/MIT and other codes. Thus, the continuity of ongoing research has been preserved from one student generation to the next.

To both gentlemen, I owe a great deal of gratitude for their tireless efforts in achieving the goals of this research.

Finally, I would like to express my gratitude for the financial support as well as for the encouraging discussions by the sponsors of this research under the MIT Energy Laboratory's Electric Utility Program.

Lothar Wolf
Principal Investigator
Associate Professor of
Nuclear Engineering

TABLE OF CONTENTS

LIST OF FIGURES

LIST OF TABLES

NOMENCLATURE

Symbol	Definition	Typical Units
A	area	ft^2
C_p	specific heat	Btu/lb ^oF
D	hydraulic diameter	ft
f	friction factor	
h	heat transfer coefficient	Btu/hr-ft^2-^oF
i	channel subscript	
j	iteration subscript	
k	thermal conductivity	Btu/hr-ft-^oF
m	mass flow rate	lb/sec
Pr	Prandtl number	
P_{ref}	reference pressure	psi
P	pressure relative to P_{ref}	psi
P_o	defined in Appendix A	psi
q'	linear heat generation rate	Btu/hr-ft
q''	heat flux	Btu/hr-ft^2
Re	Reynolds number	
T_c	clad temperature	^oF
T_f	fluid temperature	^oF
s	gap size	ft
u	axial velocity	ft/sec
v	transverse velocity	ft/sec
w	crossflow	lb/sec-ft
Δt	time step size	seconds
Δx	axial mesh size	ft
α	void fraction	
ρ	density	lb /ft^3

EXECUTIVE SUMMARY

This report summarizes the research work performed under the project,

> "LWR Core Thermal-Hydraulic Analysis -- Assessment and Comparison of the Range of Applicability of the Codes COBRA IIIC/MIT and COBRA IV-I",

whose scope of work has been outlined in the Attachment I of the letter dated November 21, 1977 to the sponsors by Dr. W. Hinkle.*

Due to the fact that the report discusses various research topics in a different order, a step-by-step discussion of the goals achieved under the various points in the order of appearance in the aforementioned reference seems to be in order:

I. PWR Analysis

1) Available information about the range of applicability of COBRA IIIC/MIT for steady-state and transient analyses has been collected and assessed. During this study it became obvious that the code has never been consistently benchmarked against another code and/or experimental evidence. Furthermore, it could be concluded that major emphasis had been put into the DNBR analysis in the past without studying other thermal-hydraulic parameters with the same intensity. This assessment set the overall framework for the research work.

2a) Using Maine Yankee data, rod ejection transient and loss of flow transients were studied extensively. Dropped rod, loss of feedwater and excess load listed under 2b through 2d were dropped after an agreement was reached with the sponsors that the power and flow transients constitute an upper envelope for the other types of transients, too.

*Managing Director of MIT Energy Laboratory Electric Utility Program.

With respect to the power transients, three significant conclusions can be drawn:

A) Oscillations occurred at the inception of boiling when very small time steps were used. Both COBRA codes failed to converge at the point where subcooled boiling starts. This failure has been corrected successfully and hence, the ability to apply either code to severe power transients is at least not limited by the use of very small time steps.

B) The comparisons with both the implicit and explicit options of COBRA IV-I reveal discrepancies in the void fraction, density and clad temperature predictions, which can be explained in terms of the oversimplified heat transfer logic in COBRA IIIC/MIT. A change in this code's heat transfer logic should improve the validity of the results.

C) As expected, COBRA IIIC/MIT fails when the flow reverses, while the explicit method of COBRA IV-I does not. However, it is worth mentioning that the results of both codes are similar up to the point where COBRA IIIC/MIT fails. But the conditions for this occurrence are, indeed, very severe. It can be concluded, then, that the code seems to perform satisfactorily for most severe power transients. (Compare Point 4 of Statement of Work.)

With respect to the loss of flow transients, the following research has been done. Four different transients were analyzed, covering a broad spectrum. The first case, which is the least severe, produced no boiling at any time during the transient. The second and fourth cases

produced boiling in steady-state as well as throughout the transient whereas the third one generates boiling only in the transient. These transients are considered to constitute an envelope of various other possible cases, and the following conclusions can be drawn:

A) Throughout the comparisons, the clad temperature predictions of the two codes are significantly different. The differences increase both as the power is increased and as the transient progresses. The major source for the observed discrepancies is again the heat transfer logic in COBRA IIIC/MIT.

B) Despite the differences in the clad temperature predictions, the DNBR predictions are in very good agreement, which simply states the insensitivity of this design parameter. This results because the heat flux predictions of the two codes are close, though the clad temperatures are different. Only the third test case is slightly affected by the different clad temperature predictions because in this case also different heat fluxes are calculated. However, in general, the DNBR predictions of both codes agree extremely well with one another.

C) Fluid variables such as density and enthalpy are predicted to be nearly the same by both codes. Therefore, it is believed that the improved implicit energy equation in COBRA IV-I has no significant effect on the predictions during the transients. This, together with the broad spectrum of transients considered, ensures the adequacy of the COBRA IIIC/MIT density and enthalpy predictions.

D) The use of COBRA IIIC/MIT for DNBR analysis should be satisfactory as compared to COBRA IV-I.

3) No additional work has been done for fuel assembly designs other than for the Maine Yankee reactor because no additional data were provided.

4a) This point is covered by the study of overly severe power transients as discussed in Point 2. Rather than reducing the flow beyond the specified limits, the power and the coolant conditions were increased such as to force flow reversal in order to employ the implicit option in COBRA IV-I.

4b) The results of the study of flow blockages will be reported below.

5) No blowdown calculations were performed with the explicit version of COBRA IV-I in the context of this research, because the method employs a pure homogeneous model which is questionable to use under these circumstances. Furthermore, it is thought that the THERMIT two-fluid code developed at MIT offers more for the money. In addition, independent study was performed with COBRA IV-BEEST for blowdown calculations which employs a best-estimate heat transfer package rather than the common RELAP41MOD5 package. Substantial differences have been observed between these two packages. These results are available to the utilities upon request.

6) No special criteria have been formulated for the upper limit of transients safely handled by COBRA IIIC/MIT because the experience

with the code indicates that it can handle safely about all of the transients to be encountered, unless they are made overly severe and unrealistic.

7) Transients which have definitely to be analyzed by COBRA IV-I are of the type which lead to flow reversal or where it is mandatory to obtain reliable clad temperatures and heat fluxes.

This concludes the statement of work. However, on top of the research reported above and in due regard of the finding that COBRA IIIC/MIT has not been assessed with respect to experimental evidence thus far, several comparisons were performed.

The first one concerns the comparison between the measured steady-state Maine Yankee core exit temperatures and the calculated results of both COBRA IIIC/MIT and COBRA IV-I. The codes predict the measured values extremely well. Most of the measured temperatures are predicted to within $5^{o}F$ by either code. Both codes agree to within $0.1^{o}F$ of each other.

The second experiment involves interbundle mixing data for inlet flow upset cases. Two cases of 25% and 5% are considered where the axial flow distribution is satisfactorily predicted by each code. Despite minor discrepancies, neither code appears to be any better than the other one in predicting the other hydraulic parameters. Both codes, however, show a substantial sensitivity to the crossflow results upon the selection of the axial mesh size whose correct value is naturally not known in advance. THERMIT, with a complete treatment of the Navier-Stokes Equations,

does not show this type of sensitivity and, furthermore, shows better agreement with the data spectrum of transients even without accounting for turbulent mixing.

The third experiment concerns the EIR two-subchannel flow blockage tests. COBRA IIIC/MIT does not predict this case very well because it simulates geometric changes via an artificially high k_{grid} factor which must be filled. On the other hand, COBRA IV-I, which models directly geometric changes, is quite successful, although changes in gap geometry call for a new set of parameters. Therefore, it is recommended that COBRA IV-I is used for flow blockage calculations as long as COBRA IIIC/MIT does not contain a better blockage simulation method.

II. BWR Analysis

1) The BWR option of COBRA IIIC/MIT has been made fully operational for steady-state and transient analysis which now can account for Levy's subcooled boiling model. Inconsistencies had to be removed in the void fraction, the flow rate and the pressure drop calculations. Other changes involved the calculation of q' on each iteration and the implementation of a physical constraint concerning P_o. During this research, it was discovered that COBRA IV-I could only be used for steady-state BWR analyses, not for transient ones. It is believed now that the BWR option works for all transients of interest.

2) The heat transfer calculations in COBRA IIIC/MIT are not adequate for the subcooled boiling regime. The differences result from both a questionable logic in the heat transfer package and an explicit

energy equation. Both items must be changed to improve the calculations. The built-in correlations have been assessed and compared to those of COBRA IV-I. No actions have been taken, however, to implement new correlations or a new methodology for the evaluation of critical power. The results obtained for the BWR cases under consideration indicate that in fact subcooled boiling should be taken into account especially when neutronic feedback calculations are involved. The effects on void fraction and density are substantial just in the core region where usually the power peaks.

3) With whatever little information was available from SAI, the Peach Bottom test of turbine trip without bypass has been simulated after the failure of the code for small time step sizes and inclusion of the Levy subcooled boiling model had been overcome. This pressurization transient was handled by COBRA IIIC/MIT quite satisfactorily although clad temperature rises in some nodes seem to be unrealistic and must again be attributed to the wrong heat transfer logic.

4) No BWR loss of flow transient has been studied. COBRA IV-I cannot be used for transient bundle-wide BWR analysis the way COBRA IIIC/MIT is set up.

5) Assessment and recommendations are given for future work in the area of BWR analyses.

Finally, it should be pointed out that with the efforts undertaken during this project, the confidence in the performance of COBRA IIIC/MIT has been remarkably increased, and the areas of questionable performance have been nailed down and their remedies are known. Thus, it is believed that with some additional efforts the latter can be quite easily removed.

CHAPTER 1

INTRODUCTION

1.1 Background

The thermal-hydraulic analysis of a Light Water Reactor core is frequently performed using subchannel computer codes. These codes are used to calculate the various thermal-hydraulic parameters (e.g., temperature, density, velocity, etc.) for either an entire core or some section thereof. The one common characteristic of all these codes is their lumping of the geometry into a manageable number of channels. A channel consists of a finite fraction of the total cross-sectional area of the core section under consideration. The size of these channels can be chosen arbitrarily, but the smallest possible channel would be the size of a subchannel. Each channel is then axially divided into a specified number of nodes. One node in any channel represents the smallest control volume for which the various conservation equations would be applied. Since each node is formed by lumping the geometry, the value for each parameter in the node represents an average over the entire volume of the node. However, if the channels are chosen appropriately then an accurate analysis of the core can be made. Consequently, subchannel codes are very important tools for the thermal-hydraulic analysis of Light Water Reactors.

However, in order to be useful tools, the range of applicability and reliability of the results of these codes must be determined for both steady-state and transient conditions. Although the ultimate validation of a code is by comparison to experiment, most experiments measure the

various thermal-hydraulic parameters only for steady-state conditions making transient comparisons very difficult to obtain. Furthermore, the experiments would usually measure discrete values for the parameters and not node average values which are what the subchannel codes predict. In view of these difficulties, the primary method for determining the range of applicability has been to compare the results of one code to those of another. This comparison can only be meaningful if the two codes use either different solution methods or different physical models. Therefore, in order to clearly identify the range of applicability of a code, comparisons of this code should be made with another code which satisfies one of the above two criteria.

Until recently, there has been no publicly available code which would satisfy either of these criteria. Most subchannel codes are based, more or less, on the same type of solution method and use the physical concept of crossflow. Although comparisons have been made among these codes, the range of applicability could not be clearly defined since these codes would be subject to the same limitations. For example, these codes would not be able to consider flow reversal, since this phenomenon would violate the assumption that the axial flow rate must be positive at all locations. However, with the development of the new code, COBRA IV-I (1, 2), useful comparisons can be made since this code does satisfy one of the above criteria. This code contains a solution scheme which is quite different from that used in other subchannel codes. In fact, COBRA IV-I is able to consider both flow reversal and natural circulation flow. Therefore, COBRA IV-I can be used to assess the range of applicability of other subchannel codes.

1.2 Comparison of COBRA IIIC/MIT and COBRA IV-I

Since both COBRA IIIC/MIT (3, 4) and COBRA IV-I are employed in the analyses discussed in this report, it is instructive to identify the major differences between these two codes. For example, both codes solve essentially the same equations, but the solution methods are not the same. In fact, COBRA IV-I contains two independent solution methods -- referred to as the implicit and explicit methods. Besides these differences, there are also differences in the heat transfer calculations of the two codes which dramatically affect the clad temperature predictions. Consequently, the main differences between the two codes are identified below.

1.2.1 Comparison of Solution Methods

The first important difference between the two codes concerns their respective solution methods. COBRA IIIC/MIT uses a marching type method which solves the temporal finite difference equations implicitly. One requirement of this method is that the axial flow rate be positive throughout the core. COBRA IV-I contains two distinct solution methods. The first method, called the implicit method, is very similar to the method found in COBRA IIIC/MIT. The implicit method is also a marching type method which solves the temporal finite difference equations implicitly. Once again, this method requires that the flow rate be always positive. The second method, termed the explicit method, is a temporally explicit pressure-velocity solution procedure. This method eliminates the positive flow requirement which then allows a wider range of flow conditions to be considered. However, the explicit method does have some limitations and, consequently, the solution methods are compared to clearly illustrate these methods.

The implicit method of COBRA IV-I employs essentially the same solution procedure as that in COBRA IIIC/MIT. The only significant differences between the two methods are the treatment of the energy equation and the procedure for inverting the crossflow matrix. In the implicit method the energy equation is solved implicitly (both spatially and temporally) which means that all enthalpies at a particular axial level are calculated simultaneously. This implicit treatment of the energy equation differs from the spatially explicit energy equation in COBRA IIIC/MIT. The primary advantage of using an implicit energy equation is that a consistent set of enthalpies and temperatures are calculated at each axial level.

The other significant difference between the implicit method of COBRA IV-I and COBRA IIIC/MIT is the way the crossflow matrix is inverted. In COBRA IIIC/MIT the matrix is inverted using a Gaussian elimination procedure. On the other hand, the implicit method of COBRA IV-I employs a Gauss-Siedel method for the inversion. The difference in these inversion procedures is only technical and should not affect the accuracy of any results.

In spite of these differences, the implicit method of COBRA IV-I and COBRA IIIC/MIT are very similar in many respects. Both methods solve the same conservation equations and, with the exception of the energy equation, these equations are solved in the same manner. Besides the similarity of solution procedures, both codes can be used to solve similar problems. COBRA IIIC/MIT and the implicit method can solve steady-state as well as transient problems. For transient problems there is no restriction on the time step size, since the temporal derivatives are solved implicitly Both the implicit method and COBRA IIIC/MIT also use the same two-phase

modeling as well as the same subcooled void fraction modeling. Hence, the implicit method of COBRA IV-I and COBRA IIIC/MIT share similar solution methods and the same hydraulic modeling.

On the other hand, the explicit method of COBRA IV-I is quite different from either COBRA IIIC/MIT or the implicit method. The explicit method uses a different solution procedure as well as treating the temporal derivatives explicitly. With explicit temporal derivatives, very small time step sizes (<0.01 seconds) are required. Furthermore, the explicit method is used exclusively for transient calculations. Hence, the explicit method would not be employed to calculate a steady-state solution. Besides having a different solution method, the explicit method also employs different hydraulic models. Only homogeneous two-phase flow is allowed which prohibits the use of any slip or two-phase friction correlation. Additionally, the homogeneous equilibrium model precludes the use of the Levy subcooled void fraction correlation. Hence, the two-phase flow modeling is limited as compared to either COBRA IIIC/MIT or the implicit method.

However, the explicit method can analyze a wide variety of problems which cannot be analyzed by either COBRA IIIC/MIT or the implicit method. For example, since there is no restriction on the axial flow direction, flow reversals and recirculation problems can be handled. However, these hydraulic conditions would only occur for severe reactor accidents (e.g., blowdown). Nevertheless, the explicit method also allows pressure drop boundary conditions which are not found in the implicit method. Consequently, more realistic core conditions can be studied. Therefore, although the

explicit method has both time step size restrictions and limited two-phase flow modeling, it does contain a more general solution method.

1.2.2 Heat Transfer Calculations

The second major area in which COBRA IIIC/MIT and COBRA IV-I differ is in their heat transfer calculations. These calculations include the prediction of the heat transfer coefficient and the heat flux. There are three main improvements in COBRA IV-I which lead to these differences. The first is the use of a new fuel-pin model. This model allows for both axial and radial conduction and, additionally, temperature dependent thermal conductivity can be considered. The second improvement is that a consistent set of heat fluxes, heat transfer coefficients and clad temperatures are calculated at each axial level. This consistent treatment is not obtained in COBRA IIIC/MIT, since the heat transfer coefficient is calculated using information from the preceding axial level. Of course, in order to obtain this consistent set, an iterative solution procedure is required at each axial level. The third improvement in COBRA IV-I is the use of a new heat transfer package. A RELAP-4 type heat transfer package is contained in COBRA IV-I. This package contains a complete steady-state boiling curve which consists of heat transfer correlations and a method for applying these correlations. The method which determines when to use the appropriate correlation depends on many parameters and is referred to as the heat transfer logic in this report. This third improvement is the most significant of the three as it has the greatest impact on the clad temperature predictions.

A comparison of the COBRA IIIC/MIT and COBRA IV-I heat transfer packages yields the following information. The COBRA IIIC/MIT package only contains

two heat transfer correlations. The Thom forced convection correlation (5) is used for single-phase heat transfer and the Thom nucleate boiling correlation (5) is applied for all two-phase conditions. The criterion for the switching correlations depends only on the quality. If the quality is greater than zero, then the nucleate boiling correlation is applied. Otherwise the forced convection correlation is used. On the other hand, COBRA IV-I has correlations for the entire boiling curve. These include the Thom forced convection correlation in single-phase flow, the Thom nucleate boiling correlation in the subcooled and nucleate boiling regimes, the Schrock and Grossman correlation (6) in the forced convection vaporization regime, and a number of other correlations in the post-CHF regime. Besides having the additional correlations, COBRA IV-I also has a different logic system for switching from the forced convection correlation to the nucleate boiling correlation. In COBRA IV-I, the criterion for switching correlations depends on the clad temperature. If the clad temperature is greater than the fluid saturation temperature, then the nucleate boiling correlation is used. Otherwise, the forced convection correlation is employed. As will be seen later, this difference in heat transfer logic leads to significant differences in the clad temperature predictions.

1.2.3 Summary

This section has highlighted the primary differences between COBRA IIIC/MIT and COBRA IV-I. These include the differences in solution procedures, modeling capabilities and heat transfer packages. The differences in solution methods stem from the fact that COBRA IV-I contains two solution procedures. The implicit method is very similar to COBRA IIIC/MIT with the exception that the

energy equation is spatially implicit. It should be noted that by using an implicit energy equation the execution time of the implicit method will be greater than that of COBRA IIIC/MIT. The other method in COBRA IV-I, the explicit method, is quite different from COBRA IIIC/MIT. This method allows for more general problems to be considered, but small time step sizes are required which will also lead to increased execution time. Additionally, the explicit method can only consider homogeneous two-phase flow. The two-phase flow modeling in the implicit method is the same as that found in COBRA IIIC/MIT. The final difference between COBRA IV-I and COBRA IIIC/MIT is in their heat transfer packages. In COBRA IV-I a wide range of correlations and a different heat transfer logic are employed. This heat transfer package is used in both the implicit and explicit methods and has a significant effect on the clad temperature predictions.

1.3 Review of Past Research with COBRA IIIC/MIT

Research with and on COBRA IIIC/MIT spans a period of about three years now, and includes a variety of different facets, some of which will be discussed in what follows.

In order to understand the various facets of research with this code at MIT, it must be recalled that COBRA IIIC/MIT is a spin-off from the MEKIN code (7). Research for the thermal-hydraulic part of this code as well as some pioneering work by Herbin (8) with an extended version of COBRA IIIC laid the groundwork for the development of COBRA IIIC/MIT (3,4). Since then further research developed along two different tracks, somewhat parallel. One path of research is concerned about the improvement, assessment and validation of the core-wide analysis tool on a bundle-wide basis which has been primarily supported by EPRI, whereas the improvement of the single-pass mixed-lattice version, COBRA IIIC/MIT has been and is sponsored by a group of New England utilities under the MIT Energy Laboratory Research Project. Naturally, each project benefits to some extent from the other, although their goals are in fact somewhat different. All research efforts within the framework of these projects are summarized in Table 1.1.

Work in the MEKIN area must be divided into two different aspects. The first is concerned about the thermal-hydraulic part alone, whereas the second one focuses upon the coupled neutronic-thermal-hydraulic. Work in the first area comprises the pioneering work by Bowring and coworkers (7), that by Rodack (9) who researched specific RIA type transients in PWRs and related topics as well as the steady-state sensitivity

study performed by Emami (10) which was concerned about both PWR and BWR systems. The latter research looked into the effect of parametric changes of the parameters on the final results and checked thoroughly the impact of the various correlations built into the code. Work in the second area was done by Valente (11) who studied specifically BWR control rod drop transients. More recent research with MEKIN has been reported by Cook (12) who had implemented corrections into MEKIN developed by the other researchers and brought the code into a shape in which it should have been two years ago. In the meantime, researchers outside MIT such as SAI (13) and BNL are currently using the code. Most of these activities required special needs thereby leading automatically to improvements in the thermal-hydraulic part, some of which are reported in this research report. Due to the special requirements of a coupled neutronic-thermal-hydraulic code the importance of various parameters are different from those which are vital from a pure thermal-hydraulic design point of view. Thus, not all of the recommendations formulated during the research of this project entered the improvement of COBRA IIIC/MIT and vice versa. On the other hand, it must be emphasized that the MEKIN studies were indeed very helpful to detect weak points and forgotten as well as untested areas of the thermal-hydraulic solution.

Unlike the MEKIN research, most of the efforts in the COBRA IIIC/MIT research concentrated mainly on one parameter of interest, namely, DNBR, as the most important design parameters for licensing purposes. Of primary importance in the early phases of the research was the assessment and validation of the single-pass method. Notably, the research by Moreno (14) and Liu (15) formed the basis for justification of this approach

for steady-state and transient analyses as compared to the multi-pass methods used by the vendors. In a second step, Chiu (16) examined the applicability of two-dimensional transport coefficients to improve the lumped energy transfer models. All these research efforts are summarized in (17) which, together with (15) and (18), comprised the state-of-the-art of the single-pass method and the status of COBRA IIIC/MIT as of September 1977, i.e., the start of the present research.

In addition, the research done by Masterson (19,20) is worth mentioning as a direct consequence of certain mathematical shortcomings inherent in the crossflow solution method of COBRA IIIC. This led to the development of COBRA IIIP/MIT which is numerically more efficient by allowing the use of iterative solution methods for sets of linear equations. This code generates converged crossflow distributions for decreasing axial mesh sizes and time increments.

Finally, it should be pointed out, for instance, that recommendations given by Rodack (9) have already been studied individually such as the comparison of various fuel pin models by Mehrabian (21).

TABLE 1.1: SUMMARY OF PREVIOUS STUDIES

Emphasis on			System		Operation				Reference
MEKIN	COBRA IIIC/MIT		PWR	BWR	S.S.	Transient	Code Used	Information/Results	
+	-		+	-	-	+	MEKIN/T.H.	PWR-RIA study, sensitivity study of T-H input parameters on fuel temperatures and coolant density, void fraction. List of most important parameters.	(9)
+	+		+	+	+	-	COBRA-IIIC/MIT	Sensitivity of COBRA solution to user input parameters and user selected correlations.	(10)
+	-		-	+	-	+	MEKIN	Coupled transient analysis, determination of energy storage in fuel.	(11)
+	-		+	+	+	+	MEKIN	Coupled steady-state and transient analysis, benchmarking, mainly power transients, state-of-the-art of MEKIN status.	(12)
+	-		-	+	-	+	MEKIN	MEKIN sensitivity studies and rod with calculation.	(13)
-	+		+	-	-	+	COBRA-IIIC/MIT	Lumped and mixed lattice approach (single pass method).	(14,17)
-	+		+	-	-	+	COBRA-IIIC/MIT	Verification of the single pass method in transients, discussion of experimental verification of COBRA.	(15,17)
-	+		+	-	+	-	COBRA-IIIC/MIT	Transport coefficients to improve results of lumped, mixed-lattice approach.	(16,17)
-	+		+	-	+	-	COBRA-IIIC/MIT	Sensitivity of COBRA solution to user input parameters.	(18)
+	+		+	-	+	+	COBRA-IIIC/MIT	Development of a new solution method based on pressure field, convergence studies.	(19,20)
+	+		+	+	+	+	-	Study of different fuel pin models.	(21)

1.4 Current Status of COBRA IIIC/MIT and COBRA IV-I

Both COBRA IIIC/MIT and COBRA IV-I were modified during this investigation. The COBRA IIIC/MIT modifications were made in order to eliminate various inconsistencies and failures. The elimination of these problems allows the code to perform successfully for both PWR and BWR analysis. These corrections are discussed in detail later in this report and a listing of the modified subroutines can be found in Appendix C. The corrections implemented in COBRA IV-I were made in order to eliminate a failure which occurred during the analysis. A discussion of this correction is found later in this report, and the modified subroutines are found in Appendix D. Besides these corrections, it should also be noted that COBRA IV-I has been updated through Fix 12 which includes all the changes made by Battelle Northwest Laboratories through June 1978. Hence, COBRA IV-I is available in its most current version.

1.5 Scope of Research

The primary objective of this research is to evaluate the applicability of COBRA IIIC/MIT for the thermal-hydraulic analysis of various Boiling Water Reactor (BWR) and Pressurized Water Reactor (PWR) cases. These evaluations are accomplished by making comparisons between COBRA IIIC/MIT and COBRA IV-I. Since COBRA IV-I represents an improved code, its results are assumed to reflect the best estimate of the actual behavior of the cases which are analyzed. Consequently, if the COBRA IIIC/MIT results agree with those of COBRA IV-I, then it can be concluded that COBRA IIIC/MIT is applicable. Likewise, when the results differ between the two codes, then the applicability of COBRA IIIC/MIT is considered

to be questionable. Therefore, comparisons between COBRA IIIC/MIT and COBRA IV-I are used as a basis for determining the applicability of COBRA IIIC/MIT.

The cases which are investigated involve some facet of thermal-hydraulic analysis for which COBRA IIIC/MIT would normally be applied. Since COBRA IIIC/MIT is widely used, the comparisons are aimed at verifying the applicability of this code for cases of practical interest. For example, COBRA IIIC/MIT is employed as part of a coupled neutronic-thermal-hydraulic analysis for both BWR and PWR cases. Consequently, the thermal-hydraulic performance of COBRA IIIC/MIT is assessed for both of these type situations. Another application of COBRA IIIC/MIT is the analysis of the Departure from Nucleate Boiling Ratio (DNBR) for a PWR. Hence, this mode of analysis is also investigated. Some comparisons with experimental results are also performed in order to further verify the applicability of COBRA IIIC/MIT. Therefore, the cases, for which comparisons were made, represent practical situations where COBRA IIIC/MIT could be applied.

Since COBRA IV-I contains two solution methods, comparisons have been made using both of these methods. The explicit method is used exclusively for severe transient cases in which the applicability of the implicit method is questionable. Since the explicit method cannot be used to calculate the steady-state solution, all steady-state comparisons are performed using the implicit method. The implicit method is also employed in transient problems which are not too severe (e.g., no flow reversal). In summary, the explicit method is only used for severe transient cases while the implicit method is applied for steady-state and

some transient cases which are representative of Anticipated Transients Without Scram (ATWS).

Each of the following chapters discusses the results of the comparisons between the two codes for one type of thermal-hydraulic analysis. These discussions focus on the applicability of COBRA IIIC/MIT for the particular type of analysis under consideration. For situations in which the two codes do not agree, the discussion is then directed towards identifying the cause of the discrepancy. The type of thermal-hydraulic analysis which is discussed in each chapter is summarized as follows.

Chapter 2 discusses the investigation of BWR bundle-wide analysis. This chapter includes both steady-state comparisons and the results of a pressurization transient.

Chapter 3 discusses the investigation of a severe power transient in a PWR. This transient simulates a rod ejection accident and can be analyzed using COBRA IIIC/MIT coupled to a neutronic solution method. However, the investigation here is limited to the thermal-hydraulic analysis only.

Chapter 4 discusses the investigation of various PWR loss of flow transients. These transients are examples of ATWS in which the minimum DNBR is the design limit for the operation of the reactor. Therefore, DNBR analysis is considered in this chapter.

Chapter 5 discusses the results of comparing the two codes with three different sets of experimental data. The first case consists of a comparison between the predictions of the codes and the measured coolant temperatures at the core exit of the Maine Yankee reactor. These exit temperatures have been measured and, hence, comparisons with the codes could be performed. The second case is a comparison of pressure and velocity

measurements, as well as the inferred crossflow distribution, with the predictions of the two codes. These measurements were made by B&W for a two-assembly set-up in which the inlet flows for each assembly differed from each other. The third case is a comparison of the two codes with flow blockage data. This data consists of pressure measurements as obtained by EIR. The results of this comparison and the above two are found in this chapter.

After discussing the investigations in Chapters 2 through 5, the conclusions and recommendations of this research are discussed in Chapter 6.

Four appendices are also included in this paper. Appendix A discusses the iterative procedure in COBRA IIIC/MIT which is used to calculate the correct flow-splitting when the BWR option is used. Appendix B summarizes the input data which was used in the various cases. Appendix C summarizes the modifications which were implemented into COBRA IIIC/MIT. And, finally, Appendix D summarizes the changes which were made in COBRA IV-I.

CHAPTER 2

BWR BUNDLE ANALYSIS

2.1 Background

The thermal-hydraulic analysis of a Boiling Water Reactor (BWR) core involves the determination of various parameters which are important for the design and operation of the reactor. For example, coolant density, coolant temperature and fuel temperature are important for their influence on the neutronic behavior of the core. Similarily, parameters such as coolant flow rate, heat flux, clad temperature, and quality are used to determine whether or not a critical heat flux condition is attained. The determination of the above quantities can be performed with a subchannel analysis, with a bundle average analysis, or with a combination of the two. A subchannel analysis would employ a detailed geometry which would use subchannels as the smallest flow channels. Typically a subchannel would have a flow area of approximatey 0.23 in^2. Due to computer limitations it is prohibitive to model an entire core on a subchannel basis. Consequently, at most one bundle would be modeled on a subchannel basis. (In this discussion a bundle is meant to be a typical BWR 7x7 or 8x8 array of fuel elements.)

On the other hand, a "bundle analysis" of a core would typically use an entire bundle as the smallest channel in the analysis. Typically, one would model a group of four bundles as a single channel (10). In modeling a channel, the individual subchannels are lumped together to give a flow area equal to the sum of all the individual subchannel flow areas. Hence, if four 7x7 BWR bundles were modeled as a single channel, the flow area of the channel would be approximately 63 in^2. The fuel rods are modeled by

using a single rod to represent the average behavior of all the rods in each channel. Hence, bundle analysis can only give average values for the quantities of interest in a channel, but an entire core can be analyzed if proper modeling is used. This type of analysis is well-suited as part of a coupled neutronic-thermal-hydraulic analysis. However, for more detailed investigations a subchannel analysis is usually required.

A third method of analysis is to use a combination of bundle and subchannel analyses. For example, one could use the bundle analysis coupled with a neturonic analysis to identify the hot assembly. A detailed analysis of the hot assembly would then be performed using a subchannel analysis. In this manner, the limiting conditions in the core can be determined.

2.2 Description of Modeling Techniques

The discussion in this chapter is limited to "bundle analysis". Investigations performed include using both COBRA IIIC/MIT and COBRA IV-I for steady-state analyses of typical 7x7 BWR assemblies. Transient analysis is also performed for a simulated pressurization transient using COBRA IIIC/MIT. Before discussing the results of these investigations it is useful to review the modeling approaches of the above two codes.

2.2.1 Description of COBRA IIIC/MIT Modeling

The modeling of BWR bundles with COBRA IIIC/MIT is simplified using the BWR option in this code. When this option is applied the transverse momentum equation is eliminated and, hence, no crossflow calculations are performed. The elimination of the transverse momentum equation is appropriate for BWR bundle analysis, since the bundles are ducted and, therefore, there

is no flow from one bundle to its neighbor. However, since there is no crossflow, boundary conditions, which are different from those used in non-BWR analysis, are required. The modeling and boundary conditions used in the BWR option are discussed below.

When the BWR option is employed the user has the ability to model any section of a BWR core. Normally an integer number of BWR assemblies are lumped together to form a single channel. Each channel need not represent the same number of assemblies. Hence, some channels could consist of two bundles while others could consist of four bundles. Typically a quarter core could be modeled using 40 channels with most channels representing four bundles. The exact modeling of the various channels is left to the discretion of the user.

Once the channels have been modeled, they are axially divided into a user-specified number of nodes. Each node represents a control volume for which the conservation equations are applied. Various thermal and hydraulic parameters (eg. enthalpy, density) are calculated in each node, but it must be remembered that values of these parameters are averaged over the node.

In each channel only one fuel rod is modeled. This rod represents the average of all the rods in the channel. If four 7x7 bundles are modeled as one channel, then this one rod represents the average behavior of 196 rods. Consistent power input to the channel is maintained by multiplying the power input of the one rod by the number of rods it represents. This single rod is axially divided into the same number of nodes as the channel.

With the channels and rods modeled, the conservation equations are applied in each node. The equations which are solved are the conservation

of mass, the conservation of energy, and the conservation of axial momentum. Since there is no crossflow between channels, the transverse momentum equation is not needed but is replaced by an additional boundary condition in order to have a closed system. The conservation equations are solved for each node with appropriate boundary conditions and constitutive equations.

The boundary conditions used with the BWR option are as follows. The first condition is that the inlet coolant temperature and system reference pressure must be specified. This condition is similar to that used in the PWR solution option. A second condition is that the total flow rate into the core must be specified by the user and is not allowed to change during the iterative procedure. Once again, this condition is always required when using COBRA IIIC/MIT. The third condition, which is employed only with the BWR option, is that equal pressure drops occur across all channels. This boundary condition is based on the assumption that the pressure in both the upper plenum and lower plenum is uniform, although not equal, and, consequently, the pressure difference across each channel is the same. In order to satisfy this condition, the total inlet flow is divided among the channels. Individual channel inlet flows will not be the same, but their pressure drops will be equal.

In order to generate the correct flow-splitting, an iterative procedure was developed and incorporated into COBRA IIIC/MIT (3). Basically, this procedure is a Newton-Raphson type method for solving a system of non-linear equations. (A detailed description of this method is included in Appendix A.) For each channel an equation is written in which it is assumed that the channel pressure drop is a non-linear function of the inlet flow rate. The condition that equal pressure drops occur across all

channels is then used to write a set of homogeneous non-linear equations. These equations are linearized and then solved. The solution to these equations yields updated inlet flows for each channel. These inlet flows represent the flow-splitting necessary to generate equal pressure drops. Of course, since the equations have been linearized, a number of iterations is usually required before a converged solution is attained. This procedure is assumed to be independent of time step size and, hence, is valid in both steady-state and transient analyses.

This brief discussion of the BWR option illustrates the modeling capability of COBRA IIIC/MIT. For BWR bundle analysis, this code offers a very convenient modeling approach. The user needs only to specify the appropriate value for one variable in order to invoke the BWR option. The option automatically takes into account the ducted nature of the BWR assemblies which eliminates the need for the transverse momentum equation. The elimination of this equation does result, however, in the need for a pressure drop boundary condition. Although the value for the pressure drop cannot be specified as a boundary condition, the condition which requires equal pressure drops across all channels is very plausible when one considers the pressure equalizing effect of the upper and lower plenums. Hence, the BWR option in COBRA IIIC/MIT is well-suited for BWR bundle analysis.

2.2.2 Description of COBRA IV-I Modeling

While COBRA IV-I does not have a BWR option, BWR bundle analysis can be performed with judicious modeling. The modeling of channels and rods is done in the same way as it was with COBRA IIIC/MIT; ie. any number of assemblies are lumped together as a channel and a single rod represents

the average behavior of all the rods in a channel. However, the transverse momentum equation is not eliminated and it is necessary to circumvent the effect of this equation. By specifying zero gap between channels, no crossflow is permitted and the transverse momentum equation is effectively eliminated. Using this technique the geometrical modeling of BWR bundles is essentially the same for both codes.

The boundary conditions which can be used with COBRA IV-I do differ from those used with COBRA IIIC/MIT. Although the need to specify the inlet temperature and reference pressure is unchanged, the user can specify the pressure drop boundary condition in one of two ways. The first option is to specify a value for the pressure drop. When this method is used, the inlet flow for each channel is adjusted such that each channel's pressure drop is equal to the input value. The total inlet flow is not held constant during the iterative procedure. This option can only be used for implicit, steady-state analyses.

The second option involves specifying the inlet flow for each channel. If the correct inlet flows are selected, then equal pressure drops will occur across all channels. This option does not change the total inlet flow during the iterative procedure, but the inlet flows must be known a priori. However, the first option requires that the core pressure drop be specified and this quantity may not be as well known as the total inlet flow. Furthermore, a comparison of COBRA IIIC/MIT and COBRA IV-I is more meaningful if both codes use approximately the same boundary conditions. Consequently, if COBRA IIIC/MIT is employed to generate the correct flow splitting and these flows are then used in COBRA IV-I, each code will have the same inlet flow and pressure drop and a meaningful comparison can be made. Unfortunately, this method can only be applied for steady-state

analysis, since individual inlet flow rates cannot be specified as a function of time in COBRA IV-I. Nonetheless, this second option can be used with COBRA IV-I in order to compare this code with COBRA IIIC/MIT in steady-state.

2.3 Steady-State Analysis

Steady-state analyses of BWR type bundles have been performed using both COBRA IIIC/MIT and COBRA IV-I. The implicit solution method of COBRA IV-I is used exclusively for BWR analysis with this code. Three cases are examined and comparisons are made in an attempt to identify similarities and differences between the two codes. Both codes use similar solution methods, but do differ in two distinct ways. The first is that COBRA IV-I has a spatially implicit energy equation as opposed to the explicit energy equation used in COBRA IIIC/MIT. Use of the spatially implicit energy equation requires a simultaneous solution for the coolant enthalpy and clad temperature at each axial level. A second distinction is that the heat transfer package used in COBRA IV-I is different from that used in COBRA IIIC/MIT. A RELAP-4 type heat transfer package is used in COBRA IV-I. This package includes correlations which cover the entire single phase and two-phase heat transfer regimes. On the other hand, the heat transfer package in COBRA IIIC/MIT only includes correlations for the single phase and nucleate boiling regimes. Besides the differences in correlations, the logic which governs the use of the correlations also differs between the two codes. Therefore, a comparison of the results of the two codes should reveal the importance of these dissimilarities.

In order to make useful comparisons of the two codes it is necessary to examine the predicted values for various parameters. For example, the enthalpy distribution should give a good indication of the performance

of the energy equation. Alternatively, instead of using the enthalpy, one could also examine the quality, the void fraction, or the density as these are all calculated directly from a given enthalpy. For the purpose of comparing the energy equations, the discussion will focus primarily on the density and void fraction as these two variables are also important from a neutronic feedback point of view. Since the clad temperature distribution is a strong function of the heat transfer package, this parameter is employed to compare the heat transfer packages of the two codes.

2.3.1. Description of Steady-State Modeling

Before comparing the predictions of the two codes, it is necessary to briefly describe the modeling used in this analysis. (A more thorough description can be found in Appendix B.) The geometry for the numerical experiments is basically the same for all cases. Five channels are modeled, with each channel representing a different position in a typical BWR core. Channel 1 consists of two 7x7 bundles. Channels 2, 3, 4, and 5 are each composed of four 7x7 bundles. The number of axial nodes is the only geometrical variable which is not held constant for all cases. Radial peaking factors are different for each channel, but the same factors are used for each case analyzed. Other variables held constant for all cases include the axial power distribution, the average heat flux, and the total inlet flow rate. For the steady-state comparisons a homogenous two-phase friction multiplier and a slip equal to unity are used.

2.3.2 Sensitivity Study of the Inlet Flow Distribution

Since the inlet flow distribution is needed as input for COBRA IV-I,

the sensitivity of this distribution to variations in the input data is examined. A base case and three variations of this case are analyzed. The base case consists of using 40 axial nodes together with the Levy subchooled void fraction correlation (22) and an inlet temperature of 527 °F. The first variation involves increasing the number of axial nodes to 60. The second variation uses 40 nodes, but this time the Levy correlation is not used. Finally, the third variation is the same as the base case except the inlet temperature is decreased to 514 °F.

The results of this sensitivity study are summarized in Table 2.1. It is seen that both the pressure drop and inlet flow distribution change as each input parameter is varied. These changes are not too large, but it is interesting to note that even a variation in node size can affect the inlet flow distribution. The variation of the inlet temperature has the most pronounced effect on both the pressure drop and inlet flow distribution. This sensitivity study indicates that when the inlet flow distribution predicted by COBRA IIIC/MIT is used in COBRA IV-I, one must use the same modeling and options in both codes in order to make useful comparisons.

2.4 Results of Steady-State Analyses

2.4.1 Description of Steady-State Cases

Three steady-state cases are used to compare COBRA IIIC/MIT and COBRA IV-I. Each case differs slightly from the other two in their respective modeling as seen in Table 2.2. The first case, which represents the base case, uses the Levy subcooled void fraction model and an inlet temperature of 527 °F. The second case only differs from the first case in that the Levy model is not used. Finally, the third case is the same as the first case except for a change of the inlet temperature to 514 °F.

TABLE 2.1

RESULTS OF INLET FLOW SENSITIVITY ANALYSIS

	T_{in} (°F)	Number of Nodes	Levy Model	ΔP (psia)	m_1 (lb/s)	m_2 (lb/s)	m_3 (lb/s)	m_4 (lb/s)	m_5 (lb/s)
Base Case	527	40	yes	9.86	66.18	122.22	215.39	148.82	127.51
First Variation	527	60	yes	9.84	66.22	122.33	215.10	148.87	127.60
Second Variation	527	40	no	9.81	66.34	122.23	214.38	149.51	127.66
Third Variation	514	40	yes	9.15	68.01	123.84	201.95	156.16	130.16

TABLE 2.2

DIFFERENCES IN MODELING

OF THE STEADY-STATE CASES

Case	T_{in} (°F)	Levy Model
1	527	yes
2	527	no
3	514	yes

Each case is analyzed first with COBRA IIIC/MIT in order to determine the inlet flow distribution. With this distribution the case is then analyzed with COBRA IV-I. The results of these analyses are presented below.

2.4.2 Results of Case 1

The first case was run using both codes as described above. In comparing the results it is impractical to report the value for every variable and, therefore, only a few representative values will be discussed. For example, the results from channel 4 approximate the average of the five channels, while those from channel 2 are the hot channel values. The results from these two channels will receive the primary emphasis.

The density distribution in channels 2 and 4 are illustrated in Figure 2.1. In either channel, there is essentially no difference between the COBRA IIIC/MIT and COBRA IV-I results. In fact, the maximum difference between any value predicted by both codes is less than 0.1%. This close agreement of the densities is also found among the enthalpies and void fractions. Consequently, any differences introduced by the different energy equations are not apparent from these results.

The clad temperature distribution is used as a means of comparing the heat transfer packages. Results from rod 2 (the hot rod) are shown in Figure 2.2. For most of the axial length the predictions of the two codes agree rather well. However, near the inlet, COBRA IIIC/MIT predicts a clad temperature which is approximately 60 ^{o}F higher than that predicted by COBRA IV-I. This large difference occurs only for one node, but indicates a dissimilarity in the heat transfer packages. A similar result is found for rod 4 as seen in Figure 2.3. Once again the COBRA IIIC/MIT results are much larger than those of COBRA IV-I at the beginning of the

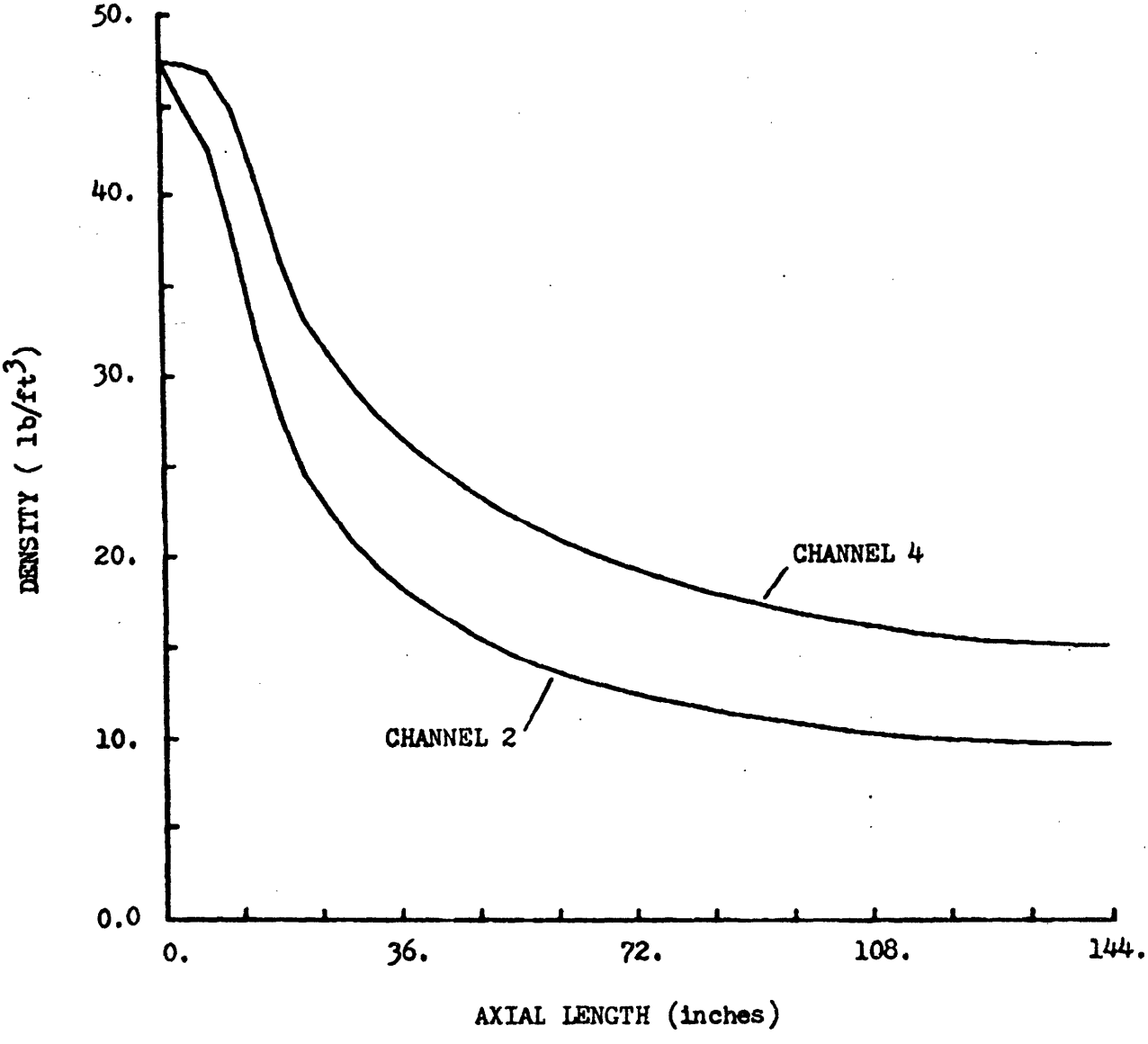

FIGURE 2.1

DENSITY VERSUS AXIAL LENGTH

COBRA IIIC/MIT AND COBRA IV-I PREDICTIONS

FOR CASE 1

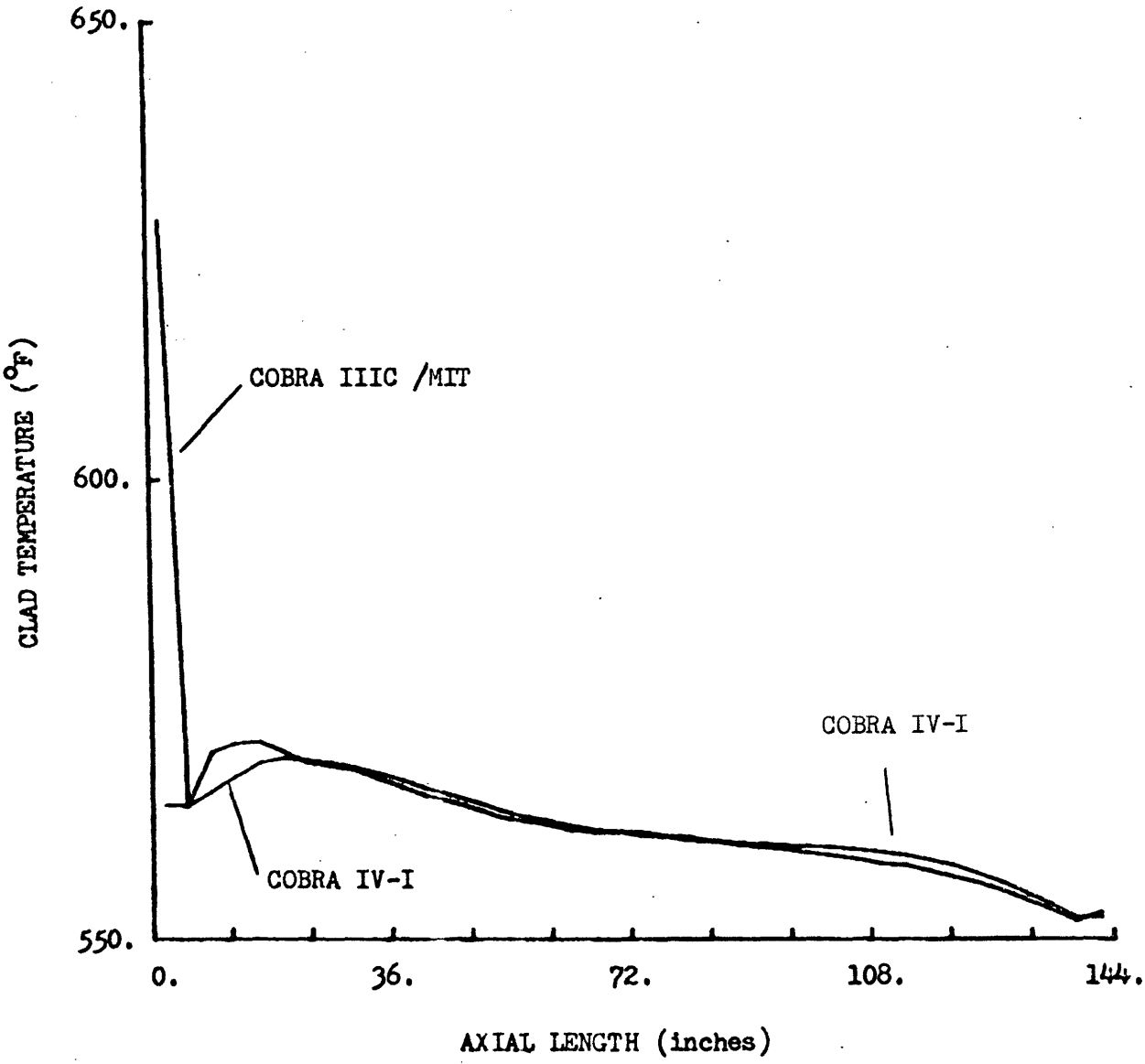

FIGURE 2.2

CLAD TEMPERATURE VERSUS AXIAL LENGTH

RESULTS FOR CASE 1, ROD 2

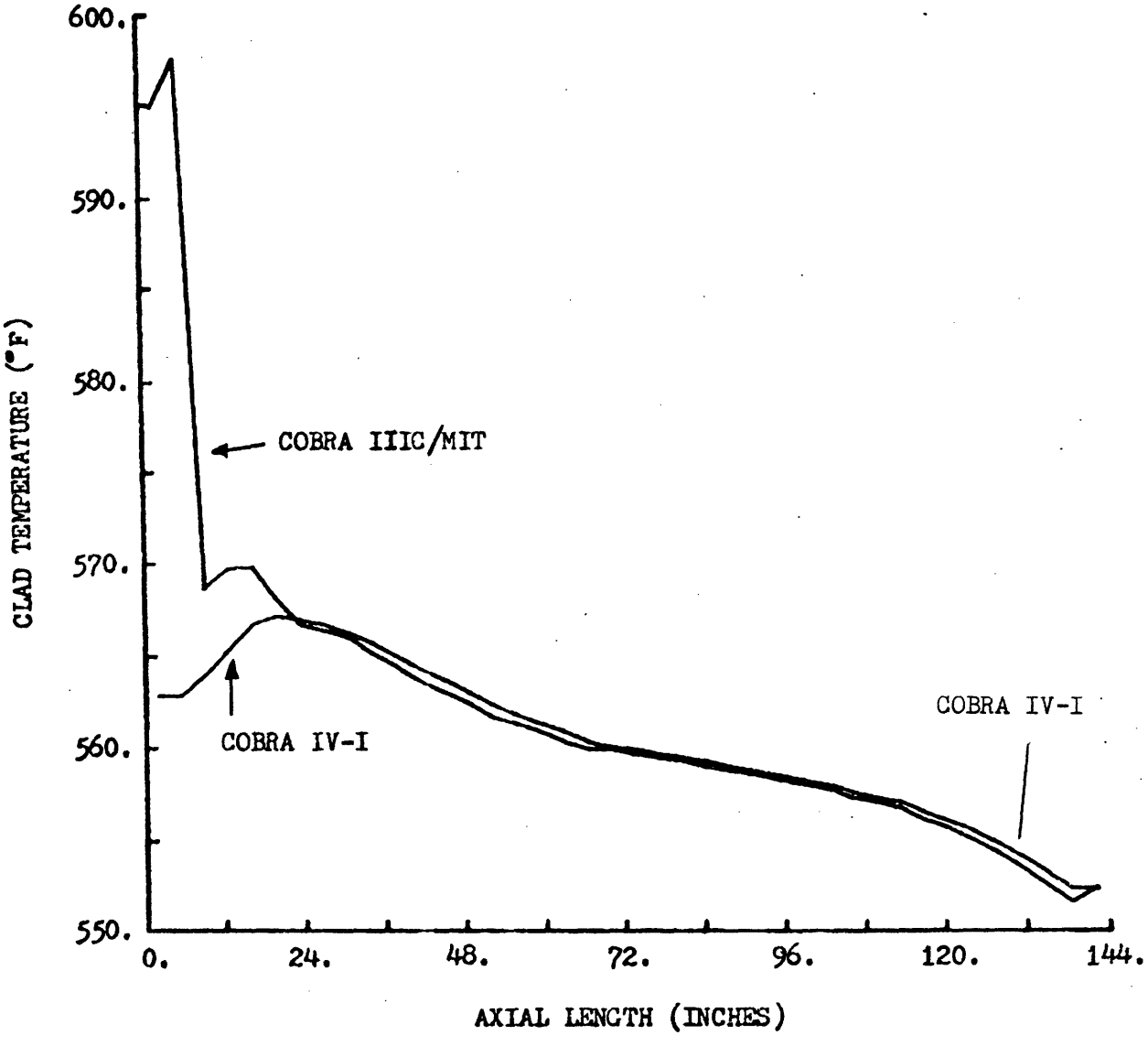

FIGURE 2.3

CLAD TEMPERATURE VERSUS AXIAL LENGTH

RESULTS FOR CASE 1, ROD 4

channel. However, for this rod the discrepancy exists for more than just the first node. These initial observations indicate that the clad temperature predictions do not agree very well.

2.4.3 Results of Case 2

As part of this investigation, a second comparison case was made. This case is the same as the above except that Levy's model is not used. As was found in the previous case, the enthalpy and density distributions are essentially identical for both codes. The density distributions for channels 2 and 4 are illustrated in Figure 2.4. Note that once boiling begins the density drops rather sharply. In this case, boiling begins in channel 2 at 18. inches and begins in channel 4 at 25.2 inches. Since the first case includes the subcooled boiling model, boiling begins earlier in each channel--at 3.6 inches in channel 2 and at 10.8 inches in channel 4. Figure 2.5 shows the density distributions with and without the Levy model for channel 4. Although the influence of the Levy model is not noticeable at high void fractions (ie. low densities), in the subcooled regime this model has a dramatic effect on the density predictions. Therefore, in order to accurately predict the density distribution, the Levy model should be used.

The clad temperature predictions for this second case point out further deviations between the two codes. Predictions from rod 2 are illustrated in Figure 2.6. The COBRA IV-I results are identical to those found in the first case, indicating that the heat transfer model is independent of Levy's model. The COBRA IIIC/MIT results do depend on the use of the Levy model, as the clad temperatures are predicted to be much higher than the COBRA IV-I results for a longer length of the rod. In fact, COBRA IIIC/MIT

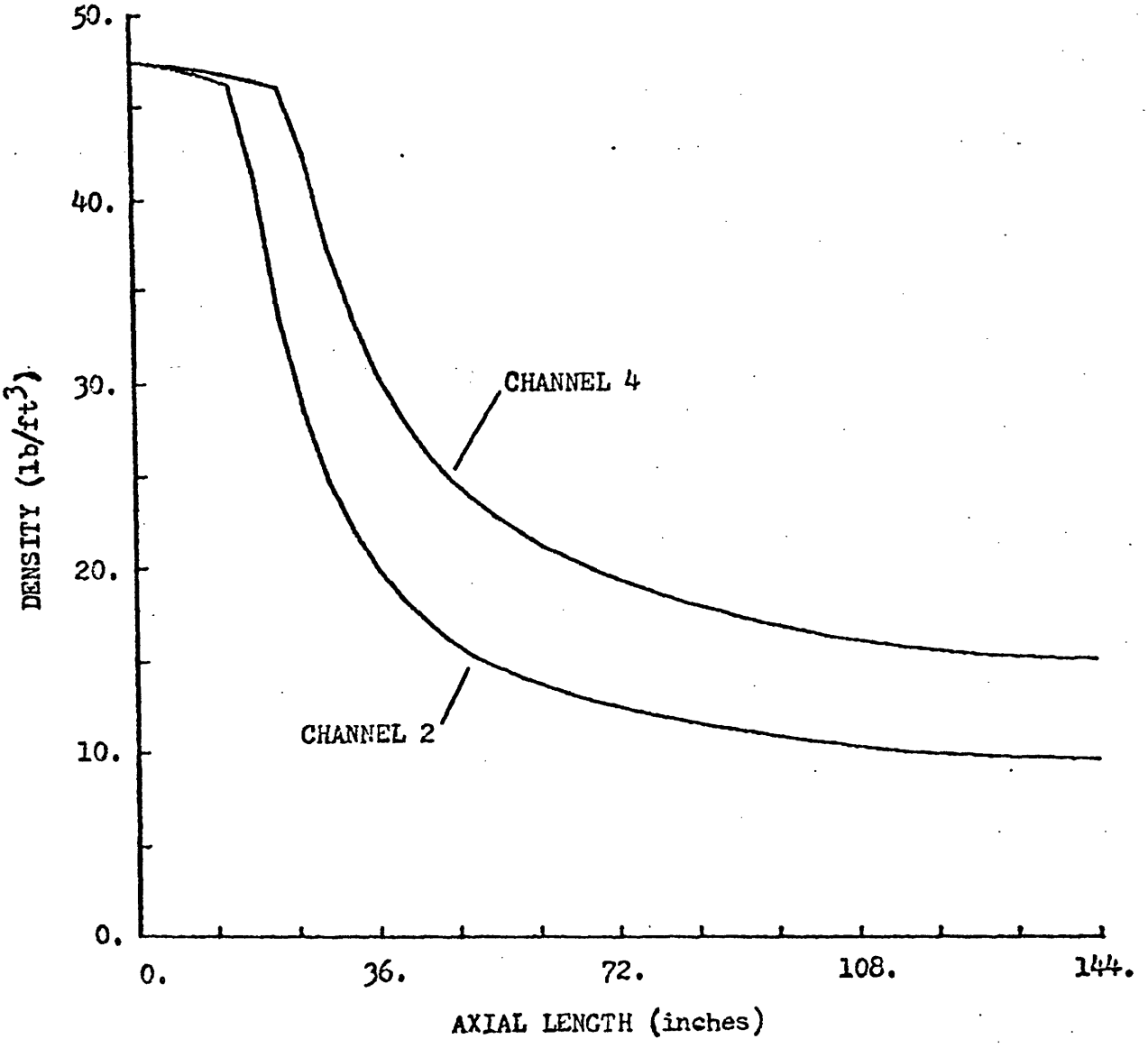

FIGURE 2.4

DENSITY VERSUS AXIAL LENGTH

COBRA IIIC/MIT AND COBRA IV-I PREDICTIONS

FOR CASE 2

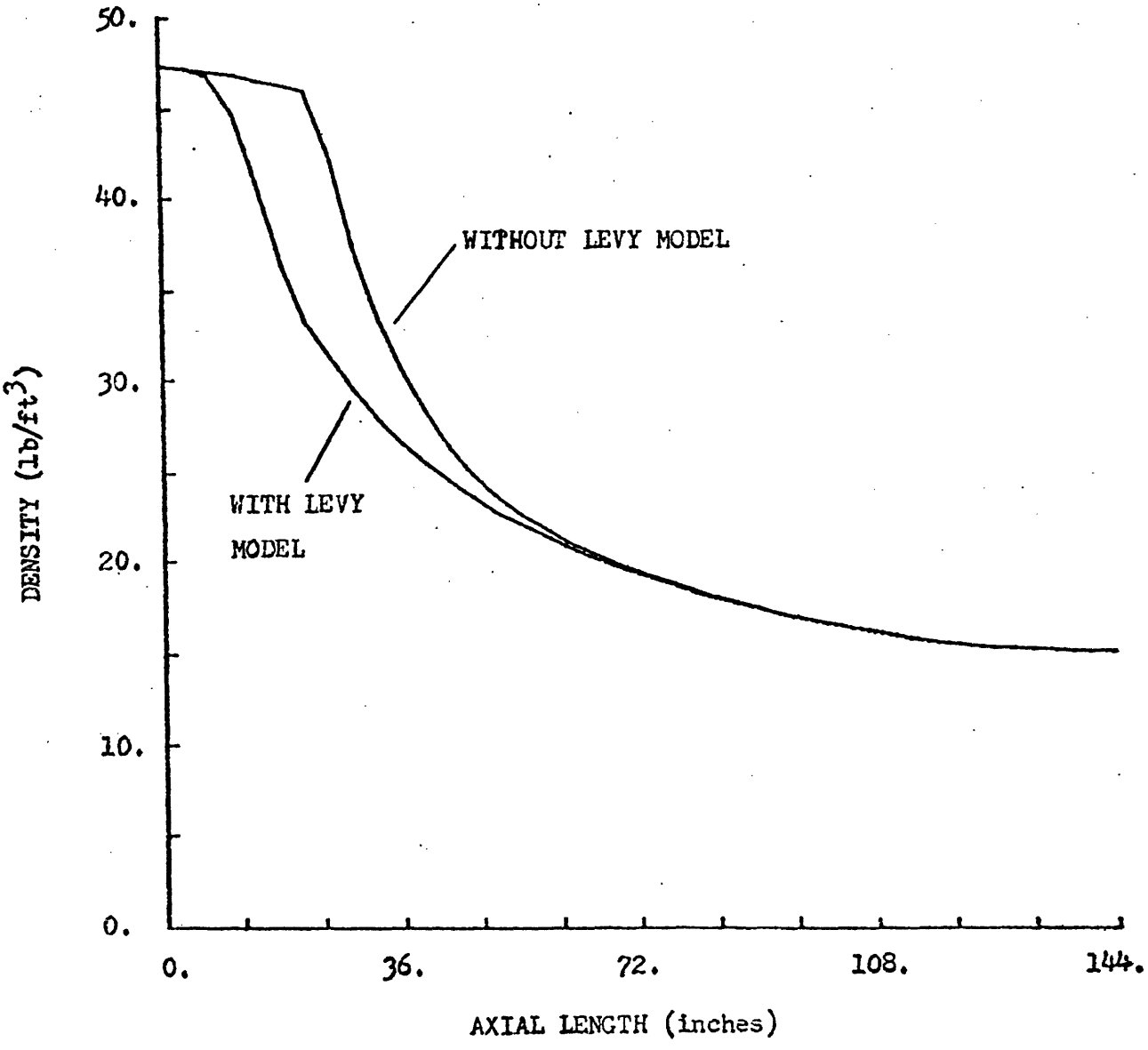

FIGURE 2.5

DENSITY VERSUS AXIAL LENGTH

COBRA IIIC/MIT AND COBRA IV-I PREDICTIONS

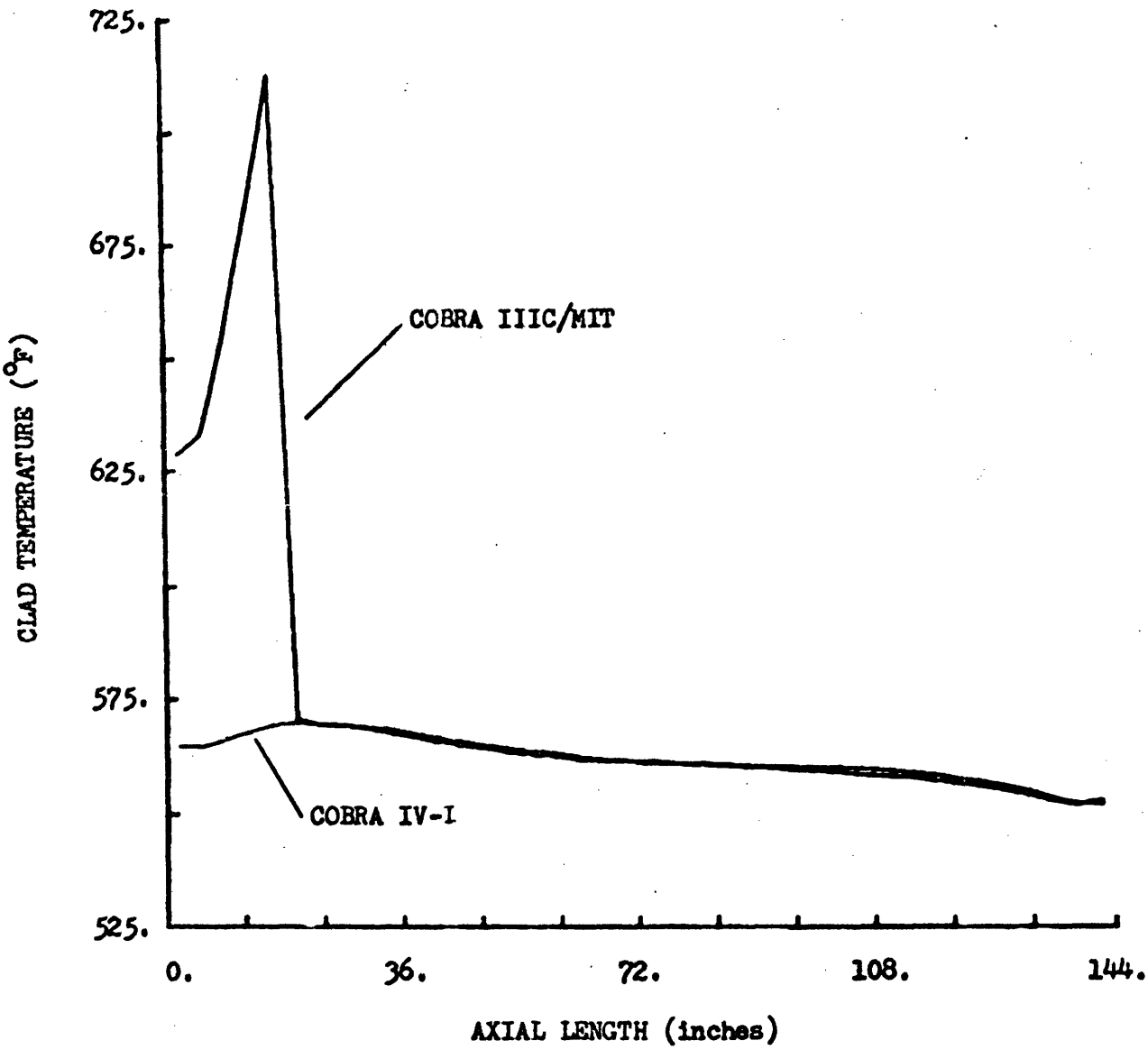

FIGURE 2.6

CLAD TEMPERATURE VERSUS AXIAL LENGTH

RESULTS FOR CASE 2, ROD 2

predicts a maximum clad temperature which is approximately 140 °F higher than that predicted from either COBRA IV-I or COBRA IIIC/MIT with the Levy model.

2.4.4 Results of Case 3

As further evidence of the importance of the Levy model, a third case was run in which the Levy model was used together with an inlet temperature of 514 °F. With a lower inlet temperature, subcooled boiling begins further up the channel. The shifted boiling front should have an impact on the COBRA IIIC/MIT clad temperature results. However, as before, the density distribution predictions of the two codes are identical. As expected, the clad temperature predictions differ significantly. Figure 2.7 illustrates the rod 4 clad temperature distribution for each code. It is interesting to note that the COBRA IV-I clad temperature predictions are the same as they were for the first two cases. The COBRA IIIC/MIT predictions are significantly greater than those of COBRA IV-I in the subcooled regime. It is also observed that the COBRA IIIC/MIT results remain larger for a longer length of the channel in this case than they did in the first case when the inlet temperature was 527 °F.

2.5 Discussion of the Steady-State Results

These widely differing results between the two codes can be explained in terms of the heat transfer models. As mentioned above, the heat transfer package can be divided into two parts. The package consists of both heat transfer correlations and a logic system which determines when and how to use each correlation. Hence, even if the same correlations are in each heat transfer package, a different logic system can lead to different

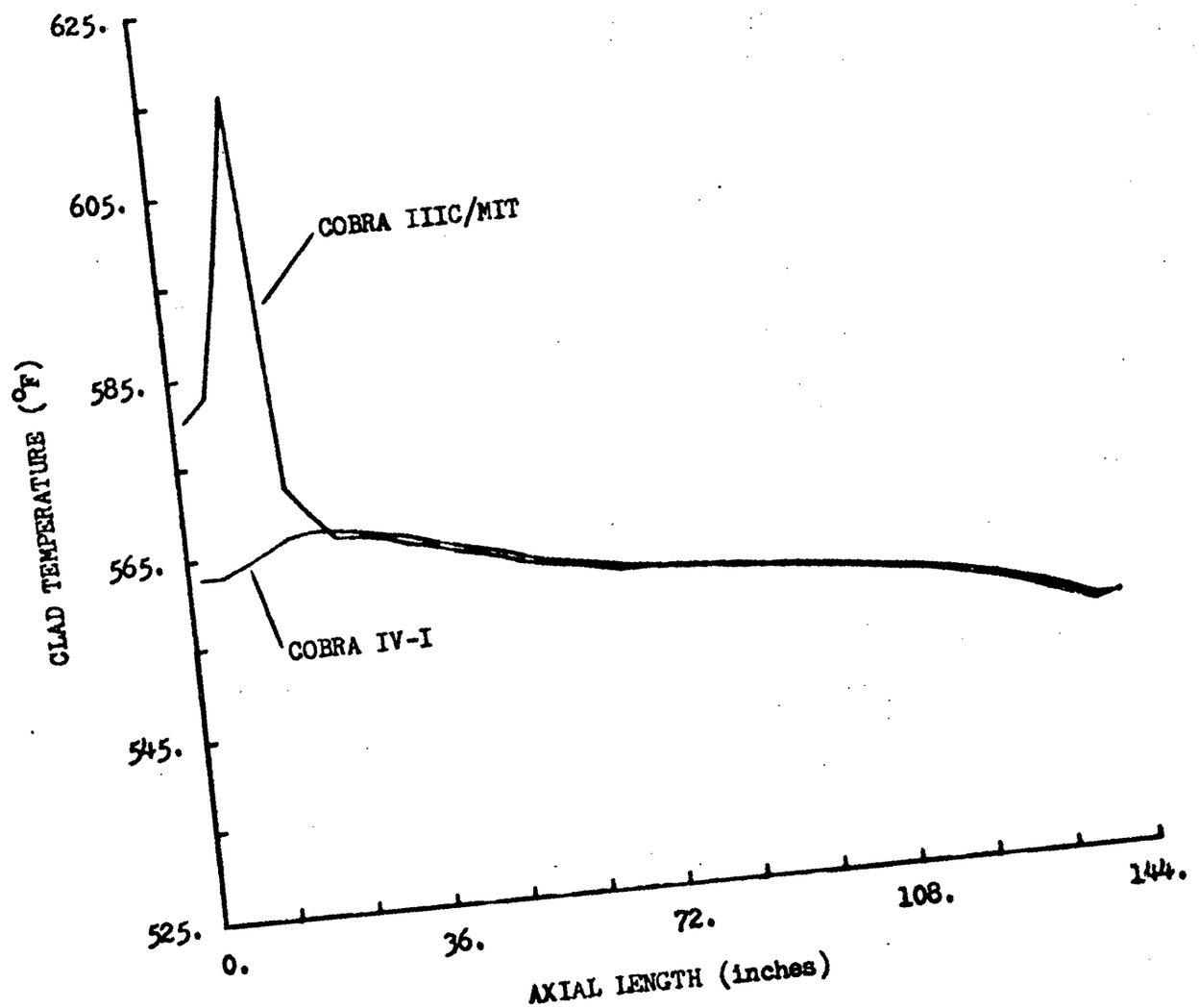

FIGURE 2.7

CLAD TEMPERATURE VERSUS AXIAL LENGTH

RESULTS FOR CASE 3, ROD 4

results. In order to investigate this latter possibility the heat transfer models in each code are examined in detail.

2.5.1 Heat Transfer Correlations

It is found that the heat transfer correlations used in each code are identical up to a void fraction of 0.8. Both codes use Thom's forced convection correlation (5) in the single phase regime and use Thom's nucleate boiling correlation (5) in the nucleate boiling regime. After a void fraction of 0.8 is reached, COBRA IV-I uses the Schrock and Grossman correlation (6) up to the point of CHF, while COBRA IIIC/MIT continues to use Thom's nucleate boiling correlation. However, only channel 2 reaches a void fraction greater than 0.8 and it does so only for the last quarter of the channel. From the previous figures of clad temperature, it was observed that the main discrepancies occur in the beginning of the channel, and over the last quarter of the channel the temperature predictions are rather close. The regime at the beginning of the channel is single phase and, yet, different temperatures are predicted even though identical correlations are used. Hence, the way these correlations are employed or the logic of the two packages must differ.

2.5.2 Heat Transfer Logic

Indeed, it is found that the logic systems in each code are different from one another. The main difference between the two codes is how each determines when to switch from the forced convection correlation to the nucleate boiling correlation. The COBRA IIIC/MIT criterion for switching correlations depends on whether or not the quality is greater than zero. If the quality is greater than zero, then the nucleate boiling correlation

is used. The quality is not simply meant to mean the thermodynamic quality, since when Levy's model is used a positive quality is predicted even though the fluid is still subcooled (ie. the thermodynamic quality is negative). Hence, a positive quality indicates the start of boiling. The COBRA IV-I criterion for switching does not depend on the quality, but instead depends on the clad temperature. If the clad temperature is greater than the fluid saturation temperature, then it begins to use the nucleate boiling correlation. However, if the heat transfer coefficient predicted by the forced convection correlation is larger than that predicted by the nucleate boiling correlation, then the forced convection correlation is used. In the cases analyzed here, the nucleate boiling heat transfer coefficient is usually four times as great as the forced convection heat transfer coefficient. Hence, for COBRA IV-I, the nucleate boiling correlation is used once the clad temperature is greater than the saturation temperature even if boiling has not started.

2.5.3 Explanation of Clad Temperature Discrepancies

Using this knowledge of the logic systems, the large differences in the clad temperature predictions can be explained. Referring back to Figure 2.3, which depicts the clad temperature distributions of rod 4 for the first case, one finds that even in the subcooled regime the clad temperature is greater than the saturation temperature. This condition means that COBRA IV-I uses the nucleate boiling correlation even at the beginning of the channel. Since subcooled boiling does not begin until the third node, COBRA IIIC/MIT uses the forced convection correlation in the first two nodes. In these two nodes, the COBRA IV-I heat transfer coefficient is approximately four times larger than that used by COBRA IIIC/MIT.

Consequently, the clad temperatures predicted by COBRA IV-I are significantly less than those predicted by COBRA IIIC/MIT. Once boiling begins, COBRA IIIC/MIT switches to the nucleate boiling correlation and the clad temperature decreases dramatically. Thus, the dissimilar heat transfer logic leads to large differences in the clad temperature predictions.

In order to examine the influence of the logic more closely, COBRA IIIC/MIT was changed so that its logic would be the same as that found in COBRA IV-I. With the logic changed, the modified COBRA IIIC/MIT was employed to analyze the first case again (inlet temperature 527 ^{o}F and the Levy model used). The clad temperature distribution of rod 4 is shown on Figure 2.8. Also on this figure are the COBRA IV-I and original COBRA IIIC/MIT temperature distributions. The modified COBRA IIIC/MIT still predicts a higher temperature in the first node, but agrees with COBRA IV-I in the second node. Thereafter, the modified COBRA IIIC/MIT is exactly the same as the original COBRA IIIC/MIT. Although the change in the heat transfer logic put the COBRA IIIC/MIT and COBRA IV-I results in closer agreement, this change alone did not produce exact correspondence between these two codes.

The reason for the remaining discrepancies between the modified COBRA IIIC/MIT and COBRA IV-I results can be attributed to the different energy equations. The explicit nature of the COBRA IIIC/MIT energy equation requires that information (eg. fluid temperature and heat flux) from the previous node be used in determining quantites (eg. heat tranfer coefficient) for a particular node. Consequently, in the first node, the nucleate boiling correlation cannot be used because the heat flux from the previous node is required and there is no previous node. By default, the forced convection correlation is employed even though the clad temperature

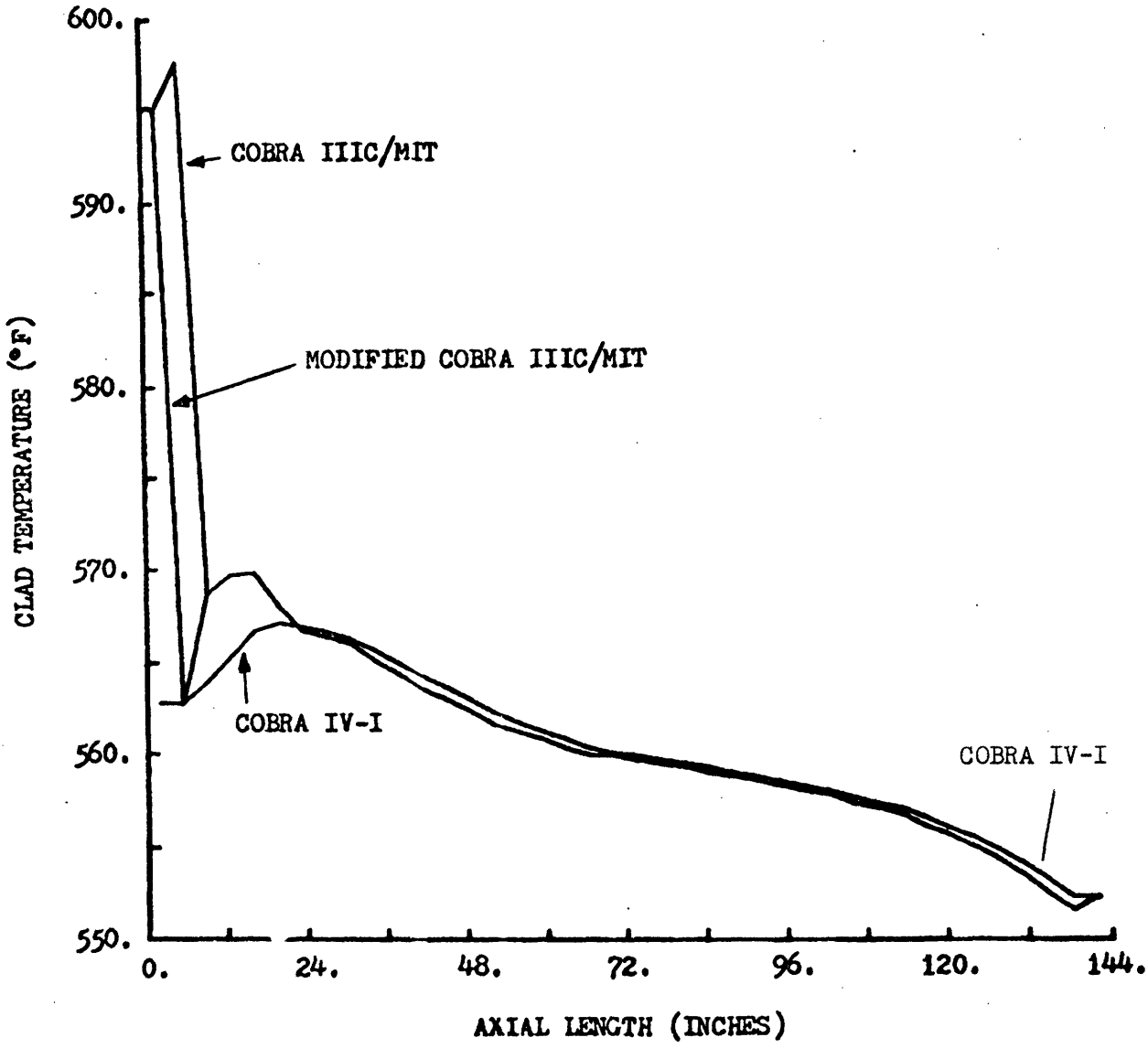

FIGURE 2,8

CLAD TEMPERATURE VERSUS AXIAL LENGTH

RESULTS FOR CASE 1, ROD 4

is greater than the saturation temperature. The application of this correlation results in a large temperature for the first node. COBRA IV-I does not have this problem since its energy equation is spatially implicit. With this equation, consistent sets of heat fluxes, clad temperatures and heat transfer coefficients are determined at each axial node. Although a number of iterations are required to obtain a converged solution, a consistent solution is obtained even in the first node. Hence, the large difference in the first node is due to differences in the energy equations which cause different heat transfer correlations to be used.

As further evidence of the effect of the different energy equations, one should note the discrepancies in the subcooled boiling regime. This regime begins at the point where the COBRA IIIC/MIT clad temperature prediction decreases dramatically (refer to Figure 2.8). In this regime, both codes are using the same heat transfer correlations, but the COBRA IIIC/MIT temperature predictions are between 1 ^{o}F and 5 ^{o}F greater than those of COBRA IV-I. As indicated above, COBRA IIIC/MIT must use information from the previous node to determine the heat transfer coefficient. Since the power distribution is increasing in this regime (see Appendix B), the heat flux for a particular node will be higher than that for the previous node. This condition means that the heat transfer coefficient, which depends on the heat flux and uses the heat flux from the previous node, will be lower than a consistent value would be. However, COBRA IV-I calculates a consistent heat transfer coefficient and, consequently, the COBRA IV-I temperature predictions are lower than those of COBRA IIIC/MIT. Once again, the differences in the energy equations lead to different clad temperature predictions.

2.5.4 Summary of Steady-State Analyses

The above steady-state BWR bundle analyses exemplify some of the similarities and differences between the two codes. The enthalpy and density distributions as predicted by each code agree extremely well with one another. This agreement occurs in spite of the fact that a wide spectrum of fluid conditions are attained--from slightly subcooled to void fractions greater than 0.8. However, the clad temperature distributions as predicted by each code are radically different from one another in the subcooled regime. Large differences are caused by both different heat transfer logic and different energy equations. The differences in heat transfer logic are concerned with the criterion for changing heat transfer correlations. The different energy equations also have a major influence on the heat transfer calculations. For a particular node, COBRA IIIC/MIT calculates the heat transfer coefficient using conditions from the previous node. This calculation produces an inconsistent set of heat transfer coefficient, heat flux and clad temperature. On the other hand, COBRA IV-I uses an iterative procedure to determine a consistent set of these variables at each node. Hence, the different heat transfer packages and different energy equations lead to significantly different clad temperature predictions.

2.6 Transient Analysis

This section discusses the results of transient BWR bundle-wide analysis. As with the steady-state cases, a five-channel geometry is employed to model typical regions in a BWR core. The transient which is examined is a pressurization transient which, in fact, simulates a

turbine trip without by-pass transient. For this type of transient analysis, attempts were made to use both COBRA IIIC/MIT and COBRA IV-I.

Unfortunately, COBRA IV-I is not able to perform in this mode of analysis. The main reason for this failure appears to be related to a lack of appropriate boundary conditions. For a realistic transient, one would require either the inlet flow for each channel as a function of time or the core pressure drop as a function of time. COBRA IV-I cannot accept individual channel inlet flow rates as a function of time. However, it is possible to specify the pressure drop as a function of time if the explicit method of COBRA IV-I is used. This latter option was employed, but meaningless results (e.g., negative flows) occurred. An attempt was then made to simply maintain a steady-state solution by requiring that the pressure drop remain constant during the transient. This unperturbed transient also produced negative flows and, hence, was deemed meaningless. Therefore, the pressure drop boundary condition does not provide the necessary boundary condition for this type of analysis.

In view of this difficulty, other boundary condition modeling was examined. The available choices are:

a) total inlet flow with implicit method;

b) total inlet flow with explicit method; and

c) pressure drop with explicit method.

The last condition, as discussed above, did not produce meaningful results. Using either the explicit or implicit method, the total inlet flow could be specified as a function of time. This total flow rate is divided among the channels in the same ratio as it is in steady-state.

Hence, if the flow splitting in steady-state produces equal pressure drops across all channels, the pressure drops will not remain equal during the transient. In order to maintain equal pressure drops, it would be necessary to know the correct flow splitting at each time during the transient. This latter option is not available in COBRA IV-I and, consequently, only the total inlet flow could be specified at each time step. Using this condition, reasonable results were predicted with either the implicit or explicit methods. However, this boundary condition is not exactly appropriate for bundle-wide analysis and no comparisons could be made with COBRA IIIC/MIT. Consequently, COBRA IV-I is not used in the transient BWR bundle analysis.

On the other hand, it is possible to use COBRA IIIC/MIT for transient BWR bundle analysis. However, while analyzing a pressurization transient, two severe problems were encountered (23, 24). Although each problem had a different cause, both resulted in a breakdown of the code if small time step sizes (0.01 seconds) were used. A few inconsistencies in the BWR method were also discovered during the investigation. Appropriate corrections were found such that both the inconsistencies and breakdowns were eliminated. These modifications are discussed in Sections 2.6.1 through 2.6.6.

After correcting these difficulties, a pressurization transient was analyzed. The objectives of this analysis are (a) to verify that the BWR option would operate in transient mode, (b) to investigate the effect of using the Levy model, and (c) to observe the effect of the pressurization transient on various core parameters. Since the code is able to analyze the pressurization transient, the first objective is satisfied. From the subsequent analysis, the second and third objectives are fulfilled, and a discussion of these are found in Section 2.7.

2.6.1 Discussion of the First Problem

Once the steady-state analysis was completed, an attempt was made to analyze a pressurization transient with COBRA IIIC/MIT. This case employs nearly the same modeling found in the second steady-state case. The only difference is that this transient case includes the application of both the Smith slip correlation and the Armand two-phase friction multiplier. Starting from a steady-state solution, which has a pressure of 1035 psia, the pressure is increased at a rate of 5% per second and a time step size of 0.01 seconds is used. With this modeling scheme, COBRA IIIC/MIT was run and after 44 time steps negative flows are predicted. These negative flows result at the inlet of channel 5 and lead to the divergence of the code. The occurrence of negative flows does not seem to be physically meaningful, and indicates that a numerical instability is causing the failure of the code.

An investigation into this breakdown was initiated and it was discovered that the prediction of negative inlet flows cause the code to diverge. As explained in Appendix A, an iterative procedure is used to update the inlet flows. The equation employed to update the inlet flow for the ith channel is

$$m_{i\ j+1} = m_{ij} + \frac{\Delta m}{\Delta p}\left[\frac{\sum P\ \frac{\Delta m}{\Delta P}}{\sum \frac{\Delta m}{\Delta P}} - P_i\right]. \qquad (2.1)$$

The only way that a negative inlet flow can be predicted is if the term

$$\frac{\Delta m}{\Delta P}\left[\frac{\sum P\ \frac{\Delta m}{\Delta P}}{\sum \frac{\Delta m}{\Delta P}} - P_i\right]$$

is negative and larger in magnitude than m_{ij}. In order to discover how this term could become large and negative, a careful examination of the

breakdown was performed.

From this analysis, the cause of the breakdown became apparent. It is found that the term, $\Delta m/\Delta P$, for a particular channel is usually positive, but could occasionally be negative. At the point of the breakdown this term is negative for channel 2. However, this term, by itself, is not a problem, but the combined term,

$$\sum \frac{\Delta m}{\Delta P}$$

is negative while the term

$$\sum P \frac{\Delta m}{\Delta P}$$

is positive. One can immediately see that these circumstances will cause the term

$$\frac{\sum P \frac{\Delta m}{\Delta P}}{\sum \frac{\Delta m}{\Delta P}} - P_i$$

to be large in magnitude and negative. A negative flow can then be predicted for a channel if $\Delta m/\Delta P$ for that channel is sufficiently large and positive. For the case being analyzed, these conditions are met and a negative inlet flow is predicted in channel 5. Once the negative flow is predicted, the code begins to predict divergent results and eventually fails.

Although the calculation of a negative $\Delta m/\Delta P$ is required for a breakdown, a negative $\Delta m/\Delta P$ by itself will not cause a breakdown. A combination of effects is necessary, but if $\Delta m/\Delta P$ is always positive then negative flows will not occur. From a physical point of view, a negative $\Delta m/\Delta P$ represents a flow instability. However, due to the high flow rates in the channels it is unlikely that such an instability exists.

The calculation of a negative $\Delta m/\Delta P$ must be attributed to a numerical cause. From the investigation, it was discovered that the pressure drop is not solely a function of the inlet flow rate. In fact, it was found that for the same inlet flow rate two different pressure drops can be predicted. Apparently, the pressure drop function is dependent on the iteration scheme. This dependence results in negative $\Delta m/\Delta P$ predictions on many occasions. Consequently, the prediction of a negative $\Delta m/\Delta P$, in itself, does not appear to be a serious problem with the code.

As was seen above, the term

$$\frac{\sum P \frac{\Delta m}{\Delta P}}{\sum \frac{\Delta m}{\Delta P}}$$

(which is defined to be P_o) is negative when the breakdown occurs. The term, P_o, is the value of the pressure drop which is the same for all channels. The prediction of a negative P_o represents a non-physical result. Since the iterative process is a mathematical procedure, the prediction of a negative P_o is not prohibited on a mathematical basis. However, on a physical basis, P_o would not be negative for a BWR core under most conditions.

2.6.2 Solution of the First Problem

In order to eliminate this problem, a number of possible corrections were examined. For example, one such correction, as suggested by R. Bowring (25), constrains $\Delta m/\Delta P$ to be non-negative. However, the value of $\Delta m/\Delta P$ can change by as much as 50% from one iteration to the next and, hence, there is a question as to which value should be used if $\Delta m/\Delta P$ becomes negative. A second correction, which was implemented, constrains

P_o to be non-negative. As discussed above, a negative P_o is a non-physical result and, furthermore, if this term is negative, then a breakdown can occur. Unlike the constraint on $\Delta m/\Delta P$, there is no difficulty in constraining P_o, since P_o normally would change by less than 0.5% from one iteration to the next. Consequently, if P_o is predicted to be less than zero, then its value from the previous iteration could safely be used. Therefore, this constraint was chosen to correct the code.

The implementation of this constraint is achieved by modifying the subroutine SEPRAT. This subroutine controls the iterative inlet flow updating procedure. It is a simple matter to add a few statements which would insure a positive P_o. A complete listing of this subroutine can be found in Appendix C.

The case which broke down was rerun with this additional constraint. It was found that with this constraint the breakdown is eliminated. At the point where the code had previously failed, it now is able to converge and no new problems are observed. None of the results predicted prior to the breakdown have changed, indicating that the additional constraint would not change the predictions of the code. Hence, the constraint on P_o simply allows convergence of the code without influencing the results of the code.

2.6.3 Discussion of the Second Problem

After correcting the above problem, an attempt was made to analyze the same pressurization transient with the only modeling change being the application of the Levy model. With this small modeling change, the transient was run, but failed to converge even at the first time step. No problems were found in the steady-state solution, which indicated that this problem

was related to the transient calculations. In fact, the failure only occurred when both the Levy model and small time step sizes (0.01 seconds) were used. When larger time step sizes were employed or the Levy model was not used, then no breakdown was found. Hence, this second problem represented an obstacle for applying COBRA IIIC/MIT to transient, BWR bundle analyses.

A detailed investigation of the breakdown identified the conditions and consequences of the failure. The code would fail when time step sizes less than 0.1 seconds are used in conjunction with the Levy model. The failure is independent of the pressurization rate or other forcing functions which indicates that there is an inherent problem in the code. When the code fails the following results are predicted:

(a) negative inlet flows;

(b) divergent pressure drops;

(c) divergent flow rate.

These results are definitely not realistic and could only be attributed to a numerical instability.

The next step in the investigation was to determine the nature of the numerical instability. In order to clearly examine the solution method, the pressure forcing function was not used. With no forcing functions applied, a transient calculation should simply maintain its steady-state solution. If the solution method were indeed stable, then no changes from the steady-state solution should occur, regardless of the time step size used. By examining this unperturbed transient any deviations from steady-state could be immediately detected and their cause identified.

Many unperturbed transient runs were made using various combinations of time step size with and without the Levy model. When Levy's model is

not used, no unusual results are detected even for time step sizes of 0.001 seconds. Likewise, when Levy's model and time step sizes greater than 0.1 seconds are used, no deviations from the steady-state solution are observed. However, when Levy's model and small time step sizes (eg. 0.01 seconds) are used, the code would begin to diverge on the first time step. After only a few time steps the code has completely diverged and failed. This inability to maintain a steady-state solution raises the question as to whether or not the BWR option in the code had been adequately tested. In fact, it was never tested seriously.

The divergent behavior of the code for the unperturbed transient can best be identified by observing the behavior of particular variables. For example, the linear heat generation rate, q', is found to fluctuate during this "transient". These fluctuations in q' only occur in the subcooled regime of each channel. In the boiling regime, q' does not fluctuate and is maintained at its steady-state value. The typical fluctuations of q' in the subcooled regime are shown in Figure 2.9. This figure reveals that q' is higher at the first time step, lower at the second time step, higher at the third time step, and finally diverges at the fourth time step. The expected constant behavior of this variable is not observed and one would conclude that an instability existed in the method.

With variables such as q' diverging, one would question whether or not the conservation equations are being solved correctly. However, for most cases analyzed, no breakdowns occur which would support the belief that the equations are being solved correctly. Still the question which persisted is why do Levy's model and small time step sizes lead to the divergence of the code?

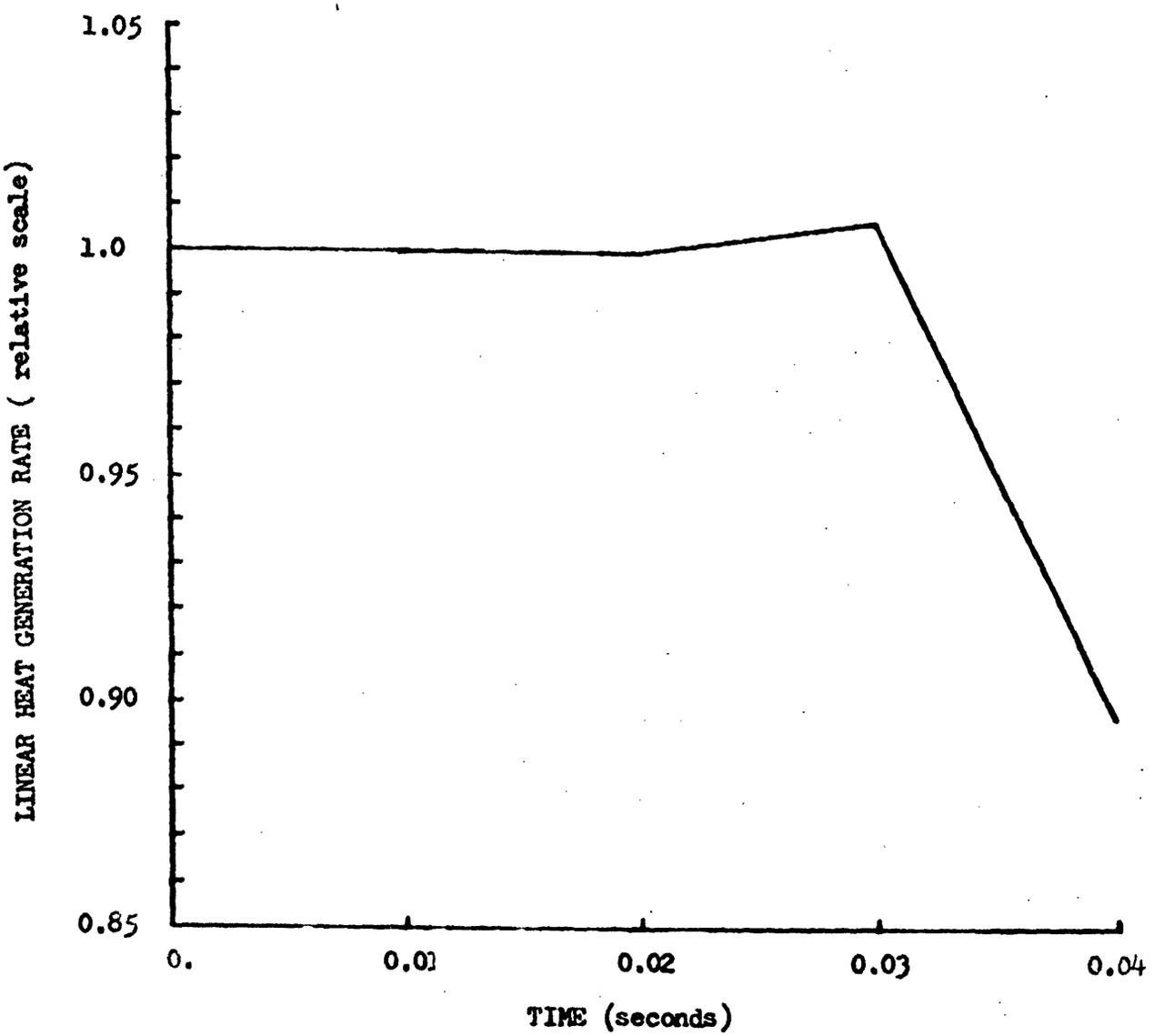

FIGURE 2.9

LINEAR HEAT GENERATION RATE VERSUS TIME

RESULTS FOR FIRST NODE IN CHANNEL 1

In order to answer this question it is necessary to review the effect of these options on the solution method. Basically, the Levy model increases the coupling between the heat transfer and hydraulic calculations. This tightened coupling is found primarily in the subcooled regime and is manifested through the density. The density acts as a link between the energy equation and the continuity and axial momentum equations. The energy equation is solved first to find the enthalpy, which in turn is used to find the density. Once the density is found, it is used first to calculate the flow rate by means of the continuity equation and then to calculate the pressure drop through the axial momentum equation. When Levy's model is not used, the density is only a function of the enthalpy. But, with the Levy model, the density is a function of enthalpy, flow rate, q', and heat transfer coefficient. One can see that the degree of coupling has increased, since when using the Levy model the flow rate is used to determine the density and in turn the density is used to determine the flow rate.

The effects of small time step sizes are most important in the continuity and axial momentum equations. Time derivatives in these equations become more sensitive to small changes as the time step size is decreased. For example, a small density variation can lead to large changes in the flow rate. With a time step size of 0.01 seconds, a 1% density change leads to a 10% change in the flow rate. Any density variation immediately leads to a significant change in the flow rate when small time step sizes are used. Hence, small time step sizes also increase the coupling between the conservation equations.

However, this strong coupling alone would not cause the code to fail. The calculation of some parameter would have to be in error and with the

strong coupling this error would be amplified. Therefore, it was assumed that some parameter was being incorrectly calculated, but this error was only detectable when the strong coupling existed.

Since the code failed when the Levy model was applied, the parameters which are used in this model were examined. The enthalpy, mass flow rate, and heat transfer coefficient were being calculated correctly, but q' was not being calculated correctly on each iteration. On the first iteration of a particular time step, q' would be calculated using

$$q' = \pi Dh\ (T_c - T_f)\ . \qquad (2.2)$$

On subsequent iterations, both the clad temperature, T_c, and the fluid temperature, T_f, are held constant. However, the heat transfer coefficient, h, can change during the iterative procedure because the mass flow rate changes as a result of the pressure drop iteration scheme. Any change in h should then be used to compute the changes in q'. These changes in q' were not being accounted for. Instead, q' was calculated on the first iteration and held constant for the remaining iterations of the time step. This calculation was not correct and turned out to be the primary cause of the code's failure.

In order to see why the failure to calculate q' on each iteration led to the breakdown, it is necessary to trace through the unperturbed transient. The steady-state solution is found as the starting point of the transient. Since each channel behaves similarily, only the behavior of channel 1 will be examined here. On the first time step, the inlet flow converges to a value which is slightly lower than its steady-state value. The reason that this value is lower is that it is virtually impossible to have an exact steady-state solution, because the steady-state solution is converged to a user-specified criterion. Any small errors

which might exist in the solution will be amplified when small time steps are used. It follows, then, that unless one starts with an exact solution, small fluctuations would be expected. However, these small fluctuations should not lead to divergence of the code.

With the converged solution from the first time step, the transient continues to the second time step. The lower inlet flow from the first time step is used as the initial guess for the inlet flow. With this lower flow, q' in the first node is calculated to be lower than its steady-state value because the heat transfer coefficient is lower. The lower q', lower flow rate, and lower h are used as input into the energy equation and the net result is a higher density. This higher density causes a deceleration of the flow and a reduction in the pressure drop for the first node. The second node uses the reduced flow and, as in the first node, q' is lower. This lower q' leads to a lower flow for the third node and reduced pressure drop. The flow continues to decrease until the nucleate boiling regime is reached, after which the flow remains constant. At the end of this first iteration, the pressure drop for this channel is lower than P_o thereby requiring an increased flow for the second iteration.

The second iteration begins with an inlet flow which is higher than its steady-state value. However, q' is not recalculated and again the density is increased. This increased density causes a reduction in the flow rate as was found on the first iteration. The calculations continue up the channel and the net result is that the total pressure drop is still lower than P_o and, hence, the inlet flow rate is increased once more. Using this higher inlet flow the code converges on the third iteration. It should be noted that the converged inlet flow is 1% greater than its steady-state value at this point in time.

The third time step uses this higher inlet flow on the first iteration. In the first node, q' is found to be higher than it was on the second time step. The increased q' leads to a density decrease and in turn the flow increases. The second node uses the increased flow to find a higher q' and lower density. This type of behavior propagates up the channel and the net result is a higher pressure drop due to the increased flow. The iterative procedure reduces the inlet flow for the second iteration. Although the inlet flow is lower on the second iteration, the flow is accelerated up the channel and the pressure drop is again higher than P_o. The inlet flow is again reduced and eventually the code converges, but the inlet flow is much less than its steady-state value.

The behavior of the inlet flow for channel 1 is illustrated in Figure 2.10. One sees that at the third time step the flow has been significantly decreased. On the fourth time step, this significantly lower flow leads to a greatly reduced q' which decelerates the flow. The pressure drop is drastically reduced and, hence, on successive iterations the flow is continually increased until the code fails.

2.6.4 Solution of the Second Problem

This second failure of the code was eliminated by calculating q' on each iteration. The reason for the success of this solution can be seen by referring to the above example. For example, at the beginning of the second iteration of the second time step a higher than steady-state inlet flow is used. This higher flow will lead to a high q' if q' is recalculated. A lower density is predicted and the flow is increased for the second node. The calculations continue and the pressure drop for the channel is found to be higher than P_o. This result causes a reduction in the inlet flow

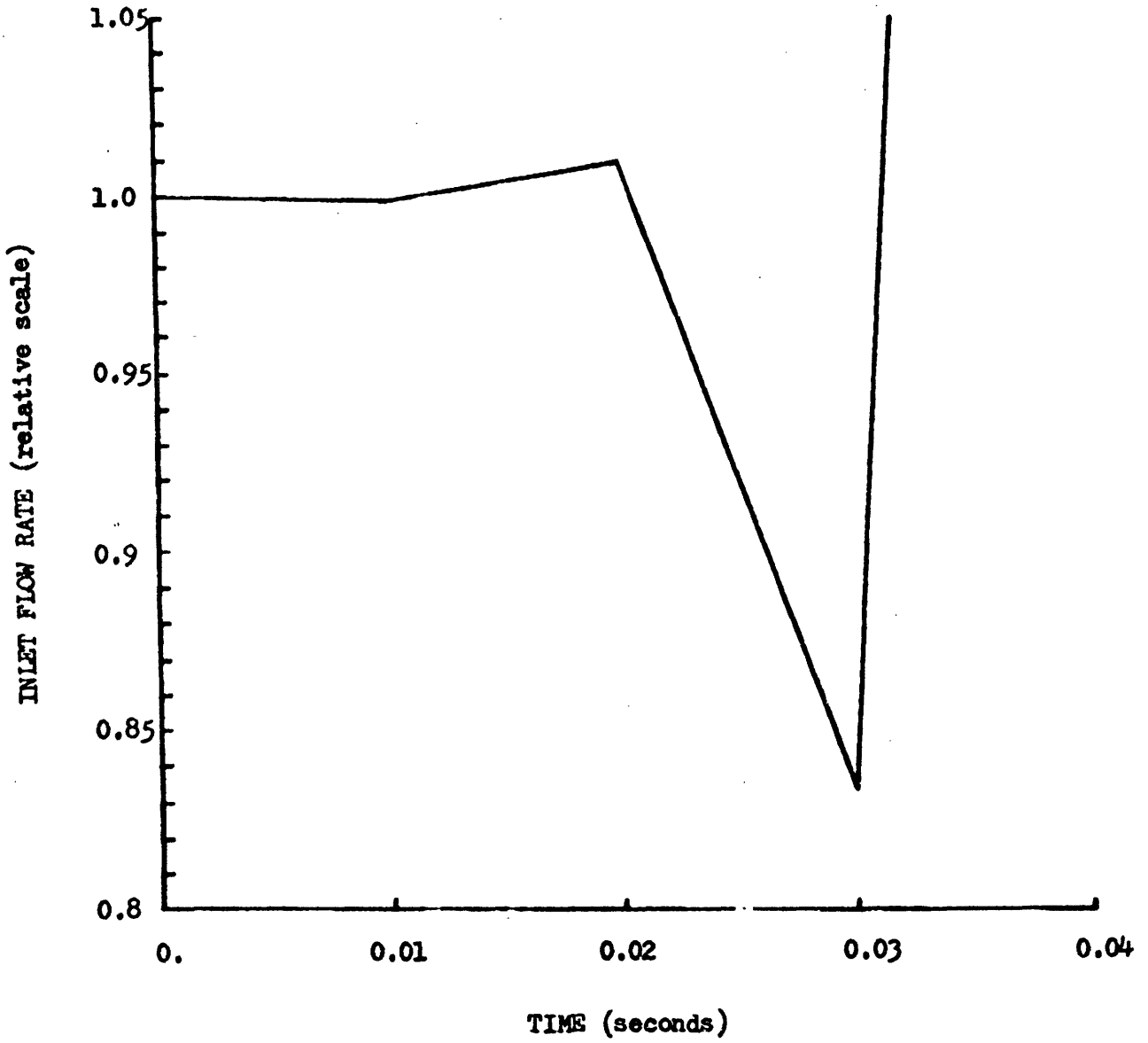

FIGURE 2.10

INLET FLOW RATE VERSUS TIME

RESULTS FOR CHANNEL 1

to a value which is closer to its steady-state value. As was seen above, the failure to recalculate q' leads to an increased inlet flow which diverges from the steady-state value. By recalculating q' on each iteration, a stabilizing effect is added to the code, which yields convergence.

In order to implement the correct calculation of q', changes were made to subroutine HEAT. Instead of using the same q' on each iteration, the equation used to calculate q' was altered so that q' would be recalculated on each iteration. This change was made in subroutine HEAT and a complete listing of the corrected version of this subroutine can be found in Appendix C.

With the code corrected, the hold steady-state transient was rerun and worked successfully. This encouraging result led to the rerunning of the pressurization transient. The code is able to analyze this transient without any abnormal behavior. Subsequent tests were made using smaller time step sizes (0.005 seconds) and pressurization rates of up to 100 psi/second. No new failures occur and it appears that the problems in the code have been successfully solved.

2.6.5 Discussion of Inconsistencies in the BWR option

Besides the problem associated with the calculation of q', a few additional inconsistencies were discovered in the BWR option during the course of this investigation. These inconsistencies involve the void fraction calculation, the flow rate calculation, and the pressure drop calculation. Each of these calculations along with their appropriate corrections is discussed below.

The void fraction is calculated before the flow rate is updated in

a particular node. Since the void fraction calculation requires the flow rate when Levy's model is used, there is a question as to which flow rate should be employed in this calculation. In a steady-state calculation, the flow rate from the previous node should be used since the flow rate does not change along the channel. For transient calculations, one can use either the previous node value or the previous iteration value. In COBRA IIIC/MIT, the value from the previous iteration was being employed in the void fraction calculation. This usage is incorrect in steady-state analysis. The solution method does not converge on the flow rate which means that the flow rate could change significantly from one iteration to the next. Hence, it is best to use the flow rate from the previous node in both steady-state and transient calculations. Subroutine SCHEME was changed such that the flow from the previous node would be used in the void fraction calculation. A listing of this subroutine is found in Appendix C.

After the void fraction is calculated, the density can be determined. Once the density is known, the flow rate can be immediately calculated. In COBRA IIIC/MIT, the flow rate was not being updated immediately and, consequently, the velocity was being calculated using the wrong flow rate. To correct this inconsistency, subroutine VOID was changed so that the flow rate would be calculated immediately after the density is known. This subroutine is listed in Appendix C.

The final inconsistency was found in the pressure drop calculation. In COBRA IIIC/MIT, an approximation is made in the equation used to calculate the pressure drop. This approximation is only required when there is crossflow, ie, when PWR semi-open cores or subchannels are analyzed. Therefore, when the BWR option is used this approximation is not needed.

The pressure drop equation was corrected to eliminate this unnecessary approximation. These corrections occurred in subroutine DIFFER and a listing of this subroutine is in Appendix C.

2.6.6 Effects of Code Changes

The improvements in the BWR option, which are discussed above, have significantly increased the applicability of COBRA IIIC/MIT. Although transient analysis with the BWR option had been attempted, many problems were encountered and the code frequently failed. These breakdowns appeared to limit the applicability of the code for many transients of interest (eg. pressurization transient). However, with the use of the above corrections these breakdowns are eliminated and, consequently, many transient cases can now be analyzed. Therefore, the limitations on the applicability of the BWR option have been removed.

Furthermore, a number of inconsistencies in the BWR option have been eliminated. The removal of these inconsistencies represents the first major change made to the BWR option. These inconsistencies are concerned with the calculation of a number of parameters. Many of these calculations are valid in the PWR option. By correcting these inconsistencies, the solution method in the BWR option is improved without significantly altering the results of the code. Therefore, these corrections represent definite improvements in the BWR option.

2.7 Results of Transient Analysis

2.7.1 Description of Transient Cases

The modeling used in the transient analysis is similar to that used in the previous studies. Once again, the five channel geometry is used.

Each channel is divided into 40 nodes yielding an axial mesh size of 3.6 inches. An inlet temperature of 527 ^{o}F is used which corresponds to a subcooling of 27.5 Btu/lb at 1035 psia. Two cases are used in this analysis. Both cases consider the same geometry and the only difference between the two cases is that the first case, case A, uses the Levy model, while for the second case, case B, the Levy model is not applied. Each case starts with a pressure of 1035 psia and the same power, and both of these variables are increased at a rate of 5% per second. These two forcing functions are applied simultaneously and the transient is run for 1.0 seconds using time step sizes of 0.01 seconds.

Since it is the intent of this analysis to investigate the effect of Levy's model and to observe the influence of the pressurization on various parameters, the transient behavior of a few selected variables will be examined. For example, the void fraction reflects the influence of using the Levy model. The case which uses the Levy model will have larger void fractions in the subcooled regime. The clad temperature distribution will also demonstrate the effect of the Levy model. As was seen in Section 2.4, the application of the Levy model can dramatically alter the clad temperature distribution. Besides illustrating the effect of the Levy model, these two variables show the influence of the transient forcing functions. An increase in pressure will cause a reduction in the void fraction. The clad temperature predictions will be affected by both the reduction in the void fraction and the increase in power. Consequently, the void fraction and clad temperature are used to report the results of the transient analysis.

2.7.2 Results of Case A

The results of the first case, which used the Levy model, illustrate the influence of the transient forcing functions. The void fraction distribution in channel 2 at the beginning and end of the transient are shown in Figure 2.11. As the transient proceeds, the beginning of subcooled boiling moves toward the end of the channel. The magnitude of the void fraction is also reduced at each point along the channel. These two observations are also found in the other channels.

The clad temperature distribution also changes during the transient. Figure 2.12 illustrates the changing distribution for rod 4. The first observation to note is that along most of the rod the temperature increases with time. Although the power was being increased, the main cause of the increasing temperatures is the increase in the saturation temperature associated with the pressure increase. During the transient, the saturation temperature increases by approximately 6 ^{o}F. In the boiling regime the temperature difference between the clad and fluid saturation temperature is given by the Thom nucleate boiling correlation,

$$T_c - T_f = 0.072\ (q")^{.5} \exp(-P_{ref}/1260.), \qquad (2.3)$$

where q" is the heat flux and P_{ref} is the reference pressure. With a 5% increase in both the heat flux and reference pressure this temperature difference has actually decreased. However, since the saturation temperature is increased, the clad temperature is also increased. Therefore, except for the first few nodes where boiling has not occurred, the increase in clad temperature can be attributed to the increased saturation temperature.

A second observation is that as the boiling front moves up the channel

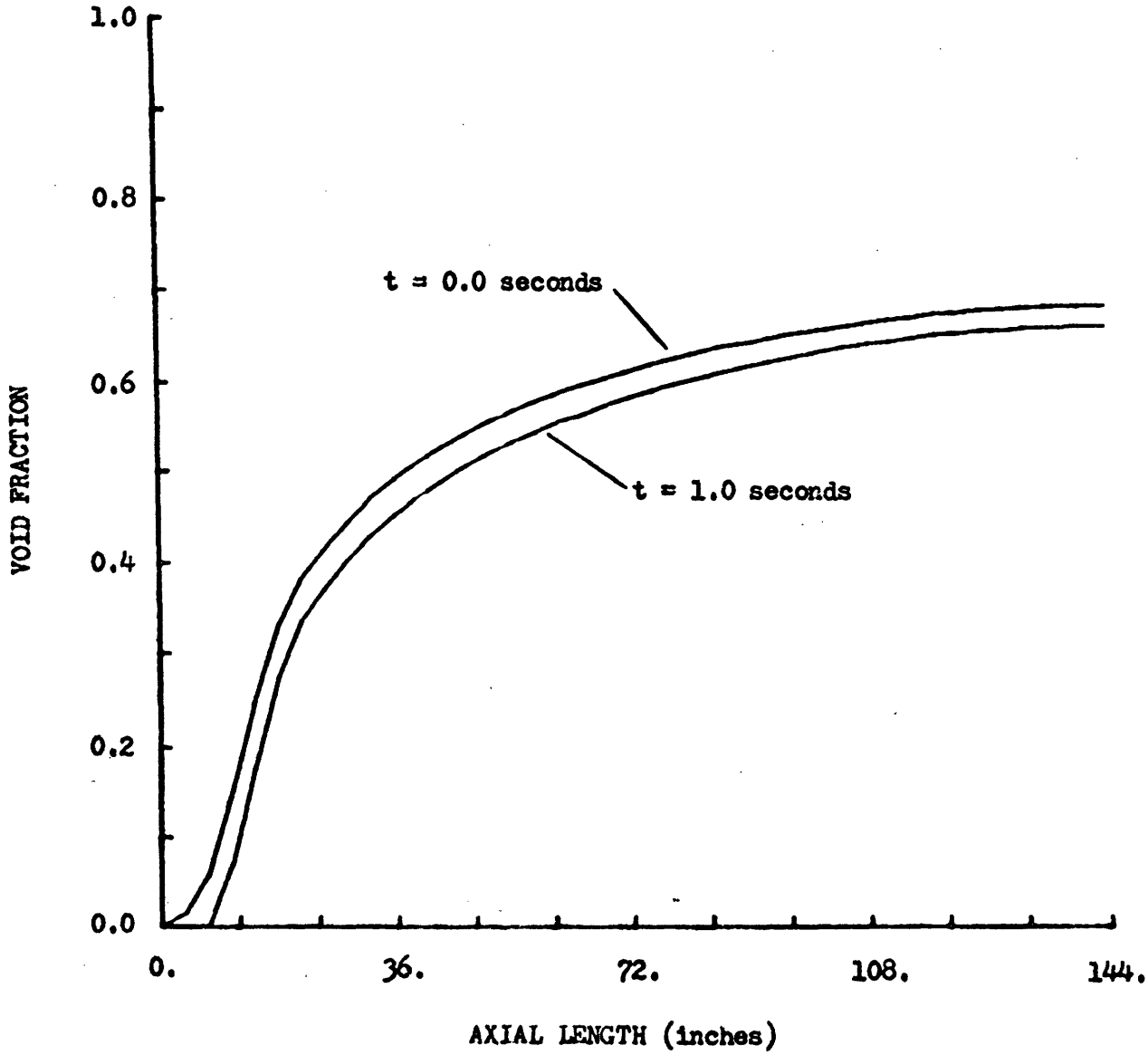

FIGURE 2.11

VOID FRACTION VERSUS AXIAL LENGTH

RESULTS FOR CASE A, CHANNEL 2

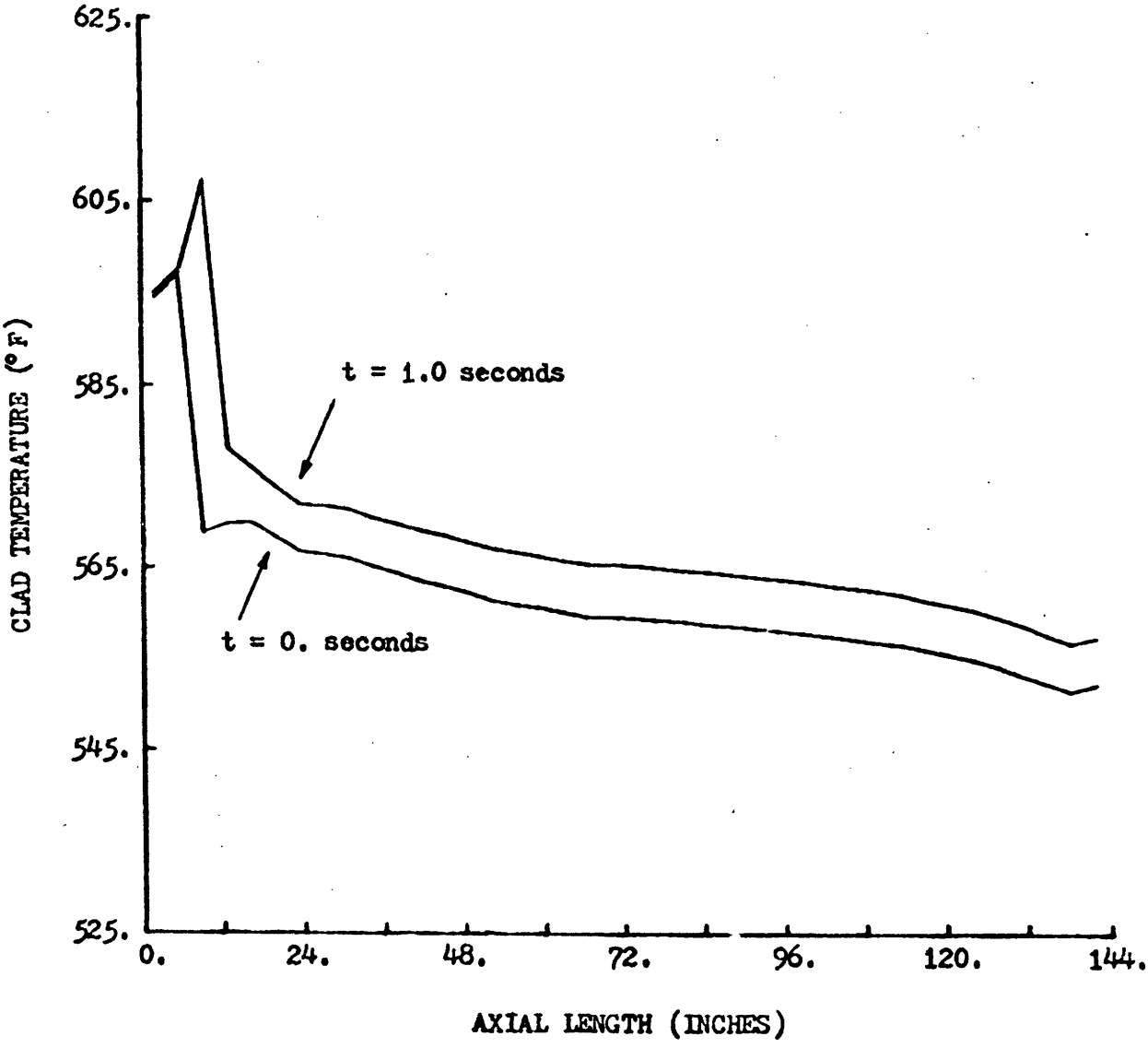

FIGURE 2.12

CLAD TEMPERATURE VERSUS AXIAL LENGTH

RESULTS FOR CASE A, ROD 4

the associated change in heat transfer correlation results in a large increase in clad temperature. As was seen in the steady-state analyses, the heat transfer logic dictates that the nucleate boiling correlation be used only if boiling has occurred. Application of this correlation results in a much higher heat transfer coefficient than would be predicted by the forced convection correlation. Hence, the large drop in the clad temperature indicates that boiling has begun. Since the pressurization tends to suppress boiling, the location along the channel where boiling begins moves toward the channel end. For example, the node, which was the first to boil at the start of the transient, does not have boiling in it later on in the transient. Consequently, the forced convection correlation is used instead of the nucleate boiling correlation and the temperature increases sharply.

A final observation, which is barely discernable, is that the clad temperatures in the first two nodes are lower at 1.0 seconds than they are at 0.0 seconds. This behavior is due to changes in the inlet flow rate. The inlet flow rate changes from one time step to the next in order to satisfy the boundary conditions. Since the forced convection correlation depends on the flow rate, a higher flow rate will lead to a higher heat transfer coefficient. The fluctuating heat transfer coefficient leads to changes in the clad temperature. This observation as well as the two others described above were typical of the clad temperature behavior in case A.

2.7.3 Results of Case B

In case B, the Levy model is not used and, therefore, the void fraction is zero until the equilibrium quality becomes greater than zero.

The void fraction distribution for channel 2 during the transient is shown in Figure 2.13. Once again, the increase in pressure during the transient causes boiling to begin further up the channel. Likewise, the magnitude of the void fraction is reduced at each location along the channel. These typical results were found in the other channels as well.

The clad temperature predictions for rod 4 are shown in Figure 2.14. The behavior of these predictions as a function of time are similar to those found in case A. First, it is seen that the predictions at 1.0 seconds are larger than those predicted in steady-state. This result is again due to the increased saturation temperature. Secondly, the shifting boiling front causes large differences between the predictions at 0. seconds and those at 1.0 seconds. These large differences occur in nodes which were boiling in steady-state, but which stop boiling as the pressure is increased. Again these differences can be attributed to the heat transfer coefficient which is used. Finally, small fluctuations in the clad temperature predictions at the beginning of the channel were observed. These fluctuations result from the changing inlet flow rate which directly influences the heat transfer coefficient. Results for the other rods exhibited similar behavior during the transient.

2.8 Discussion of Transient Results

The two transient cases analyzed can be used to illustrate the influence of the Levy model. The most obvious influence of this model is to increase the magnitude of the void fraction in the subcooled and initial part of the boiling regimes. As seen in Figure 2.15, the use of the Levy model predicts larger void fractions for the first third of the

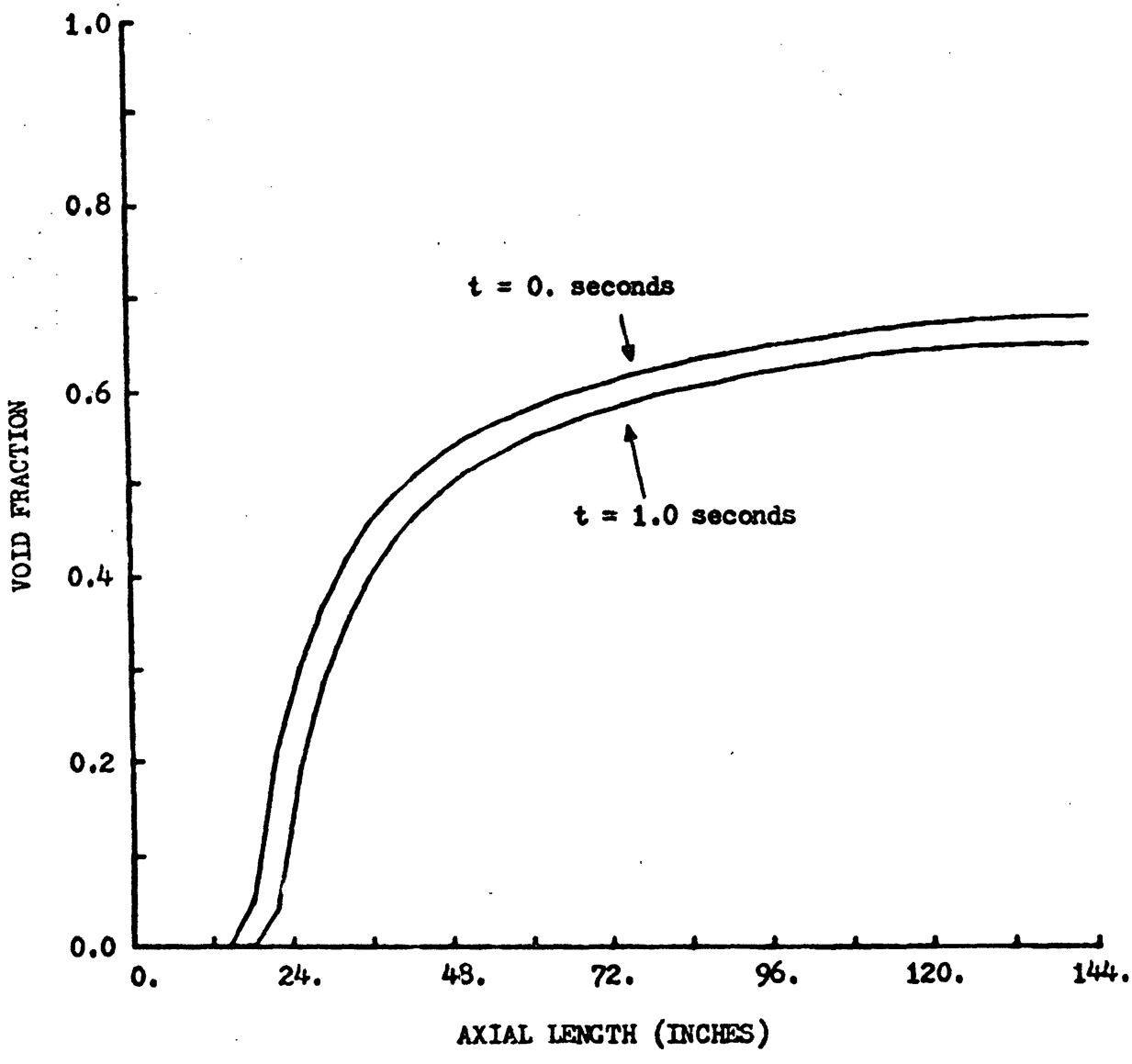

FIGURE 2.13

VOID FRACTION VERSUS AXIAL LENGTH

RESULTS FOR CASE B, CHANNEL 2

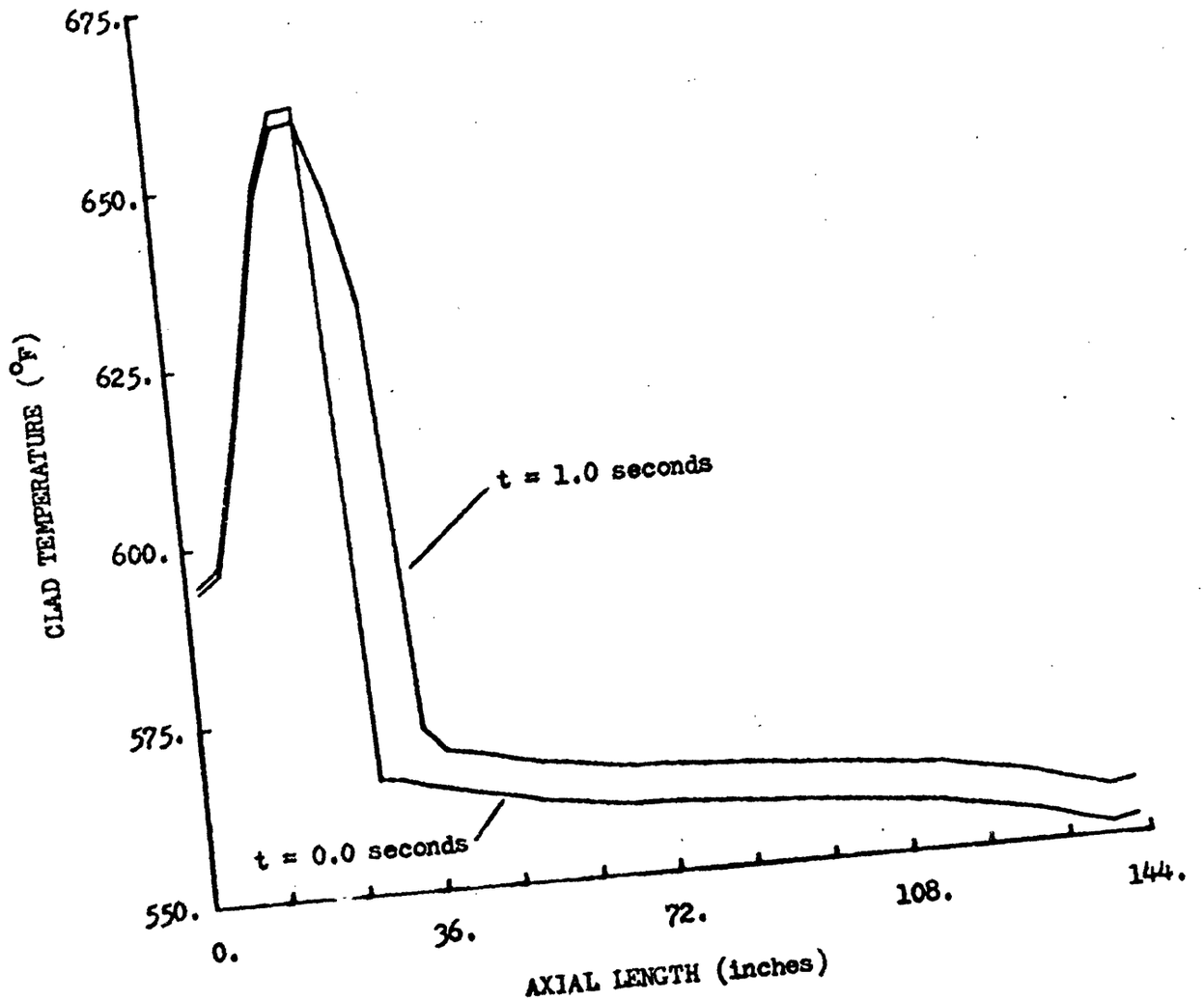

FIGURE 2.14

CLAD TEMPERATURE VERSUS AXIAL LENGTH

RESULTS FOR CASE B, ROD 4

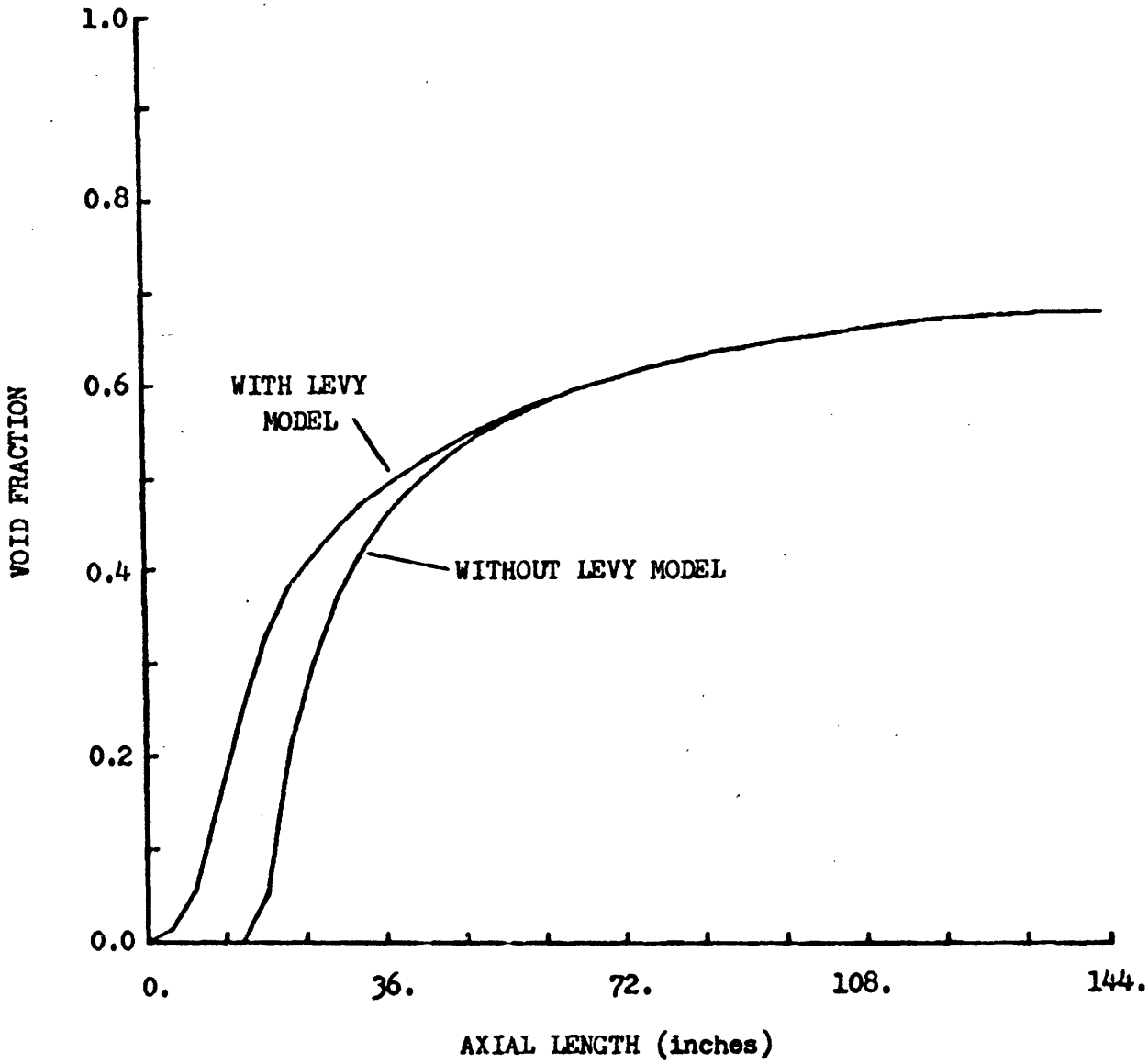

FIGURE 2.15

VOID FRACTION VERSUS AXIAL LENGTH

RESULTS AT 0.0 SECONDS FOR CHANNEL 2

channel. Also, the beginning of boiling is predicted to occur earlier. At the end of the transient, the relative differences between the two cases remain the same. Figure 2.16 illustrates the void fraction distribution at 1.0 seconds. The curves for both cases have decreased in magnitude and the start of boiling has shifted toward the top of the channel. However, the differences in the predictions of the two cases are unchanged.

Besides influencing the void fraction, the Levy model also has a large effect on the clad temperatures. Figure 2.17 shows the clad temperature predictions with and without the Levy model. Once again, the dramatic differences in these predictions are caused by the heat transfer logic. Since boiling begins near the inlet when the Levy model is used, the nucleate boiling correlation begins to be employed closer to the inlet for case A. In fact, case A applies the nucleate boiling correlation almost 12 inches earlier than case B. As was seen before, the large difference between the forced convection and nucleate boiling heat transfer coefficients leads to large differences in the clad temperature predictions.

A similar result occurs at the end of the transient. As illustrated in Figure 2.18, the temperatures are still significantly different in the subcooled boiling regime. The main difference between the results at the end of the transient and those at the start is that the temperature has increased sharply in a few positions. These increases occur in nodes which stop boiling during the course of the transient. As the pressure increases, some nodes stop boiling and, consequently, they begin to use a lower heat transfer coefficient. This switch in heat transfer coefficient begins to drive the clad temperature up, because the heat flux has not

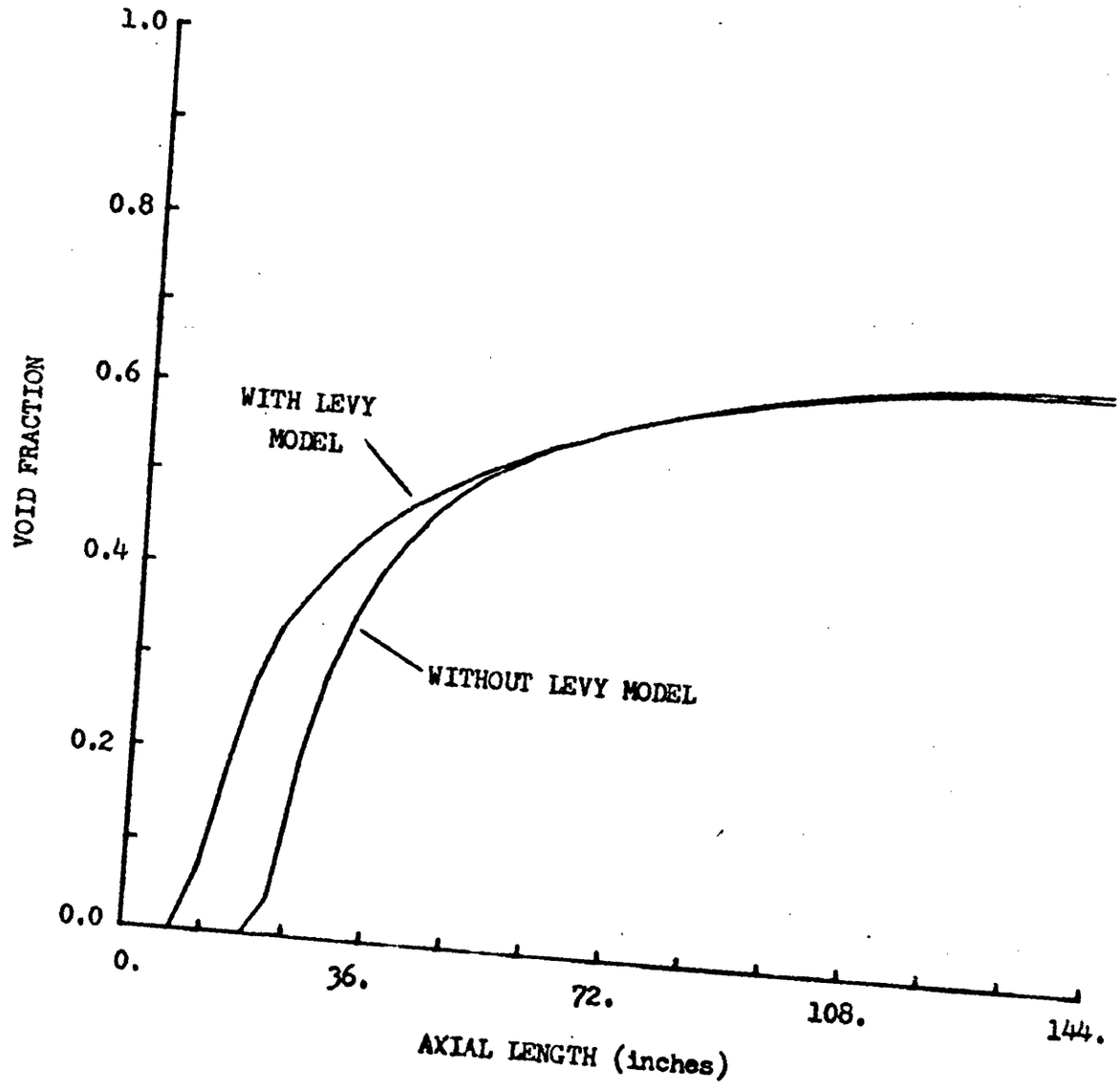

FIGURE 2.16

VOID FRACTION VERSUS AXIAL LENGTH

RESULTS AT 1.0 SECONDS FOR CHANNEL 2

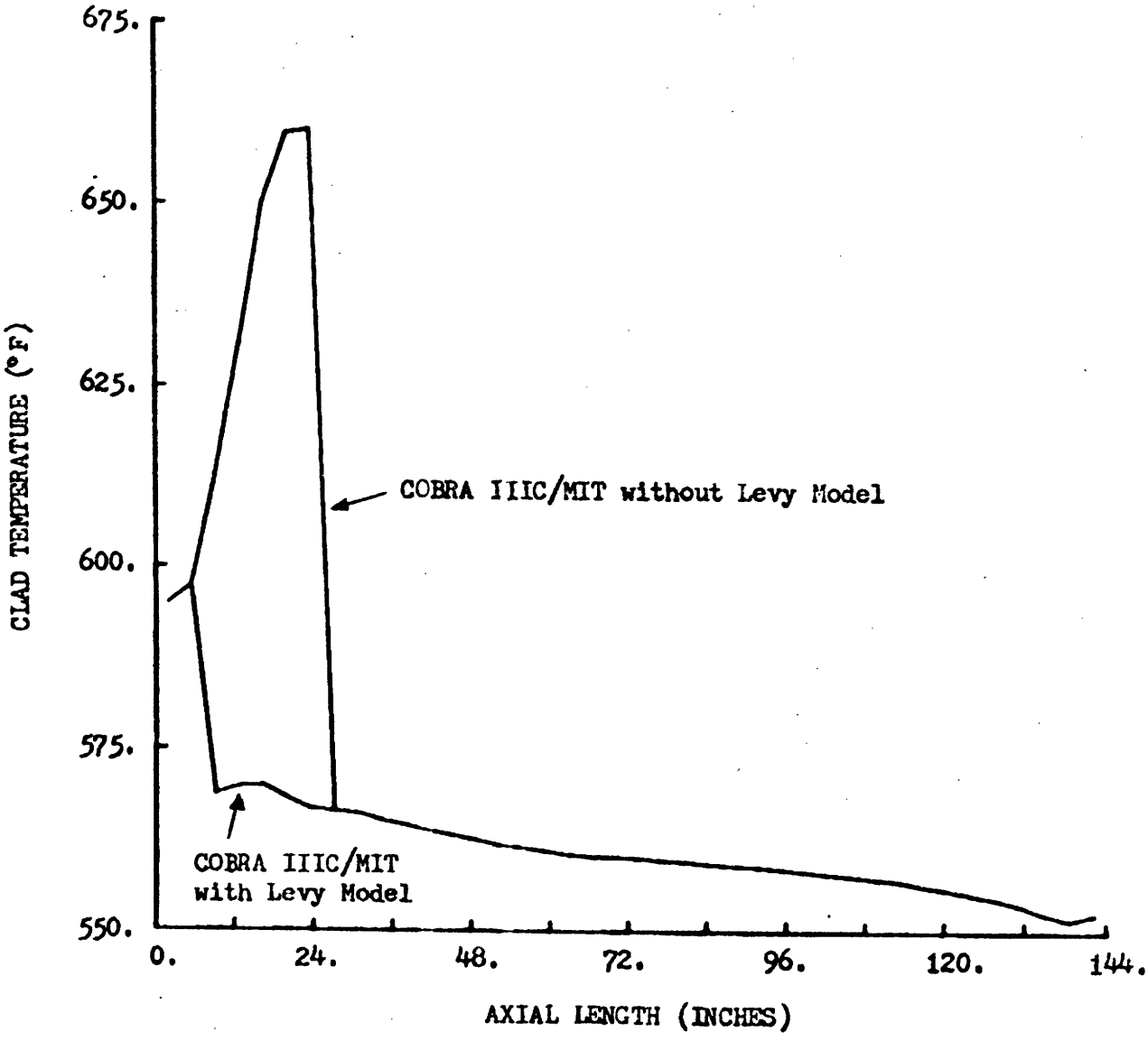

FIGURE 2.17

CLAD TEMPERATURE VERSUS AXIAL LENGTH

RESULTS AT 0.0 SECONDS FOR ROD 4

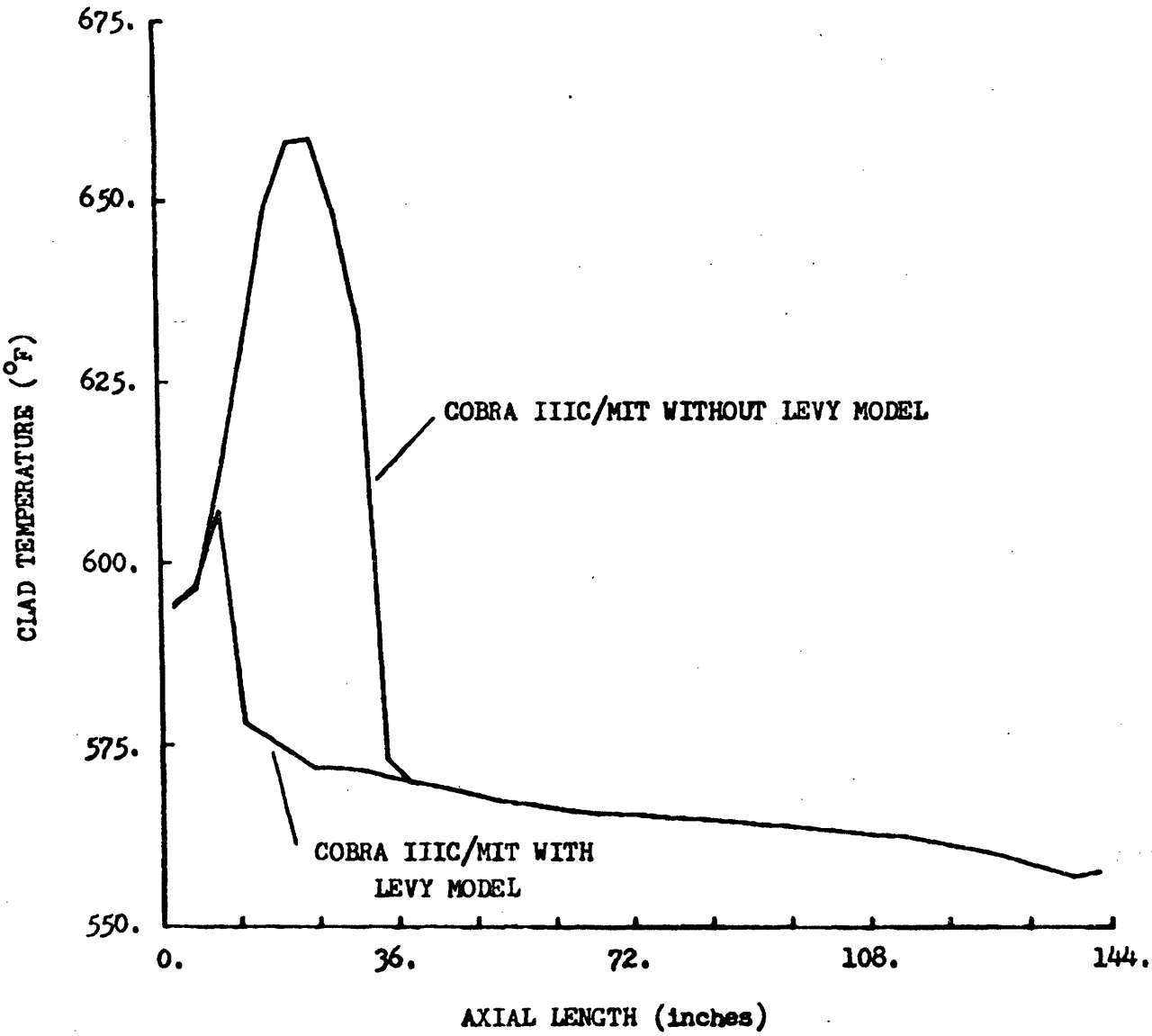

FIGURE 2.18

CLAD TEMPERATURE VERSUS AXIAL LENGTH

RESULTS AT 1.0 SECONDS FOR ROD 4

decreased.

2.8.1 Summary of Transient Results

The results of the transient analysis can be summarized as follows. First of all, it is found that the increase in pressure affects both the void fraction and clad temperature distributions. The start of boiling moves toward the exit and the magnitude of the void fraction is reduced. Clad temperatures in the boiling regime are increased due to the increase in saturation temperature. The movement of the boiling front also causes sharp increases in the clad temperature. A second result concerns the impact which the application of the Levy model has on the void fraction and clad temperature distributions. As would be anticipated, the case which uses the Levy model predicted higher values for the void fraction over much of the boiling length. The clad temperatures in the subcooled boiling regime are predicted to be smaller when the Levy model is applied since the start of boiling is predicted to occur earlier. Hence, both the use of Levy model and the increase in pressure influence the void fraction and clad temperature distributions.

2.9 Conclusions

The main intent of the investigations discussed in this chapter has been to evaluate BWR bundle analysis. In order to perform this evaluation, both COBRA IIIC/MIT and COBRA IV-I have been used. These codes are compared for various steady-state cases in an attempt to identify significant differences. Transient analysis has been performed with COBRA IIIC/MIT alone. From these investigations, a number of conclusions can be drawn.

First of all, the use of COBRA IV-I for steady-state analyses is deemed acceptable. With the boundary conditions obtained from COBRA IIIC/MIT, COBRA IV-I is able to adequately model the BWR bundles. The close agreement between the density and enthalpy predictions of the two codes verifies that COBRA IV-I could model ducted BWR bundles in steady-state.

A second conclusion is that the heat transfer calculations in COBRA IIIC/MIT are not adequate for the subcooled boiling regime. These inadequacies result from both a questionable logic system and an explicit energy equation. The logic used to determine the proper heat transfer coefficient is overly sensitive to boiling and does not take into account the amount of wall superheat (ie. $T_c - T_{sat}$). Consequently, when the Levy model is not used and there is no subcooled boiling, the clad temperature can be over 100 ^{o}F greater than the saturation temperature. With this much superheat, some boiling should occur and the nucleate boiling heat transfer correlation should be used even though boiling is not predicted. The temperature predictions should not be as sensitive as they are to the use of the Levy model. Therefore, a logic system similar to that used in COBRA IV-I, which is independent of the Levy model, should be implemented in COBRA IIIC/MIT. However, a new logic system alone is not sufficient to produce consistent heat transfer calculations. The explicit nature of the energy equations leads to an inconsistent set of heat transfer coefficients, heat fluxes and clad temperatures at each axial level. In particular, the heat transfer coefficient is based on information from the previous node. For example, if the power is increasing along the rod and subcooled boiling exists, then the predicted heat transfer coefficient will be lower than a

consistent value would be. It follows that with a lower heat transfer coefficient, higher clad temperatures will be predicted. A consistent heat transfer coefficient would improve the heat transfer calculations and a method for achieving this result should be implemented in COBRA IIIC/MIT. Hence, improvements in both the heat transfer logic and the procedure for calculating the heat transfer coefficient are required to improve the heat transfer calculations for subcooled boiling in COBRA IIIC/MIT.

Thirdly, although transient analyses have been performed with COBRA IIIC/MIT, further testing of this code for transient, BWR bundle analyses is required. The problems discovered while attempting to use this code illustrate the need for adequate testing of the code. No new problems were found, but it is possible that some difficulties might still occur.

A fourth conclusion is that, with the exception of the heat transfer calculations, COBRA IIIC/MIT could satisfactorily analyze a BWR pressurization transient. As would be expected, the increase in pressure leads to an increase in the saturation enthalpy and the void fraction is reduced. Due to the heat transfer dependence on boiling, the reduction in void fraction leads to increased clad temperatures in a few nodes. This result can be explained in terms of the heat transfer logic, but is probably not a realistic result. With improved heat transfer capabilities, the code should yield more realistic results for the parameters of interest.

Finally, the results indicate that the Levy model should be used in BWR bundle analyses. Although this model has little effect in the high void fraction regimes, it has a great influence in the subcooled regime. When this model is used, boiling is predicted to start earlier and the

magnitude of the void fraction is increased in the initial stages of boiling. These effects are very important for neutronic feedback calculations and should be accounted for in order to accurately analyze the BWR bundles.

CHAPTER 3

ANALYSES OF SEVERE POWER TRANSIENTS

3.1 Introduction

The thermal-hydraulic calculations in MEKIN (7) are performed using COBRA IIIC/MIT. Since MEKIN can be used to analyze very rapid power transients (eg. rod ejection accident), it is imperative that COBRA IIIC/MIT be able to analyze these transients. This requirement implies that COBRA IIIC/MIT must yield realistic results even when very small time steps (0.0025 seconds) are used. With very small time step sizes, rapid density changes can lead to convergence difficulties. For example, the sudden start of boiling during a rapid power transient can lead to large density changes which, in turn, cause large flow rate changes. Depending on the situation, the code may require a large number of iterations in order to converge. Alternatively, on some occasions the code may fail to converge. This latter characteristic is not desirable and the circumstances leading to its occurrence must be identified.

Therefore, in order to assess the applicability of COBRA IIIC/MIT, various severe power transients were investigated. These investigations involve using both COBRA IIIC/MIT and COBRA IV-I. Comparisons between the two codes are made for the various cases. Since COBRA IV-I contains two distinct solution methods, some comparisons are made between COBRA IIIC/MIT and the implicit method of COBRA IV-I, while others are made between COBRA IIIC/MIT and the explicit method of COBRA IV-I. Through comparisons of the results, differences in the two codes are identified.

For example, although both COBRA IIIC/MIT and the implicit solution method of COBRA IV-I are similar in many regards, they do differ in their

energy equations and heat transfer packages. These differences become apparent when the results are compared. On the other hand, the explicit solution method is inherently much different from that in COBRA IIIC/MIT. Hence, comparisons between these latter two methods should reflect the differences between these methods. Another use of these comparisons is to evaluate the adequacy of COBRA IIIC/MIT. The improvements in the energy equation and the addition of the explicit solution method make COBRA IV-I better suited to handle severe transients. Consequently, it is possible to determine whether or not COBRA IIIC/MIT is predicting realistic results in severe power transients through comparisons with COBRA IV-I.

3.2 Modeling Sequence

The transients discussed in this chapter are simulated rod ejection transients. The main characteristic of this type of transient is a large power increase during a very small time period. For example, the power can increase from a zero power condition to 10 times its full power value in less than 0.1 seconds. These transients are called power transients, since the rapid power increase and subsequent decrease drives the thermal-hydraulic calculations during the transient. Hence, the use of simulated rod ejection transients permits the performances of COBRA IIIC/MIT and COBRA IV-I to be evaluated for these severe power transients.

The modeling used in these power transients can be divided into three parts. The first part involves the geometrical layout of the channels. This layout includes such specifications as channel area and length, rod dimensions, and other parameters relevent to the geometry. The second part involves the selection of the thermal-hydraulic models used

in the analysis. For example, the use of the Levy model or some mixing correlation may be specified. Finally, the third part involves the operating conditions and transient forcing functions. In this part, various operating conditions are specified as well as any changes in these conditions as a function of time. A complete description of the modeling used in each case can be found in Appendix B and a brief description follows.

The geometrical layout is the same for all transient cases. Two channels are used with each representing a part length 14 x 14 PWR fuel assembly. Typical values are used for the flow area, rod dimensions, fuel parameters, and gap size. The total length of each channel is 59.2 inches (150 cm). This small section is used so that a power history could be determined in an economical way with MEKIN. Each channel is divided into 5 axial nodes which result in node sizes of 11.84 inches (30 cm).

The thermal-hydraulic models are essentially the same in each case. The only exception is whether or not the Levy model is used. In cases comparing COBRA IIIC/MIT and the explicit method of COBRA IV-I, the Levy model is not used. The reason for not using this model is that it cannot be applied with the explicit method of COBRA IV-I, because the equations in this method are solved assuming a homogenous equilibrium model and this assumption precludes the use of the Levy model. In cases comparing COBRA IIIC/MIT with the implicit method, the Levy model is always used. The other thermal-hydraulic models which are applied are described in Appendix B.

The operational conditions and transient forcing functions for the various cases are nearly identical. Each case uses an inlet temperature

of 635 ^{o}F and a reference pressure of 2100 psia. Cases 1 thru 3 use an inlet mass flux of 2.48 Mlb/hr/ft^2 and an average heat flux of 10 Btu/hr/ft^2. Case 4 uses an inlet flux of .25 Mlb/hr/ft^2 and an average heat flux of 1000 Btu/hr/ft^2. These input data are summarized in Table 3.1. All cases employ a uniform axial power distribution and peaking factor of 1.52 and .48 in channels 1 and 2, respectively. The power forcing function is also the same for all cases. Hence, except for case 4, the operational conditions are identical.

3.3 Results for Case 1

The first case is analyzed with the original version of COBRA IIIC/MIT. This version does not contain the corrections suggested in Chapter 2. Using this version, with the Levy model included, the power transient was run. The initital run used a time step size of 0.01 seconds. It worked successfully although some curious results occur once boiling starts. These results include large increases in both the flow rate and pressure drop. A second phase of the investigation was an attempt to analyze the transient with time step sizes of 0.0025 seconds. This run failed to converge at the point where boiling started. After a thorough investigation, the cause of the failure and a solution for it have been found. This problem and its solution as well as the results with a time step size of 0.01 seconds are discussed below.

3.3.1 Initial Results

The initial results of this case were obtained using a time step size of 0.01 seconds. The transient was run and it is found that subcooled boiling begins at 0.12 seconds in channel 1. Once boiling begins, the

TABLE 3.1

SUMMARY OF INPUT DATA

Case	T_{in} (°F)	P_{ref} (psia)	G_{in} (Mlb/hr-ft^2)	q" (Btu/hr-ft^2)	Levy Model
1	635	2100	2.48	10	yes
2	635	2100	2.48	10	yes
3	635	2100	2.48	10	no
4	635	2100	0.25	1000	no

mass flow rate and pressure drop increase sharply. As illustrated in Figure 3.1, the exit mass flow rate increases significantly at the start of boiling. After a few time steps, the flow rate has decreased to a value near its pre-boiling value. The transient behavior of the pressure drop in channel 1 is shown in Figure 3.2. The pressure drop increases at the point of boiling, but becomes negative on the next time step. Eventually, it returns to its pre-boiling value. Hence, both the flow rate and pressure drop experience sharp increases at the point of boiling, but after a few time steps they return to their pre-boiling value.

The reason for this behavior can be understood by examining the transient behavior of the density. As seen in Figure 3.3, the channel exit density decreases discontinuously at the start of boiling. This large density change is then used to calculate the flow rate through the continuity equation:

$$m_j = m_{j-1} - \Delta x A \Delta \rho / \Delta t - w \Delta x. \qquad (3.1)$$

Although the crossflow, w, does increase at the start of boiling, the density gradient, $\Delta \rho / \Delta t$, is so large that the flow is accelerated. (note that $\Delta \rho / \Delta t$ is negative). This acceleration results in the large flow rate increase.

After boiling has started, the density does not change by large amounts during the transient. This result leads to a reduced density gradient and the flow rate stabilizes. Consequently, the flow rate returns to its pre-boiling value.

Once the flow rate is calculated, the pressure drop is computed using

$$P_j - P_{j-1} = a' \Delta x - \frac{\Delta x}{A} \frac{\Delta m}{\Delta t} + 2u \frac{\Delta \rho \Delta x}{\Delta t} + \frac{uw \Delta x}{A}. \qquad (3.2)$$

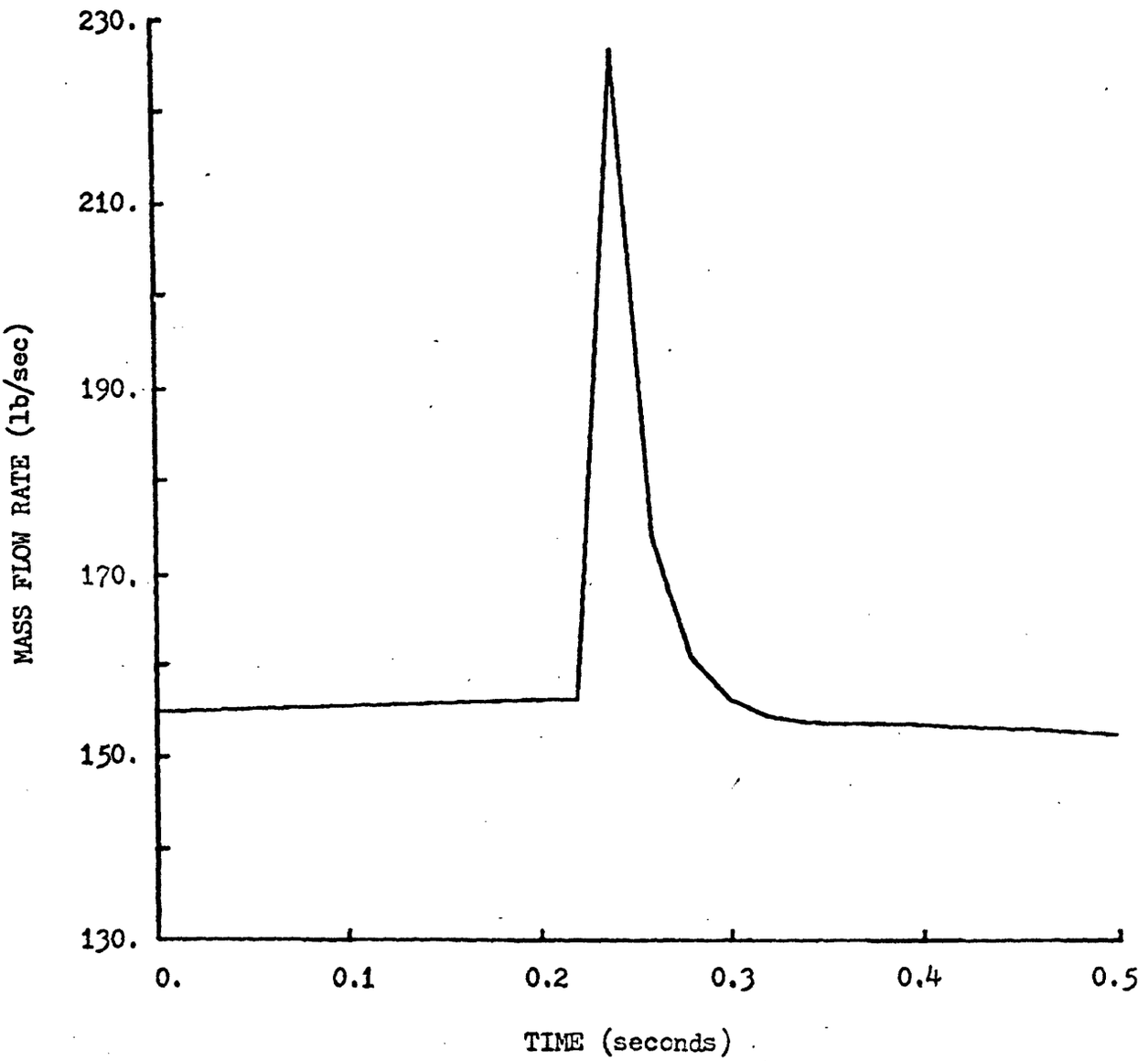

FIGURE 3.1

EXIT MASS FLOW RATE VERSUS TIME

RESULTS FOR CASE 1, CHANNEL 1

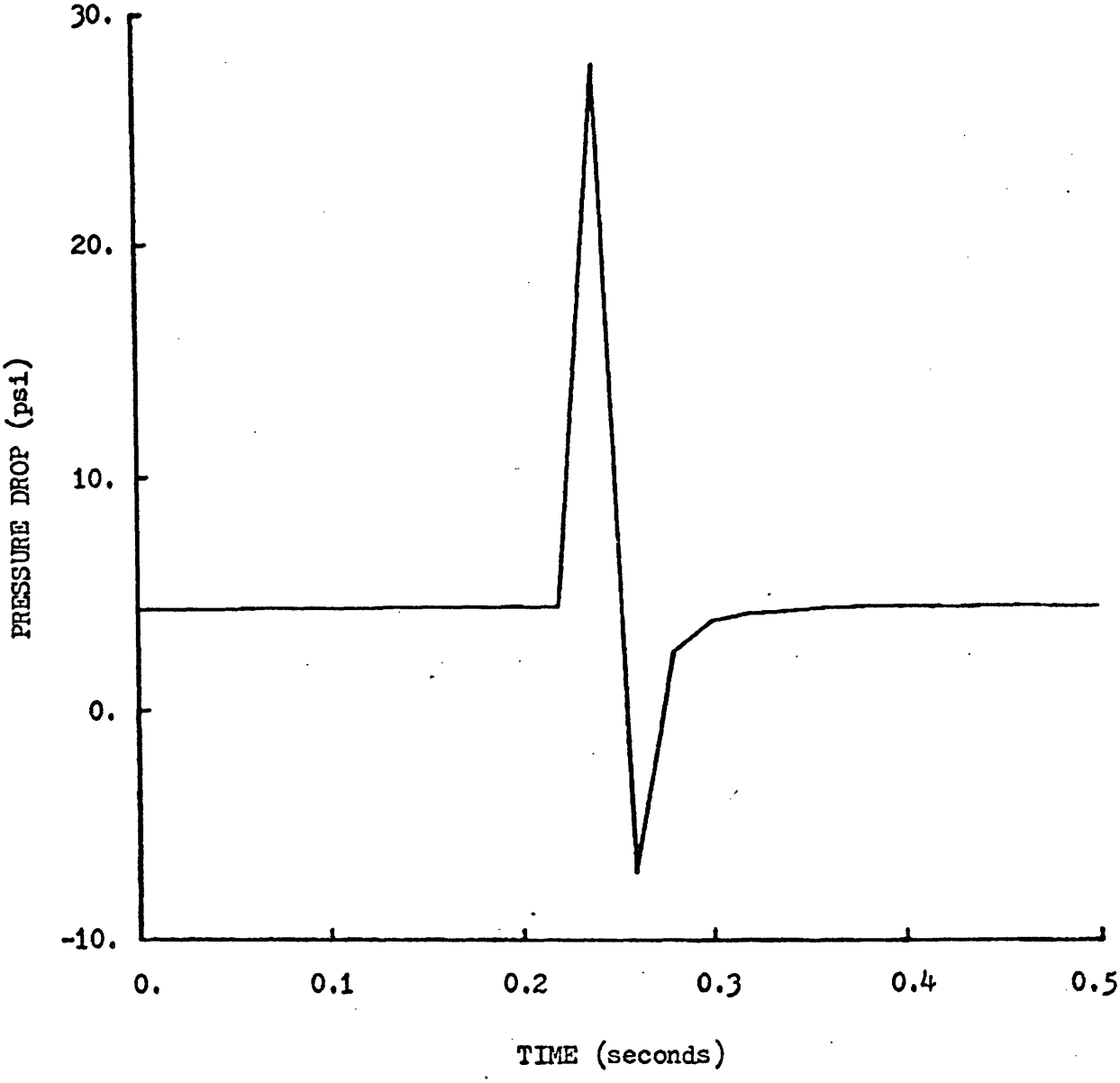

FIGURE 3.2

PRESSURE DROP VERSUS TIME

RESULTS FOR CASE 1, CHANNEL 1

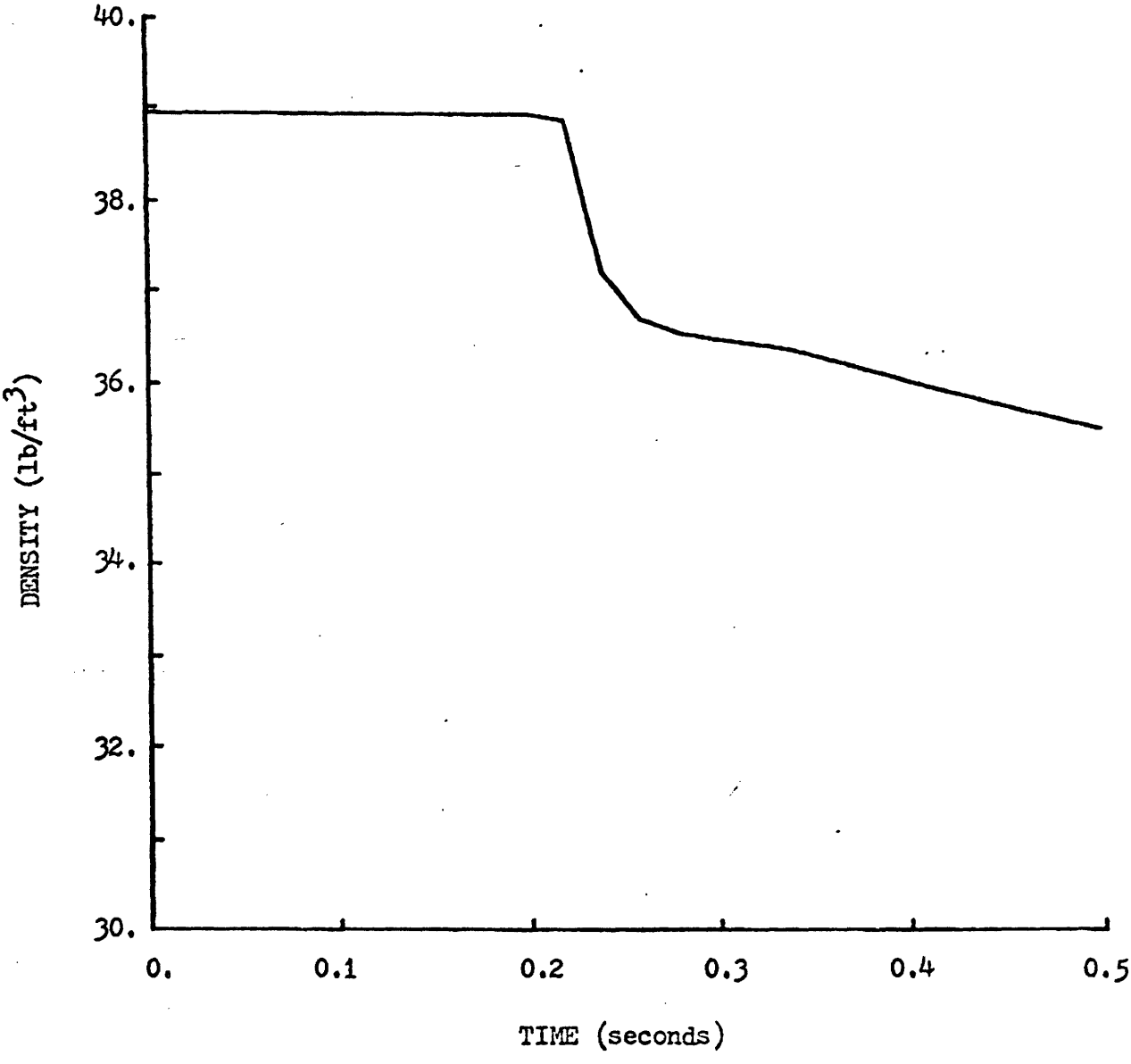

FIGURE 3.3

EXIT DENSITY VERSUS TIME

RESULTS FOR CASE 1, CHANNEL 1

When the density is changing slowly, the $a'\Delta x$ term is the largest term on the right hand side of this equation. The term, a', is always negative and varies slowly as a function of time. If the density decreases abruptly, the flow rate will increase sharply. These two effects cause the second and third term of equation 3.2 to be negative and large in magnitude. Consequently, the pressure drop will increase sharply.

On the next time step, the flow rate has decreased due to the lower density gradient. The decrease in flow rate is large enough to cause the right hand side of equation 3.2 to be positive. This result means that the pressure drop is negative. After the flow rate stabilizes, the pressure drop returns to its pre-boiling value. Hence, the rapid density change, caused by the start of boiling, can explain the observed increases in the flow rate and pressure drop.

3.3.2 Discussion of the Code Failure

When this case was run with a time step size of 0.0025 seconds, it was found that the code failed to converge at the point when boiling started. As is found in the above case, the start of boiling causes the pressure drop and flow rate to increase sharply. However, the code is unable to converge even after 100 iterations. This behavior was deemed unacceptable and an investigation into the breakdown was initiated.

The initial phase of this investigation examines the influence of both small time step sizes and the application of the Levy model on the results. Even though the code converges when time step sizes greater than 0.0025 seconds are used, both the flow rate and pressure drop increase at the start of boiling. The amount of these increases depends on the time step size used; the smaller the time step size, the larger

the increase. For example, with a time step size of 0.01 seconds the flow rate increases by 70 lb/sec, while with a time step size of 0.0025 seconds the flow rate increases by 156 lb/sec. These differences are a consequence of the fact that at the start of boiling the density decreases by an amount which is independent of time step size. Hence, the magnitude of the density gradient would depend only on the time step size and the increases in the flow rate and pressure drop would be larger when smaller time step sizes are used.

When Levy's model is not used, no large increases in the flow rate or pressure drop occur even at the point where saturated boiling begins. Apparently, the density decrease is not as large when saturated boiling begins as that which occurs when subcooled boiling begins. The smaller density gradient does not lead to large increases in flow rate and pressure drop. Hence, the density gradient, which influences the flow rate and pressure drop, is a strong function of the time step size and the application of the Levy model.

The next phase of the investigation reviews the procedure for calculating the density. For a particular node in a channel, the method for computing the density depends on whether or not the fluid in the node boils. If boiling is not present, then the density would be set equal to the inverse of the specific volume which would correspond to the value of the enthalpy in the node. If boiling is present, then the density would be calculated using

$$\rho = \rho_f(1 - \alpha) + \rho_g \alpha. \qquad (3.3)$$

The void fraction, α, is calculated with a user-specified correlation and is strongly dependent on the quality. Since the density depends on

the void fraction, the quality is important for the density calculation.

The calculation of the quality can be done in one of two ways. The first method does not include the effect of subcooled boiling and simply uses the thermodynamic equilibrium quality. If this method is used, the quality is only a function of the enthalpy. The second method does include the effect of subcooled boiling through its application of the Levy model. When the Levy model is used, the quality is a function of the flow rate, the heat flux, and the enthalpy. Hence, if the second method is used, the coupling among the various variables is tightened.

The third phase of the investigation examines the actual cause of the failure. At the point where boiling starts the code fails to converge. Since the convergence criterion is based on the flow rate, the value of the flow rate on each iteration is studied. As illustrated in Figure 3.4, the flow rate oscillates between two values and is unable to converge. A careful review of the results shows that, after a few iterations, two different solutions are obtained and the code oscillates between them.

This oscillatory behavior results from the first node in channel 1 having a positive quality only on odd numbered iterations. On even numbered iterations, the quality in this node is zero. This behavior is seen in Figure 3.5. When the quality is positive, a higher flow rate is predicted as compared to that predicted when the quality is zero. The flow is predicted to be higher because a positive quality results in a larger density decrease. Hence, the prediction of a positive quality on alternate iterations leads to the oscillatory flow rate.

The prediction of a positive quality on alternate iterations is a result of the coupling between the flow rate, density and quality. On

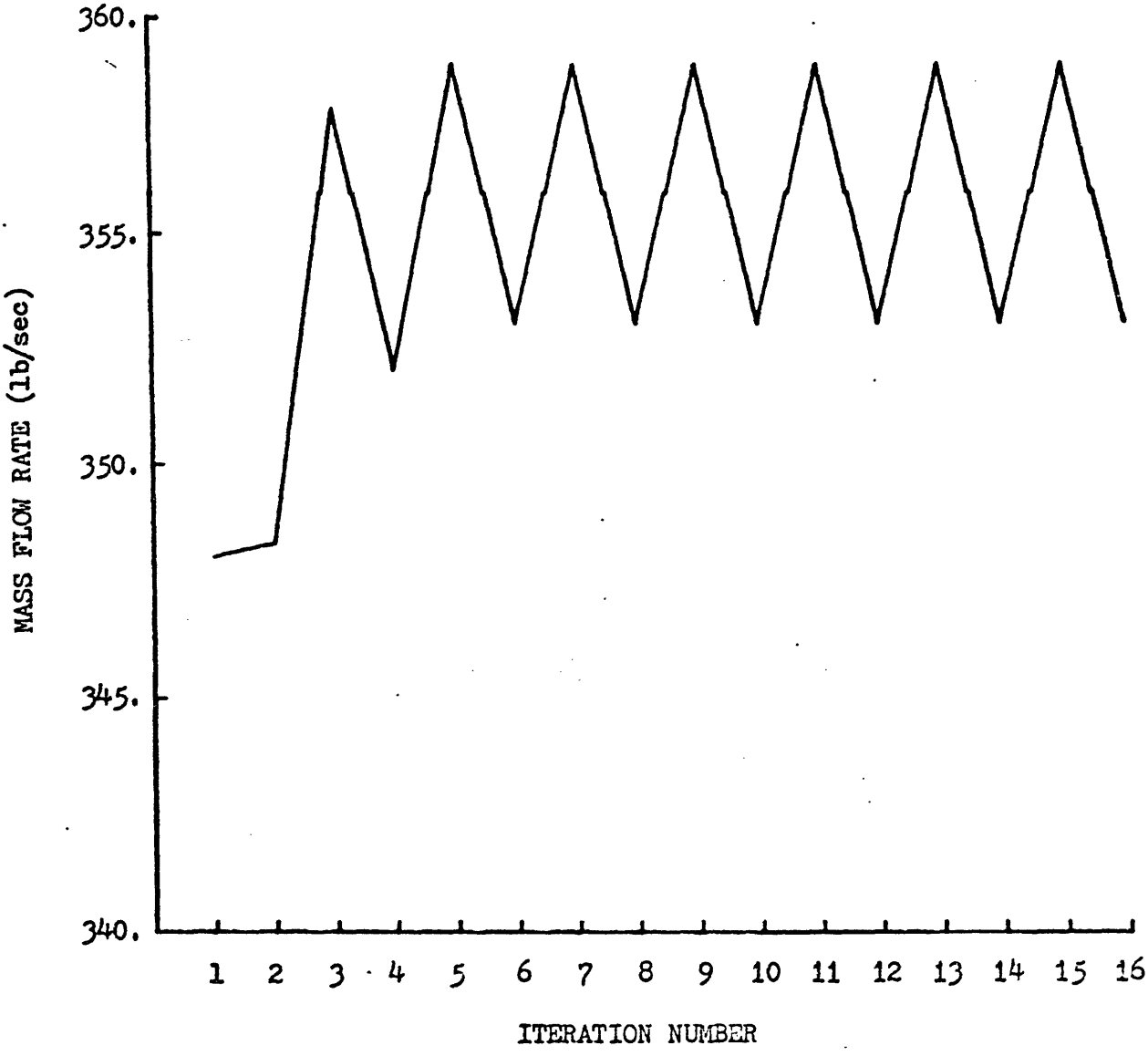

FIGURE 3.4

MASS FLOW RATE VERSUS ITERATION NUMBER

AT TIME OF BREAKDOWN

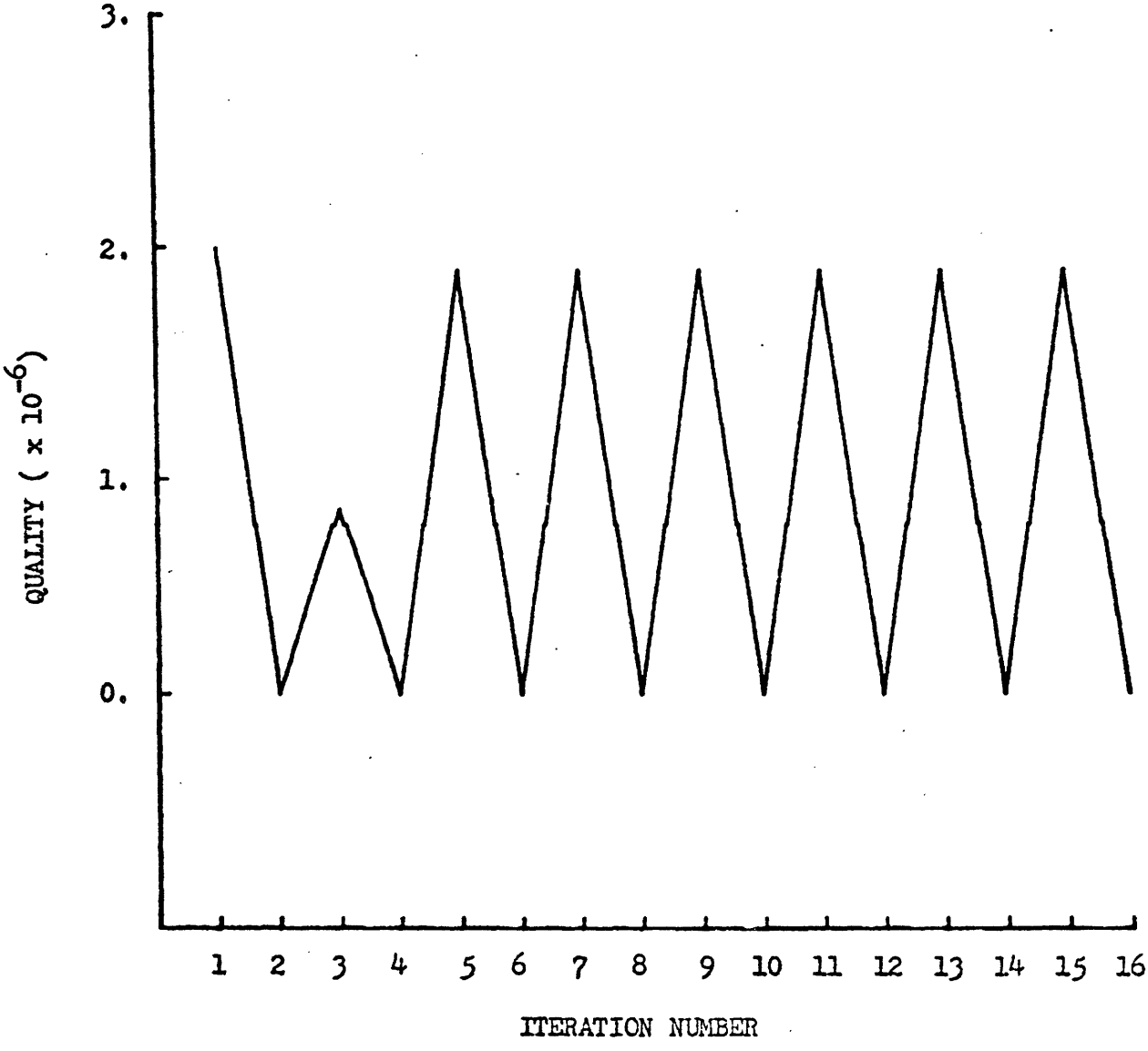

FIGURE 3.5

QUALITY VERSUS ITERATION NUMBER

AT TIME OF BREAKDOWN

the first iteration, a positive quality is predicted for the first node in channel 1. This positive quality leads to a decrease in the density which, in turn, causes a flow rate increase. On the second iteration, the increased flow rate is sufficiently high to prevent the prediction of a positive quality. Consequently, the density is higher than it was on the first iteration and the new flow rate is lower. On the third iteration, the lower flow rate results in a positive quality and the flow rate increases for this iteration. With this higher flow rate, the quality on the fourth iteration is zero again. This behavior is repeated and the code oscillates between two solutions.

3.3.3 Solution of the Code Failure

Once the problem had been identified, it was necessary to find a solution. Only physical solutions are examined so that the solution will be valid for all cases using the Levy model. The problem arises because the prediction of a positive quality results in a large flow rate increase. The large flow rate, in turn, results in a zero quality on the next iteration. Hence, the problem could be viewed in one of two ways. The first would concern the reasons why the prediction of a positive quality leads to such a large increase in the flow rate. And the second would concern the actual calculation of the quality with the Levy model.

As is seen above, the prediction of a positive quality leads to a density decrease which, in turn, results in a flow rate increase. The amount of this density decrease is especially large when subcooled boiling occurs because the pre-boiling density is much higher than the fluid saturation density. Once the quality is positive, the density is calculated using equation 3.3. However, as pointed out by Sliz (26), the

calculation of the density with this equation in the subcooled boiling regime is not exactly correct. The fluid is still subcooled and, consequently, the subcooled fluid density should be used instead of the saturated fluid density. This correction reduces the density discontinuity at the point where boiling begins. Accordingly, the flow rate should not increase as much as it had previously. If the flow rate increase were reduced, the quality on the second iteration might remain positive which could lead to convergence.

This correction is implemented by making changes in subroutine VOID and a listing of this subroutine is in Appendix C. The code was rerun with this correction, but again it fails to converge. Apparently, the reduction in the flow rate increase is not enough to eliminate the oscillations. Even though this correction does not solve the problem, the density calculation is improved and this correction should be used in the code.

After correcting the density calculation, the Levy model was examined in order to find a method for eliminating the oscillations. During this examination, two inconsistencies were found in the code's usage of the Levy model. The first inconsistency involves the evaluation of the fluid properties in the model. In Levy's original paper (22) the properties are evaluated at the saturation temperature. However, the code was evaluating these properties at the subcooled temperature. In order to eliminate this problem, subroutine SCQUAL was changed so that the properties in the Levy model would be evaluated at the saturation temperature. The second inconsistency involves the heat transfer coefficient which is used in the model. The model should use the Dittus-Boelter correlation to calculate the heat transfer coefficient. However, the Thom correlation

was being used. Once again this inconsistency was corrected by making changes in subroutine SCQUAL. Unfortunately, the correction of these inconsistencies did not eliminate the breakdown.

Hence, the problem of the oscillatory quality predictions remained. Physically, if a positive quality is predicted for a particular node at a particular point in time, then the iterative flow redistribution should not eliminate this positive quality. Furthermore, if the quality is prevented from oscillating, then the solution could converge. Hence, a correction was found which prevents the quality from beccming zero once is has been predicted to be positive in a particular node. This correction is implemented in subroutine SCQUAL which is listed in Appendix C.

The way in which this correction works can be described as follows. On the first iteration, the quality in each node is calculated and these values are stored in a new array, DATA($XPOLD+I+MC*(J-1)). Then, on the second iteration, the quality is recalculated. A damping scheme uses the present iteration value and the previous iteration value to calculate the new quality. As implemented now, 99% of the present iteration value is added to 1% of the previous iteration value. Consequently, if a positive quality is predicted on the first iteration, then the quality calculated on the second iteration will be at least 1% of the first iteration value. The iterative procedure continues by storing the new qualities in the DATA array. Note that once a quality is predicted to be positive it will remain positive during the iterative procedure.

With this solution, the code is able to converge at all times during the transient. Hence, the elimination of the oscillatory quality predictions allows the code to converge. In order to observe the effect of this correction, the case which uses a time step size of 0.01 seconds

was rerun. No significant changes in the results are observed when this corrected version of the code is used. Hence, this correction is deemed an acceptable solution to the non-convergence problem.

3.3.4 Summary

The results of this first case indicate that, at the start of subcooled boiling, COBRA IIIC/MIT experiences difficulties when small time step sizes are used. The large density drop, associated with the start of boiling, leads to large increases in the flow rate. When a time step size of 0.01 seconds is used, the code is able to converge, even though large increases in the flow rate occur. However, the large increases in the flow rate cause oscillations in the results when a time step size of 0.0025 seconds is used. These oscillations prevent the code from converging. This oscillatory behavior has been investigated and a number of corrections are implemented into the code in order to eliminate this behavior and allow convergence.

The first correction changes the method for calculating the density when subcooled boiling occurs. The fluid saturation density, ρ_f, in equation 3.3 is replaced with the subcooled fluid density. This correction is based on the physical fact that when subcooled boiling occurs, the fluid is still subcooled rather than being saturated. It should also be noted that the two-phase specific volume calculation is changed for the same reason.

The second correction changes the method for evaluating variables used in the Levy model. Specifically, the fluid properties and heat transfer coefficient were not being evaluated as suggested in Levy's paper. These inconsistencies do not affect the oscillatory behavior,

but are corrected so that the Levy model would be consistent.

The final correction is the insertion of a damping scheme in the Levy model. This scheme eliminates the oscillations by insuring that once a positive quality is predicted that it would not become zero on subsequent iterations. In order to implement this correction, a new variable, DATA($XPOLD+I+MC*(J-1)) is added to store the values of the qualities for all nodes. The use of this new variable requires changes in subroutines CORE and BLOCK DATA so that it would be properly dimensioned. These two subroutines are listed in Appendix C.

With these corrections implemented, the code is able to converge when small time step sizes are used. This solution is considered to be satisfactory for this problem since it both eliminates the problem and has a physical basis. Hence, with the corrected code, it is now possible to make comparisons with COBRA IV-I.

3.4 Case 2 Results

The corrections discussed in Sections 2.6 and 3.3 were incorporated into COBRA IIIC/MIT so that the severe power transient could be analyzed. Since the intent of this analysis is to compare COBRA IIIC/MIT with COBRA IV-I, the implicit method of COBRA IV-I is initially used to analyze this transient. Unfortunately, COBRA IV-I developed oscillations at the point when boiling begins. These oscillations are similar to those found in COBRA IIIC/MIT. Consequently, subroutines SCQUAL and VOID were changed using the same corrections used for COBRA IIIC/MIT. With these corrections, COBRA IV-I is able to successfully analyze the transient. These corrections and a listing of subroutines VOID and SCQUAL can be found in Appendix D.

With both codes corrected so that they could analyze the severe power transient, comparisons of their results are performed. Throughout this analysis a time step size of 0.0025 seconds is used. Comparisons of the heat transfer and void fraction predictions are used to determine whether or not the improved energy equation and heat transfer package in COBRA IV-I are actually necessary for this type of transient. Consequently, the clad temperature and void fraction predictions are the primary variables which are compared.

3.4.1 Discussion

As was found in the BWR analysis, the clad temperature predictions between the two codes are different. Figure 3.6 shows the maximum clad temperatures differ by as much as 10 ^{o}F during the transient. This difference is not as great as those seen in the BWR cases, but could again be explained in terms of the different heat transfer logic. The COBRA IV-I predictions never exceed the fluid saturation temperature by more than 5 ^{o}F, because this code's logic system is based on the value of the clad temperature. On the other hand, the COBRA IIIC/MIT predictions do exceed the saturation temperature by up to 10 ^{o}F since this code's logic system is based on the quality.

As a further illustration of the clad temperature predictions, Figure 3.7 shows the axial clad temperature distributions for both codes at two times during the transient. The COBRA IV-I predictions are consistently uniform indicating that the Thom nucleate boiling correlation is used along the entire rod. The COBRA IIIC/MIT predictions are uniform just prior to the start of the boiling, but change significantly once boiling is initiated. Before the start of boiling, the Thom forced

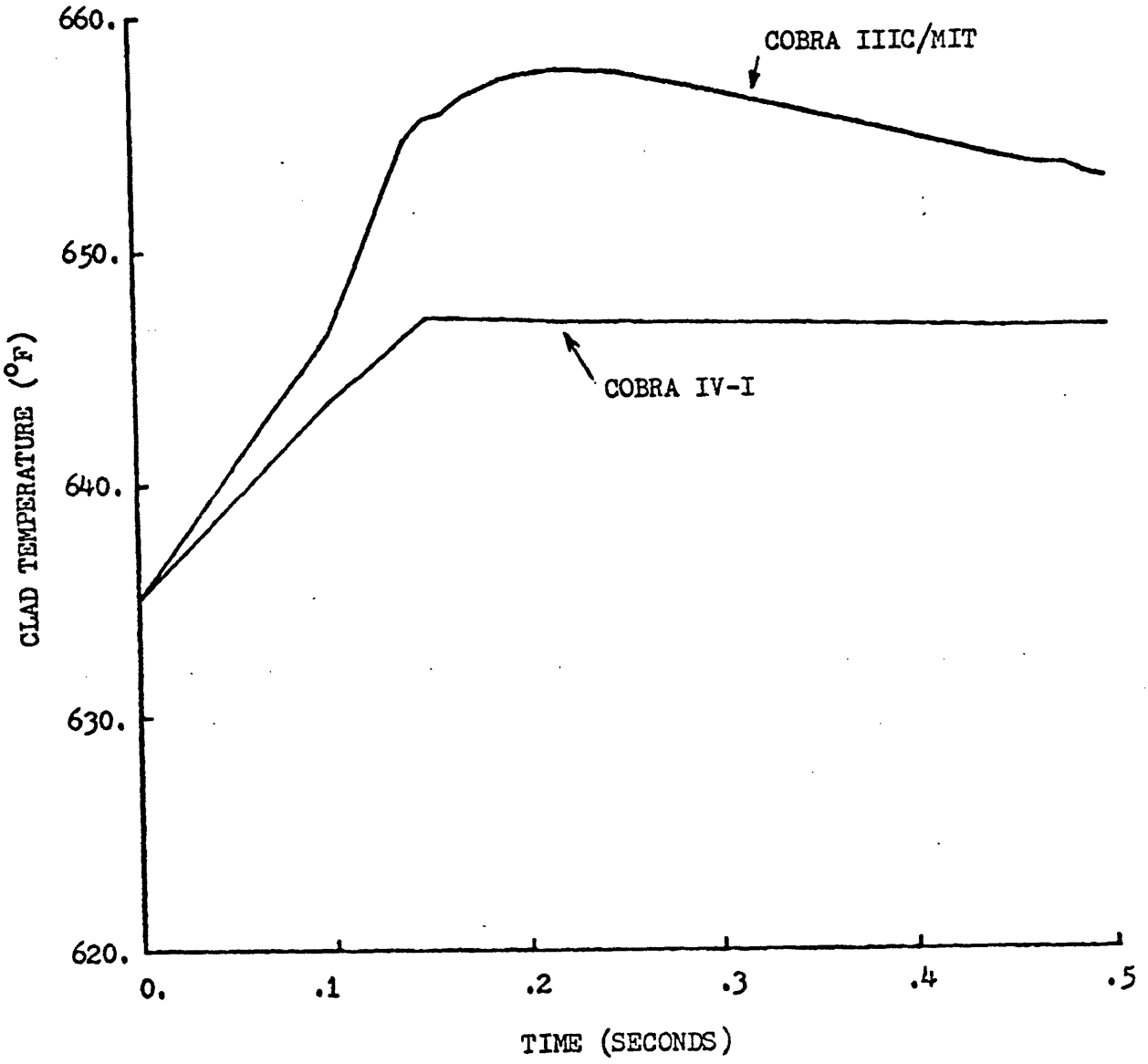

FIGURE 3.6

MAXIMUM CLAD TEMPERATURE VERSUS TIME

RESULTS FOR CASE 2

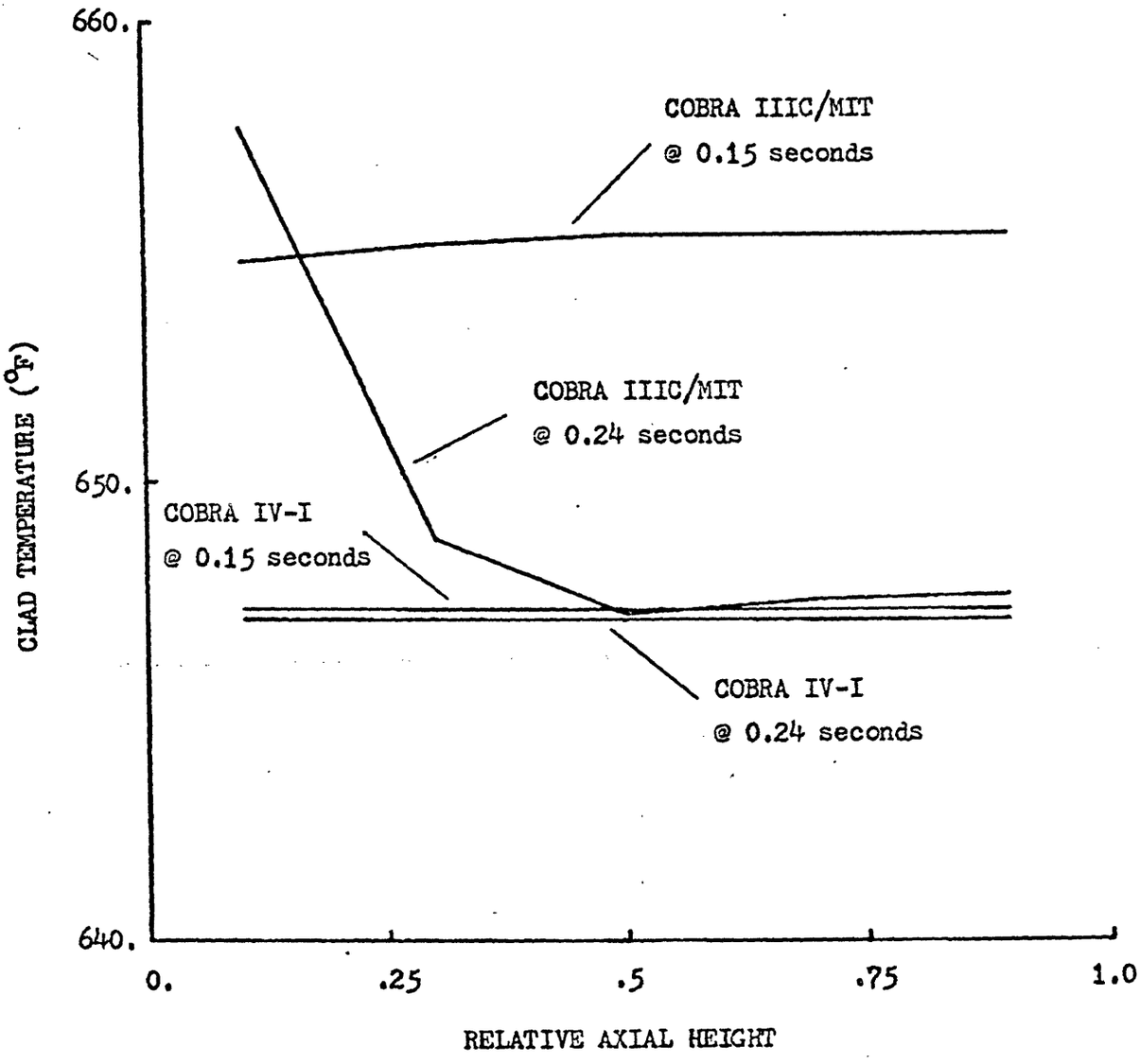

FIGURE 3.7

CLAD TEMPERATURE VERSUS AXIAL HEIGHT

RESULTS FOR CASE 2

convection correlation is used along the entire rod. However, with the start of boiling, only those nodes with boiling switch to the forced convection correlation. Consequently, two correlations are in use and the net result is a non-uniform temperature distribution. Hence, the strong dependence of the COBRA IIIC/MIT heat transfer logic on boiling results in the differences in the clad temperature predictions.

Besides predicting different clad temperatures, the two codes also predict different void fractions. This result differs from the steady-state BWR comparisons in which the density and void fraction predictions are nearly identical. The exit void fraction predictions, as illustrated in Figure 3.8, differ between the two codes in two distinct ways. First of all, COBRA IIIC/MIT predicts boiling (ie. positive void fraction) to occur earlier than does COBRA IV-I. Secondly, the COBRA IIIC/MIT predictions are greater than those of COBRA IV-I during the transient. Since each code is using both the same power history and the Levy model, the reason for these differences is not readily apparent.

After a re-examination of the Levy model, the reason for the differences can be explained. The use of the Levy model causes the void fraction to be a function of the heat flux, the mass flow rate, and the enthalpy. The void fraction would increase with an increase in either the heat flux or the enthalpy and would decrease with an increase in the flow rate. These three variables are compared and it is found that only the heat flux differs between the two codes. This result was not expected since the power distributions are identical for each code. However, the differences in clad temperatures and heat transfer coefficients result in different heat fluxes. The COBRA IIIC/MIT heat flux predictions are larger than those of COBRA IV-I which would lead to earlier and larger

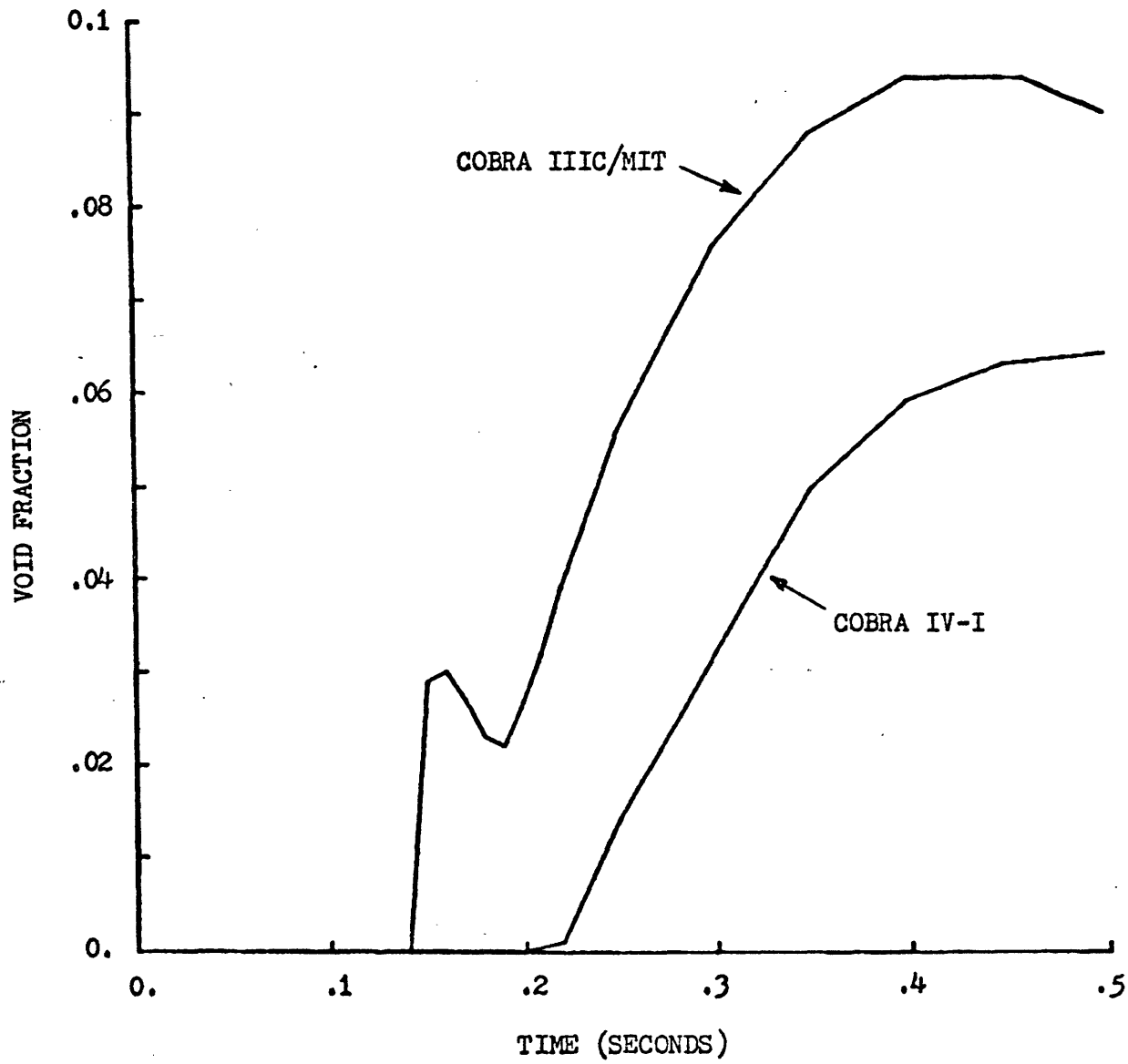

FIGURE 3.8

VOID FRACTION VERSUS TIME

RESULTS FOR CASE 2

subcooled void fraction predictions. Since the higher heat fluxes result from the differences in clad temperatures and heat transfer coefficients, the differences in the void fraction prediction could be indirectly attributed to the different heat transfer logic in the two codes.

The results of the first case show that the pressure drop would increase sharply at the inception of boiling. This result is observed in the COBRA IIIC/MIT run, but no large increase or decrease is observed in the COBRA IV-I run. As seen in Figure 3.9, the COBRA IIIC/MIT pressure drop predictions oscillate when boiling started. On the other hand, the COBRA IV-I predictions remain nearly constant throughout the transient. This difference in behavior can be attributed to the differences in the energy equations in the two codes. The more implicit nature of COBRA IV-I equation would prevent large density changes by insuring a consistent energy solution at each axial level. Without a large density decrease, the pressure drop would not increase significantly. Hence, the improved energy equation in COBRA IV-I would prevent the pressure drop oscillations which are seen in the COBRA IIIC/MIT results.

3.4.2 Summary

This second case has been used to compare COBRA IIIC/MIT and the implicit method of COBRA IV-I for a severe power transient. Once again, these comparisons reveal differences in the clad temperature predictions. These differences can be attributed to the different heat transfer logic in the two codes. The void fraction predictions also differ between the two codes, and result from different heat flux predictions which are caused by the different heat transfer logic. The pressure drop increase at the start of boiling, which is observed in the COBRA IIIC/MIT run, is

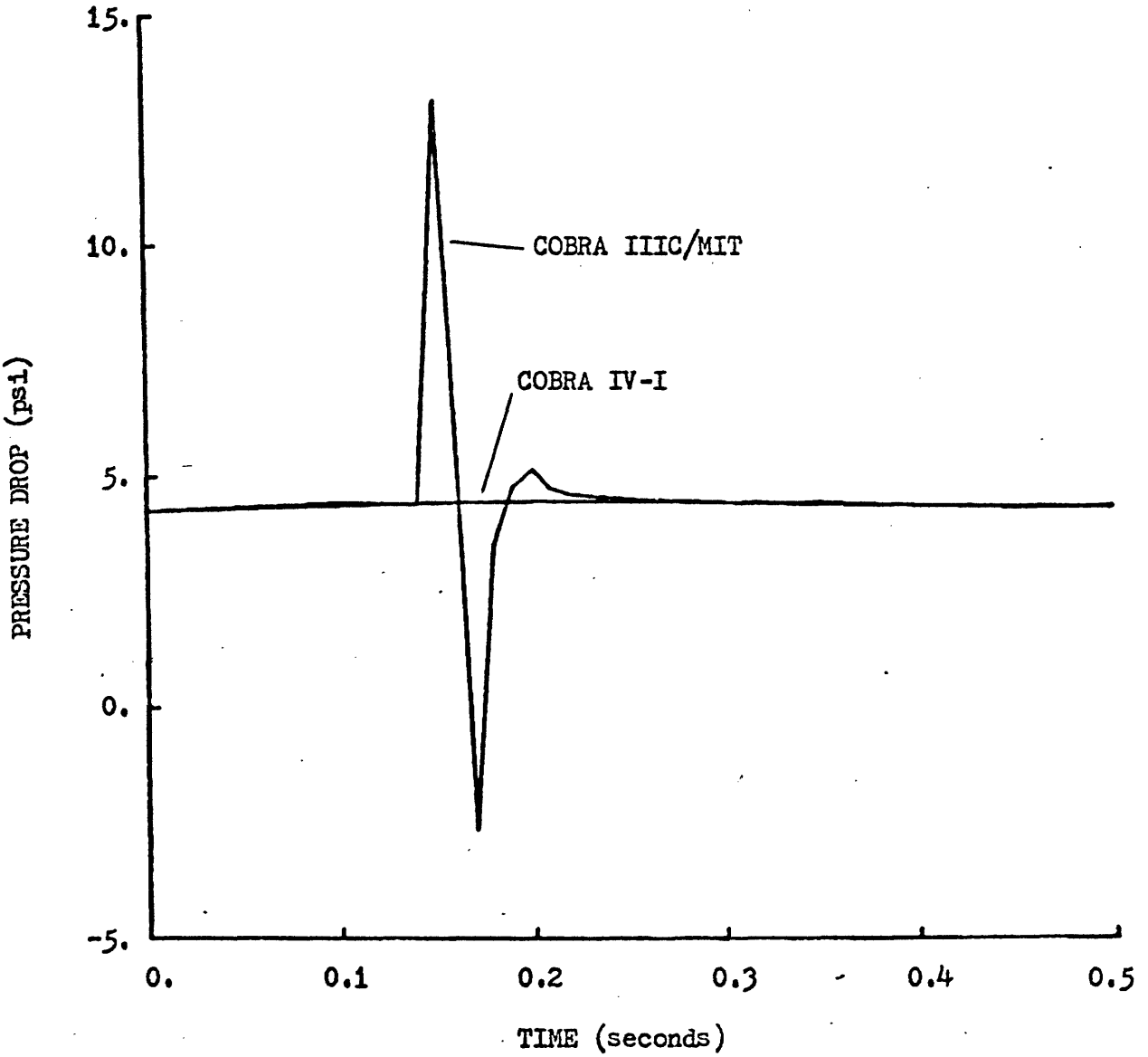

FIGURE 3.9

PRESSURE DROP VERSUS TIME

RESULTS FOR CASE 2

not observed in the COBRA IV-I run. This difference results from the difference in the energy equations. Hence, both the different heat transfer package and energy equation in COBRA IV-I result in different predictions by the two codes.

3.5 Case 3 Results

The third case which is investigated is used to compare COBRA IIIC/MIT and the explicit method of COBRA IV-I. Once again, the severe power transient serves as a basis for comparison. Since the explicit method does not allow the use of the Levy model, COBRA IIIC/MIT was run without this model. Consequently, no subcooling boiling is allowed and boiling does not start until the equilibrium quality was greater than zero. Other modeling parameters are the same as in the previous two cases and a time step size of 0.0025 seconds is used.

3.5.1 Discussion

The intent of this analysis is to evaluate the results of COBRA IIIC/MIT with respect to those of the explicit method of COBRA IV-I. Since the explicit method uses an improved solution scheme, comparisons of these two codes for the severe power transient would point out any inadequacies in COBRA IIIC/MIT. Therefore, variables such as the density and clad temperature are compared in order to evaluate the two codes.

The first comparisons are made between the density predictions of the two codes. As illustrated in Figure 3.10 the predicted exit densities of the two codes are in close agreement up to the point where boiling begins. COBRA IIIC/MIT predicts boiling to occur approximately 0.02 seconds earlier than does COBRA IV-I. Furthermore, the COBRA IIIC/MIT

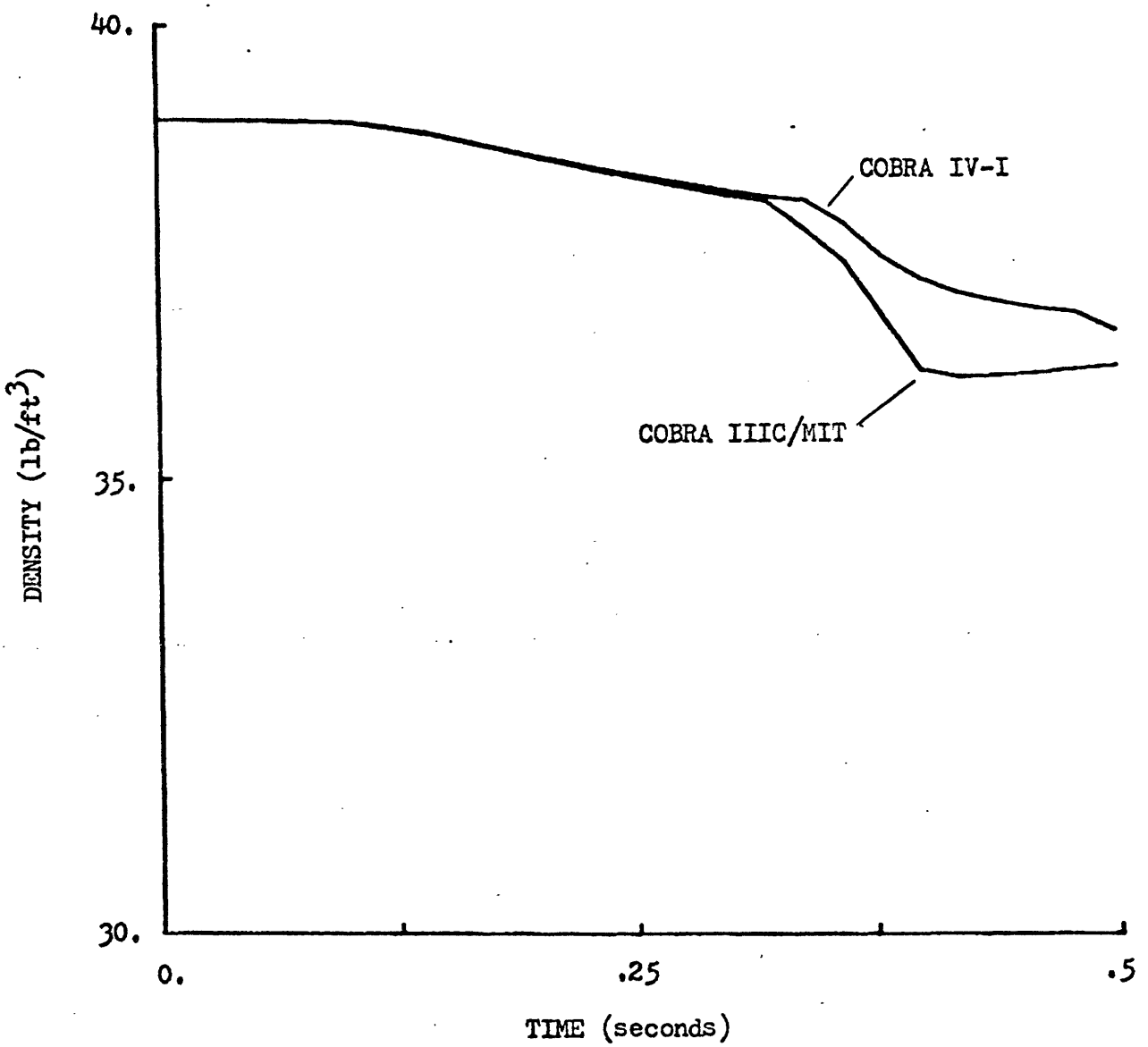

FIGURE 3.10

EXIT DENSITY VERSUS TIME
RESULTS FOR CASE 3, CHANNEL 1

densities are lower after boiling began. The COBRA IIIC/MIT results show that the density begins to increase near the end of the transient which indicates that the amount of boiling is reduced. On the other hand, the COBRA IV-I results show a continuously decreasing density which indicates that the peak void fraction has not yet occurred. Similar differences as found for the density, are also found in the enthalpy predictions which imply that COBRA IIIC/MIT uses a higher heat input into the channel than does COBRA IV-I.

This higher heat input is caused by the higher heat flux and clad temperature predictions of COBRA IIIC/MIT. As seen in Figure 3.11, the clad temperature predictions of COBRA IIIC/MIT are again higher. These higher temperatures lead to higher heat fluxes as seen in Figure 3.12. Note that the COBRA IV-I heat flux predictions peak earlier than those of COBRA IIIC/MIT, but the COBRA IIIC/MIT predictions are higher for most of the transient. The large increase in heat flux at 0.38 seconds is caused by the transition to a different heat transfer coefficient because boiling has started. These results again indicate the significant impact which the heat transfer logic has on the predictions of COBRA IIIC/MIT.

3.5.2 Summary

This case has been used to compare COBRA IIIC/MIT and the explicit method in COBRA IV-I. These comparisons illustrate that the results of the two codes are similar with one another until boiling begins. With the start of boiling, the different logic systems cause different density predictions, since the heat flux is predicted to be higher by COBRA IIIC/MIT. The different logic also leads to different clad temperature predictions.

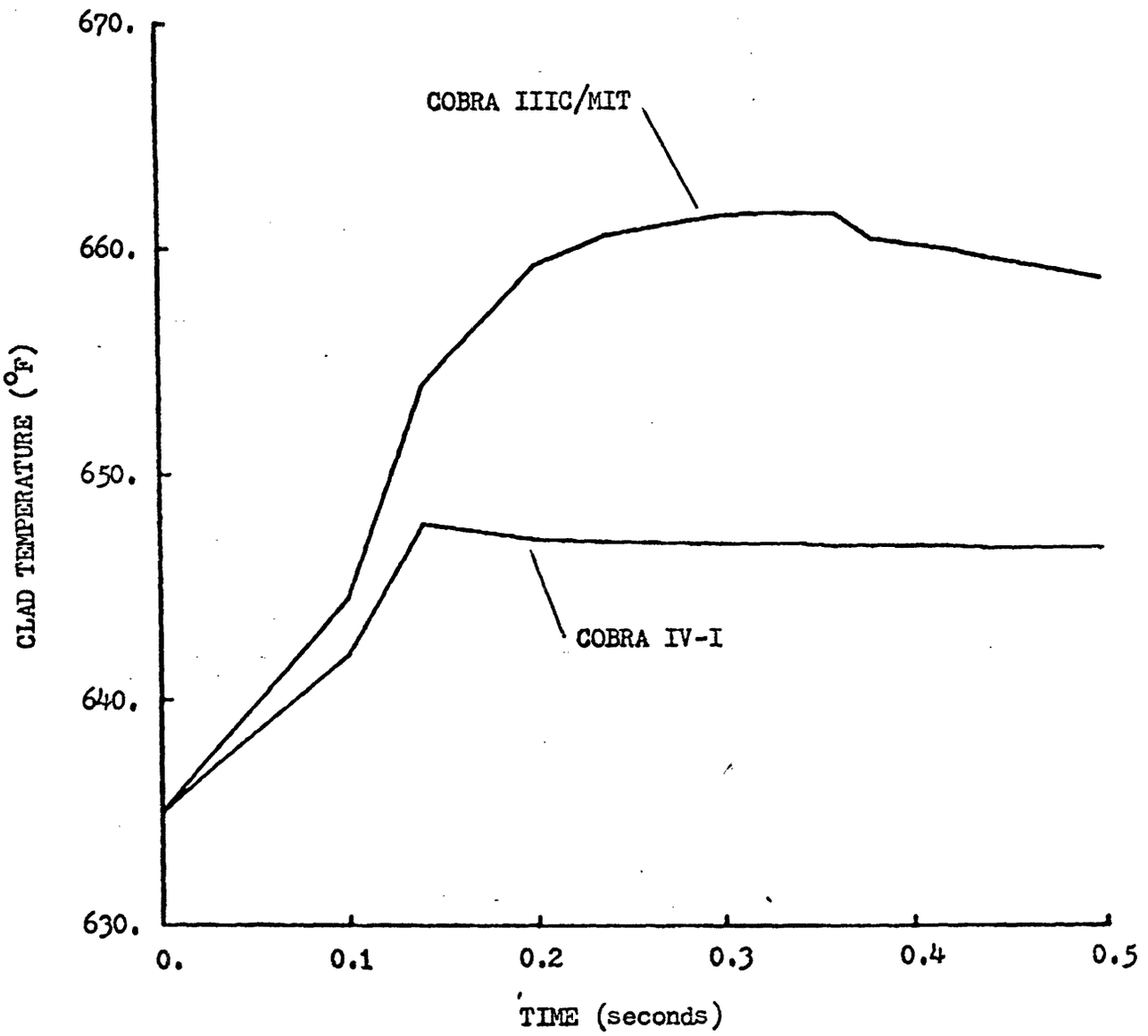

FIGURE 3.11

MAXIMUM CLAD TEMPERATURE VERSUS TIME

RESULTS FOR CASE 3

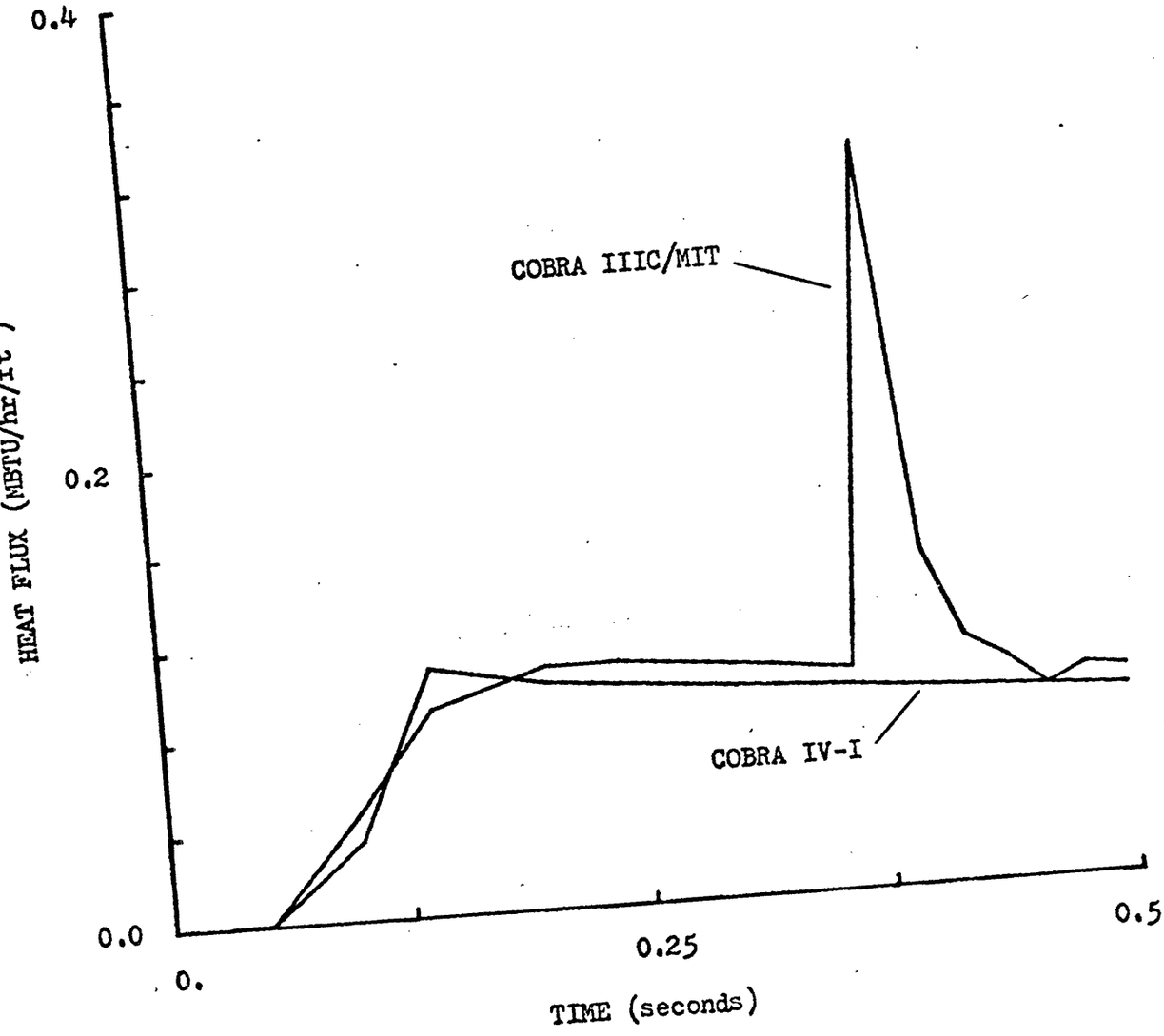

FIGURE 3.12

HEAT FLUX VERSUS TIME

RESULTS FOR CASE 3

Hence, the differences in heat transfer packages are found to be the primary causes of dissimilarities in the predictions of the two codes.

3.6 Case 4 Results

Although the results of the three previous cases have shown some differences between the two codes, there is no indication that COBRA IIIC/MIT is not applicable. These differences could be explained in terms of the heat transfer logic and with similar logic systems the results of the two codes should be in better agreement. Hence, the intent of this fourth case is to investigate a transient in which COBRA IIIC/MIT would not be applicable. Such a case would be one in which the flow reverses due to the sudden voiding of a node in a channel. The explicit method of COBRA IV-I could handle such a reversed flow condition and could be used to find this condition. Once this transient is identified, COBRA IIIC/MIT could be run to examine its behavior for this transient.

3.6.1 Discussion

A number of runs were made using the explicit method of COBRA IV-I in order to find a transient in which the flow reversed. Starting with the transient analyzed in the previous three cases, the power was increased up to 100 times what it had been. In other words, the steady-state average heat flux was 1000 Btu/hr/ft^2. Even with this large increase in power, the sudden voiding at the start of boiling does not lead to a flow reversal. Using this higher power, the inlet mass flux was then reduced to 0.25 Mlb/ft^2/hr and the transient was rerun. For this case, reverse flow does occur at approximately 0.11 seconds into the transient.

The flow reverses at the interface between the boiling and non-boiling sections of the channel. This result indicates that the sudden density change, introduced by the inception of boiling, is sufficient to stop and actually reverse the flow. The flow returns to a positive value after 2.5 milliseconds and remains positive thereafter.

COBRA IIIC/MIT is then used to analyze this extremely severe case. At approximately 0.1 seconds into the transient, reverse flow is predicted and the code fails. This failure is expected, since COBRA IV-I has predicted a reverse flow condition. Once again, the flow reversal occurs at the interface between the boiling and non-boiling regimes. Also, the time of the reverse flow prediction is nearly the same as that predicted by COBRA IV-I. Most predictions prior to the flow reversal are also in good agreement. Hence, although COBRA IIIC/MIT fails when the flow reversal occurs, its results are similar to those of COBRA IV-I up to the point of failure. Furthermore, the point of flow reversal seems to be reliably predicted by each code.

3.6.2 Summary

As is seen in the above analysis, the prediction of a flow reversal leads to the failure of COBRA IIIC/MIT. This limitation does not apply to the explicit method of COBRA IV-I. Yet, the comparison of the results of the two codes up to the point of the flow reversal indicates that COBRA IIIC/MIT is performing satisfactorily. It is found that, with the exception of the clad temperatures, the two codes agree rather well for most predictions. However, if calculations beyond the point of flow reversal are required, then only COBRA IV-I could be used.

The severe transient examined in this section is just one example

of a flow reversal transient. The sudden change in density caused by the inception of boiling leads to the flow reversal. Boiling occurs in only one channel which means that the large density decrease occurs only in this channel. With this density decrease, the difference in pressure between the two channels becomes very large causing a large crossflow from the boiling channel to the non-boiling channel. As seen in Figure 3.13, the crossflow when boiling occurs is much greater than when no boiling occurs. If the crossflow is large enough and the flow rate is small enough, a negative flow rate can be predicted. This result can be seen with the aid of equation 3.1 repeated here:

$$m_j = m_{j-1} - A\Delta x\Delta\rho/\Delta t - w\Delta x. \qquad (3.1)$$

Although the density term would be positive, the crossflow term could be sufficiently large to cause m_j to be negative. However, the flow rate, m_{j-1}, must be small enough in order for this result to occur. Hence, a combination of low flow rate and sudden density decrease would be required for a flow reversal condition.

3.7 Conclusions

The results of the analyses in this chapter reveal three significant conclusions regarding the applicability of COBRA IIIC/MIT and COBRA IV-I. The first conclusion concerns the oscillations which occur at the inception of boiling when very small time steps are used. Both COBRA IIIC/MIT and the implicit method of COBRA IV-I fail to converge at the point when subcooled boiling begins. This failure could be considered to be a limitation, but through the use of a physically based correction this limitation is eliminated. Hence, the ability to apply either code to a severe power transient is not limited by the use of very small time

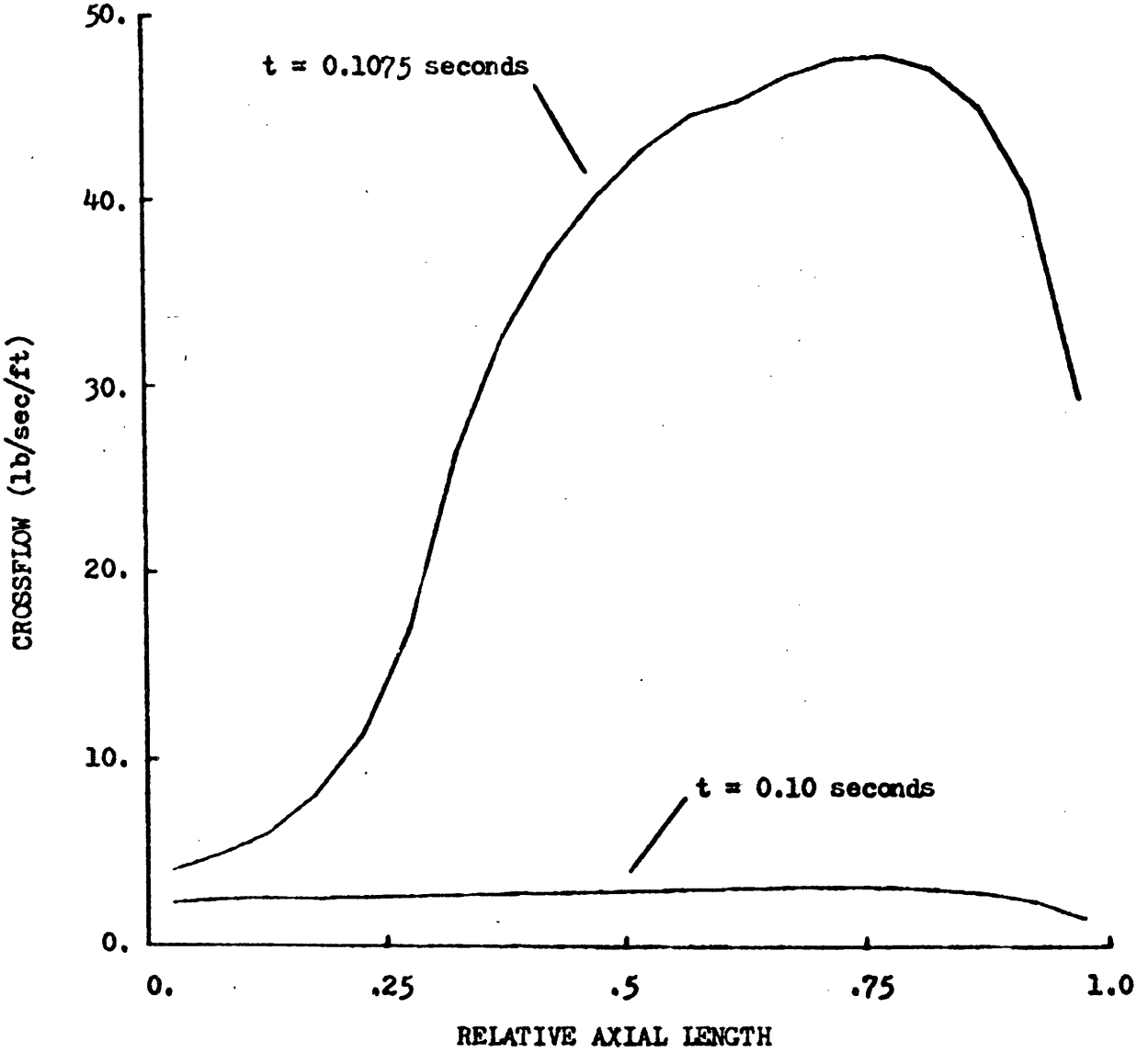

FIGURE 3.13

CROSSFLOW VERSUS AXIAL LENGTH
COBRA IV-I CROSSFLOW PREDICTIONS
DURING REVERSE FLOW TRANSIENT

step sizes.

The second conclusion concerns the validity of the COBRA IIIC/MIT results during a severe power transient. Although the comparisons with both the implicit and explicit methods of COBRA IV-I reveal discrepancies in the void fraction, density and clad temperature predictions, these discrepancies could be explained in terms of the heat transfer logic. Prior to the beginning of boiling, the predictions of the two codes are very similar. The start of boiling only affects the COBRA IIIC/MIT heat transfer logic and results in the different predictions. If the two codes use the same logic systems, then their results should be in better agreement. Hence, although the COBRA IIIC/MIT results do differ from those of COBRA IV-I, a change in the COBRA IIIC/MIT logic system should improve the validity of this code's results.

The third conclusion concerns the applicability of COBRA IIIC/MIT when a flow reversal occurs. As expected, this codes fails when the flow reverses, while the explicit method of COBRA IV-I does not. However, the results of the two codes are similar up to the point of the COBRA IIIC/MIT failure. These results illustrate that COBRA IIIC/MIT would not be applicable if a flow reversal occurs, but the conditions for this occurrence are, indeed, very severe. Another observation is that COBRA IIIC/MIT appears to be applicable up to the point of the flow reversal. Therefore, although COBRA IIIC/MIT would not be applicable if a flow reversal occurs, the code seems to perform satisfactorily for most severe power transients.

CHAPTER 4

LOSS OF FLOW TRANSIENT ANALYSES

4.1 Introduction

Although COBRA IIIC/MIT can be used in a coupled neutronic-thermal-hydraulic calculation, another common use of this code is the calculation of the Departure from Nucleate Boiling Ratio (DNBR) for both steady-state and transient conditions. This parameter is extremely important for the design and operation of a PWR due to its safety related significance. Consequently, the accurate prediction of the DNBR is of paramount importance. COBRA IIIC/MIT has been used successfully to calculate the DNBR for many steady-state and transient conditions (27). This success has led to the common use of COBRA IIIC/MIT for DNBR calculations.

With the development of COBRA IV-I, which is an improved code, the COBRA IIIC/MIT DNBR predictions can be assessed. This assessment would be based on the assumption that COBRA IV-I, with its improved energy equation and RELAP-4 heat transfer package, should yield better results and, therefore, could be used as a standard to which other codes could be compared. By comparing the COBRA IIIC/MIT predictions with those of COBRA IV-I, the adequacy of COBRA IIIC/MIT for DNBR calculations can be determined.

For the purpose of comparing COBRA IIIC/MIT to COBRA IV-I, a series of loss of flow transients are examined. This type of transient is representative of an ATWS for which the minimum DNBR is the design limit. Furthermore, this type of transient could be severe enough to illustrate any inadequacies in the COBRA IIIC/MIT predictions. By assuming no scram and complete loss of the primary coolant pumps, the Minimum Departure

from Nucleate Boiling Ratio (MDNBR) would decrease very rapidly and boiling could occur despite the high operating pressure. Due to the severity of this transient, differences between the COBRA IIIC/MIT and COBRA IV-I predictions could arise and be identified. Therefore, loss of flow transients are used to assess COBRA IIIC/MIT for typical DNBR analyses.

4.2 Description of Modeling

The overall modeling approach uses a single stage method (14, 15). This method combines an assembly to assembly analysis with a subchannel analysis. The hot rod and the subchannels around it are modeled on a subchannel basis while the remainder of the core is modeled using a few large channels. Using the combined modeling scheme, only one run is required to determine the DNBR along the hot rod.

For the purpose of comparing COBRA IIIC/MIT and COBRA IV-I, the single stage method is used for the DNBR analysis of the loss of flow transients. A 1/8 section of the Maine Yankee core is modeled for the application of this method. The hot rod is surrounded by nine subchannels in order to provide sufficient detail for the DNBR analysis. Seven larger channels are then employed to model the remainder of the 1/8 core. Typical geometrical values for the Maine Yankee reactor are used to specify the actual dimensions of these channels. The data are summarized in Appendix B.

A total of four loss of flow transients are analyzed using this single stage method. Each case employs the same layout for the channels, but each also uses different values for one or more of the following parameters; average heat flux, inlet temperature, rate of flow loss,

or radial power factors. As seen in Table 4.1, the values for these parameters vary from case to case. The first case represents a conventional loss of flow transient since the various input values are typical of a PWR. The second case is similar to the first, but the average heat flux is increased. Likewise, the third case differs from the first in its rate of flow loss. Both the second and third cases are more severe versions of the first case. Finally, the fourth case increases both the average heat flux and inlet temperature relative to the first case. This fourth case is the most severe case analyzed. All cases assume that no scram occurs so that the power remains at 100% throughout the transient. Therefore, these four cases cover a wide range of possible loss of flow transients.

Since the purpose of investigating these transients is to assess the predictions of COBRA IIIC/MIT, both codes employ exactly the same modeling for each case which is analyzed. This approach insures that any differences which might occur would not be due to different modeling. Furthermore, only the implicit method of COBRA IV-I is used during these investigations. Therefore, with both COBRA IIIC/MIT and the implicit method of COBRA IV-I modeled in exactly the same manner, the four loss of flow transients were run and the results are discussed below.

4.3 Case 1 Results

The initial comparisons of COBRA IIIC/MIT and COBRA IV-I are performed using a transient which could be considered to be a typical loss of flow transient. Realistic values for the operating and transient conditions are used. The inlet temperature and inlet flow rates are typical of a PWR core. Furthermore, the power distribution is based on neutronic

TABLE 4.1

COMPARISON OF DATA USED

IN LOSS OF FLOW CASES

CASE #	$\bar{q}''$ (MBtu/hr/ft^2)	T_{in} (^oF)	RATE OF FLOW DECREASE	RADIAL POWER FACTORS
1	.1695	541	4.44%/sec	Set A
2	.3	541	4.44%/sec	Set A
3	.1695	541	7.77%/sec	Set B
4	.3	570	4.44%/sec	Set B

considerations only. Similarly, the rate of flow decrease is based on the actual coastdown characteristic of a primary coolant pump. With these conditions, the transient is analyzed and the results are compared.

4.3.1 Discussion

Since the analysis of a loss of flow transient would usually be concerned with the calculation of the DNBR, most comparisons use this variable to evaluate the results of the two codes. These comparisons are made for the rod 9 predictions, since this rod was determined to be the hot rod from peaking factor considerations. Comparisons of the temporal MDNBR behavior are also performed to further evaluate the two codes.

Besides the DNBR comparisons, the density, enthalpy, and clad temperature predictions of the two codes are also compared. These variables are used to evaluate the influence of both the energy equations and heat transfer packages of each code. The rod 9 clad temperatures are employed for the clad temperature comparisons. Since channel 11 is adjacent to rod 9, the density and enthalpy predictions in this channel are also used in these comparisons.

The DNBR predictions for rod 9 are compared in Figure 4.1. Both the comparisons at 0.0 seconds and at 9.0 seconds are in rather good agreement. Although the COBRA IIIC/MIT predictions are consistently greater than those of COBRA IV-I, the maximum difference between the predictions at any one point is 2.8%. Furthermore, most the predictions are within 0.1% of one another. This close agreement is also found in the MDNBR predictions, which are listed in Table 4.2. The maximum difference in any MDNBR prediction is again found to be 2.8%. Once again, the COBRA IIIC/MIT predictions are consistently greater than those of COBRA IV-I. The only

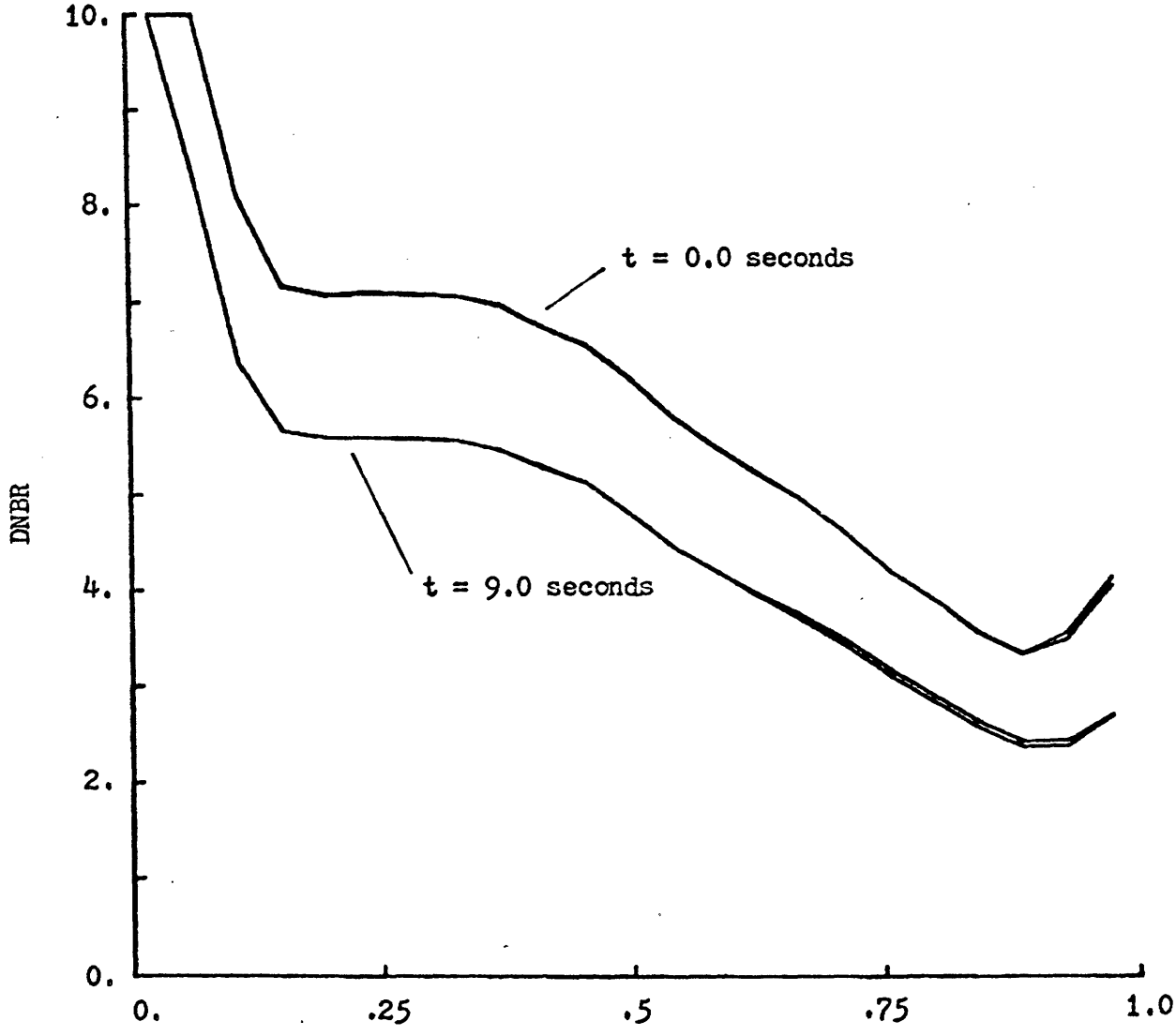

FIGURE 4.1

DNBR VERSUS AXIAL HEIGHT
RESULTS FOR CASE 1, ROD 9

TABLE 4.2

MDNBR VERSUS TIME DATA

RESULTS FOR CASE 1

TIME	COBRA IIIC/MIT		COBRA IV-I	
(sec)	MDNBR	ROD	MDNBR	ROD
0.	3.327	9	3.321	9
1.	3.251	9	3.228	7
2.	3.149	7	3.132	9
3.	3.067	7	3.027	7
4.	2.955	7	2.930	7
5.	2.860	7	2.810	7
6.	2.746	7	2.700	7
7.	2.639	7	2.581	7
8.	2.529	7	2.467	7
9.	2.418	7	2.350	7

significant difference in these results is the predicted location for the point of MDNBR. However, both rods 7 and 9 use the same power factors and, hence, it might be expected that the point of MDNBR could have moved from one rod to the other. Overall, the DNBR predictions of the two codes are very similar.

With the DNBR predictions in close agreement, the density predictions are compared next. These predictions are examined to see if any discrepancies exist. Comparisons are made at both 0.0 seconds and 9.0 seconds. Both of these comparisons show extremely good agreement, as illustrated in Figure 4.2. While the maximum difference at any one location is approximately 0.3%, most results agree to within 0.05%. These results indicate that COBRA IIIC/MIT is performing quite well.

However, even though the DNBR and density calculations compare favorably, the clad temperature predictions are different. As illustrated in Figure 4.3, the results of the two codes agree rather well at 0.0 seconds, but differ significantly at 9.0 seconds. The good agreement at 0.0 seconds is a consequence of the fact that both codes are using the same heat transfer correlation along most of the rod. Since no boiling occurs, COBRA IIIC/MIT always uses the forced convection correlation. COBRA IV-I uses the forced convection correlation until the clad temperature exceeds 643 ^{o}F (saturation temperature). After this temperature is reached, the nucleate boiling correlation is used. However, the heat transfer coefficients predicted by each code are nearly the same and, consequently, the two codes agree rather well at 0.0 seconds.

On the other hand, the predictions at 9.0 seconds are significantly different from each other over the last one third of the rod. These differences result from the differences in heat transfer logic. Over

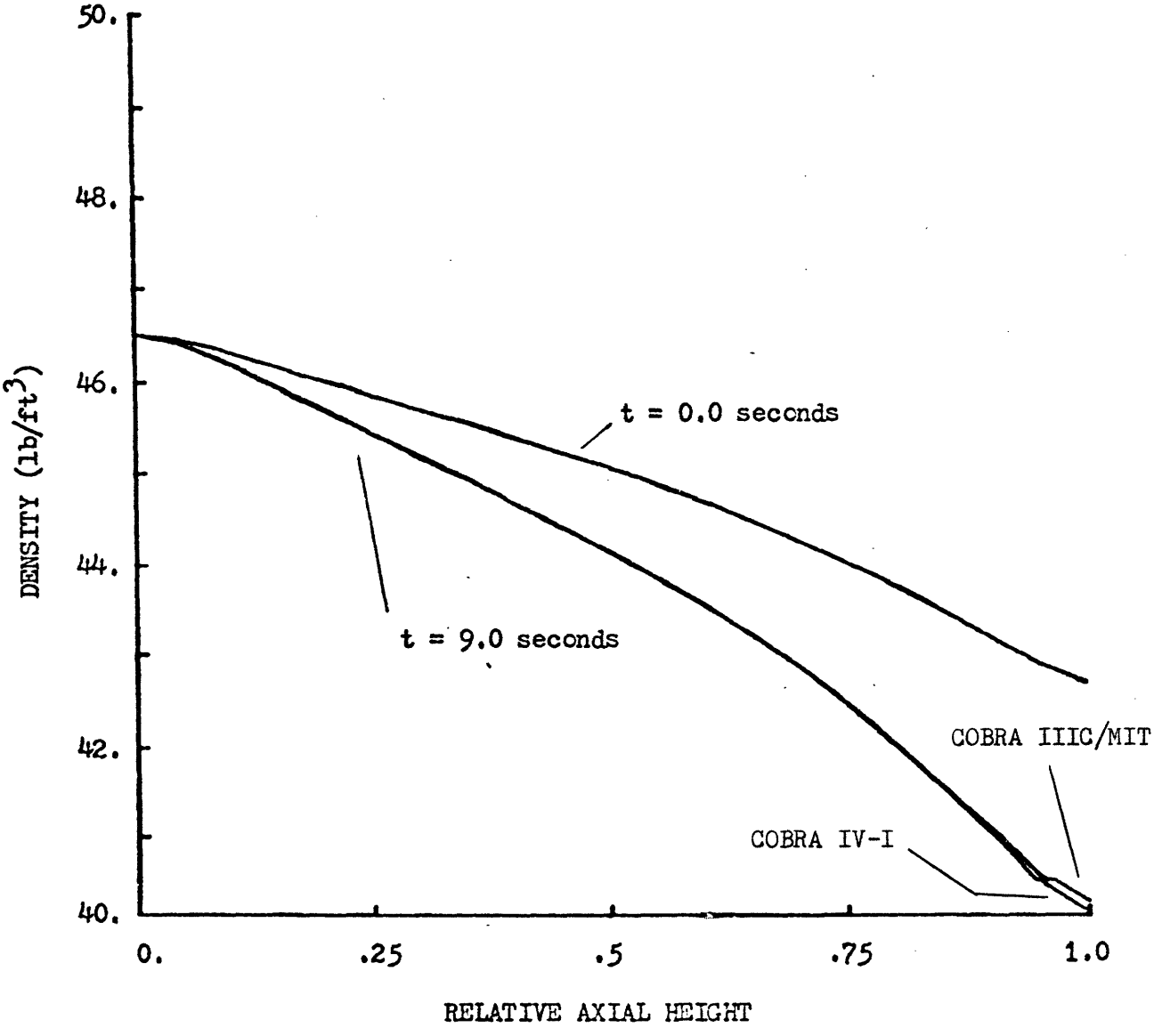

FIGURE 4.2

DENSITY VERSUS AXIAL HEIGHT

RESULTS FOR CASE 1, CHANNEL 11

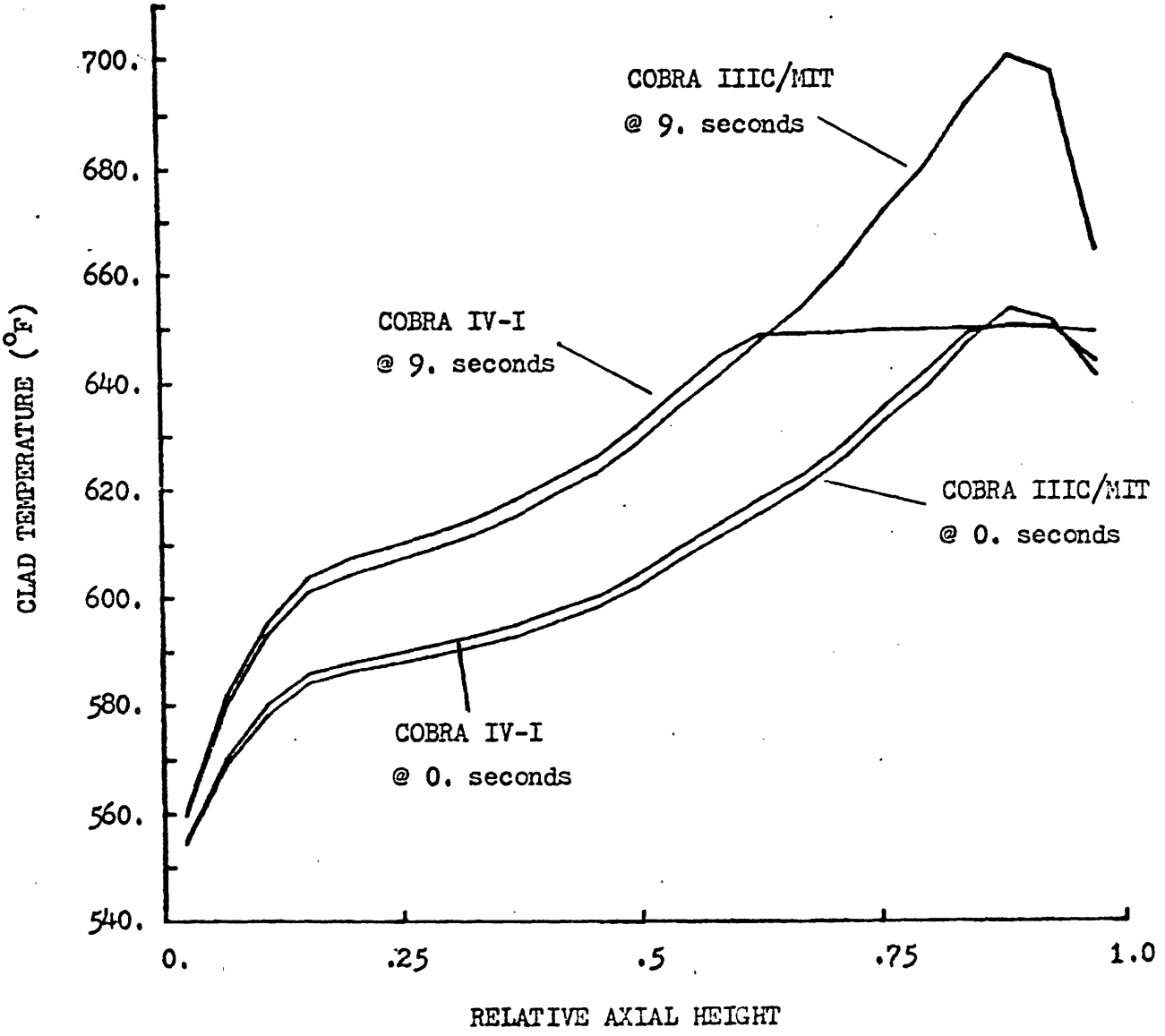

FIGURE 4.3

CLAD TEMPERATURE VERSUS AXIAL HEIGHT

RESULTS FOR CASE 1 , ROD 9

the first two thirds of the channel, both codes are using the forced convection correlation. Since the flow has been reduced relative to steady-state, the heat transfer coefficient is lower and the clad temperatures are higher. Once the clad temperature exceeds the fluid saturation temperature, COBRA IV-I begins using the nucleate boiling correlation which then maintains the clad temperature at approximately 7 ^{o}F above the saturation temperature. Since no boiling occurs COBRA IIIC/MIT does not switch correlations and continues to use the forced convection correlation. Consequently, the COBRA IIIC/MIT clad temperatures greatly exceed those of COBRA IV-I. Once again, the differences in heat transfer logic cause the observed discrepancies in the clad temperature predictions.

4.3.2 Summary

The comparisons made for this first case reveal that COBRA IIIC/MIT and COBRA IV-I are predicting similar results. For example, the DNBR comparisons show that the codes are in good agreement in spite of the fact that their clad temperatures differ. These latter differences, which result from differences in the heat transfer logic, do no alter the heat flux predictions and, therefore, the DNBR results are unaffected. Good agreement is also found not only among the density predictions, but also among the enthalpy and pressure drop predictions. Hence, except for the clad temperature predictions, the two codes agree rather well throughout the transient.

4.4 Case 2 Results

After completing the analysis of the first case, a second case is

studied to further compare the two codes. This second case uses a higher average power than does the first case, but otherwise it is identical to the first. The use of a higher power results in boiling even in steady-state and the DNBR predictions are very low. At the end of the transient (ie. 9.0 seconds), qualities of up to 17% are present in some of the channels. Hence, the higher power increases the severity of this transient.

4.4.1 Discussion

Using this second case, comparisons are again made among the various parameters of interest. The first variable to be compared is the DNBR. As in the first case, the DNBR predictions of the two codes are very similar. In fact, the MDNBR predictions, which are listed in Table 4.3, are in better agreement here than in the first case. All predictions are within 1% of each other and the predicted location of the MDNBR is the same for both codes. Furthermore, the DNBR predictions for rod 9 compare very well throughout the transient. As seen in Table 4.4, the results at both 0.0 seconds and 9.0 seconds are in very good agreement along the rod. This correspondence is found even though both boiling and non-boiling regimes are encountered. Hence, although this transient is rather severe, the DNBR predictions of the two codes compare very well with respect to one another.

Comparisons of the density and enthalpy predictions reveal that again the two codes are predicting similar results. For example, the density predictions are within 0.5% of each other at any point during the transient. Similarly, the enthalpy predictions of the two codes agree to within 0.3% of one another. This good correspondence indicates

TABLE 4.3

MNDBR VERSUS TIME DATA

RESULTS FOR CASE 2

TIME	COBRA IIIC/MIT		COBRA IV-I	
(sec)	MDNBR	ROD	MDNBR	ROD
0.	1.408	9	1.404	9
1.	1.348	9	1.347	9
2.	1.278	9	1.278	9
3.	1.210	9	1.108	9
4.	1.140	9	1.140	9
5.	1.076	9	1.085	9
6.	1.002	7	1.007	7
7.	0.912	7	0.918	7
8.	0.809	7	0.816	7
9.	0.706	7	0.711	7

TABLE 4.4

DNBR COMPARISONS

RESULTS FOR CASE 2, ROD 9

	t = 0.0 SECONDS		t = 9.0 SECONDS	
HEIGHT (in.)	COBRA IIIC/MIT	COBRA IV-I	COBRA IIIC/MIT	COBRA IV-I
3.0	10	10	10	10
8.9	5.907	5.895	4.646	4.637
14.8	4.540	4.528	3.558	3.552
20.8	4.007	3.996	3.139	3.119
26.7	3.934	3.924	3.077	3.042
32.7	3.930	3.920	3.050	3.009
38.6	3.901	3.891	2.998	2.956
44.5	3.865	3.856	2.946	2.899
50.5	3.789	3.779	2.855	2.801
56.4	3.642	3.634	2.727	2.672
62.4	3.508	3.501	2.602	2.544
68.3	3.294	3.284	2.418	2.356
74.3	3.051	3.045	2.165	2.152
80.6	2.856	2.877	1.950	1.963
86.2	2.710	2.702	1.787	1.787
92.2	2.530	2.525	1.630	1.632
98.1	2.330	2.324	1.468	1.470
104.0	2.084	2.071	1.297	1.296
110.0	1.862	1.849	1.148	1.157
115.9	1.637	1.624	1.000	1.000
121.8	1.460	1.451	0.856	0.850
127.8	1.408	1.404	0.763	0.754
133.7	1.513	1.515	0.732	0.729

that COBRA IIIC/MIT is performing satisfactorily.

Still, the clad temperature predictions are very different from each other. As seen in Figure 4.4, even the steady-state clad temperature distributions are dissimilar. Although the distributions are similar up to approximately 650 ^{o}F, the distributions diverge after this temperture is reached. At this temperature, COBRA IV-I begins using the nucleate boiling correlation and, consequently, the clad temperatures remain constant thereafter. On the other hand, COBRA IIIC/MIT continues to use the forced convection correlation until boiling begins. Once boiling starts, COBRA IIIC/MIT begins using the nucleate boiling correlation and the clad temperature decreases discontinuously which results in the peaked behavior of these predictions. Note that the peak clad temperature is predicted to occur just prior to the start of boiling. The differences between the predictions of the two codes are apparently caused by the differences in heat transfer logic.

As a means of verifying that the clad temperature discrepancies are caused by the difference in logic, COBRA IIIC/MIT was modified so that its logic system would be similar to that in COBRA IV-I. The steady-state solution was calculated using this modified version and the results are compared. As illustrated in Figure 4.5, the change in logic results in much better agreement between COBRA IIIC/MIT and COBRA IV-I. These results verify that the difference in heat transfer logic is responsible for the large discrepancies in the clad temperature predictions.

The clad temperature predictions at 9.0 seconds exhibit behavior similar to that found in steady-state. As seen in Figure 4.6, the comparisons of both codes reveal that the COBRA IIIC/MIT predicts large temperature peaks during the transient, while the COBRA IV-I results

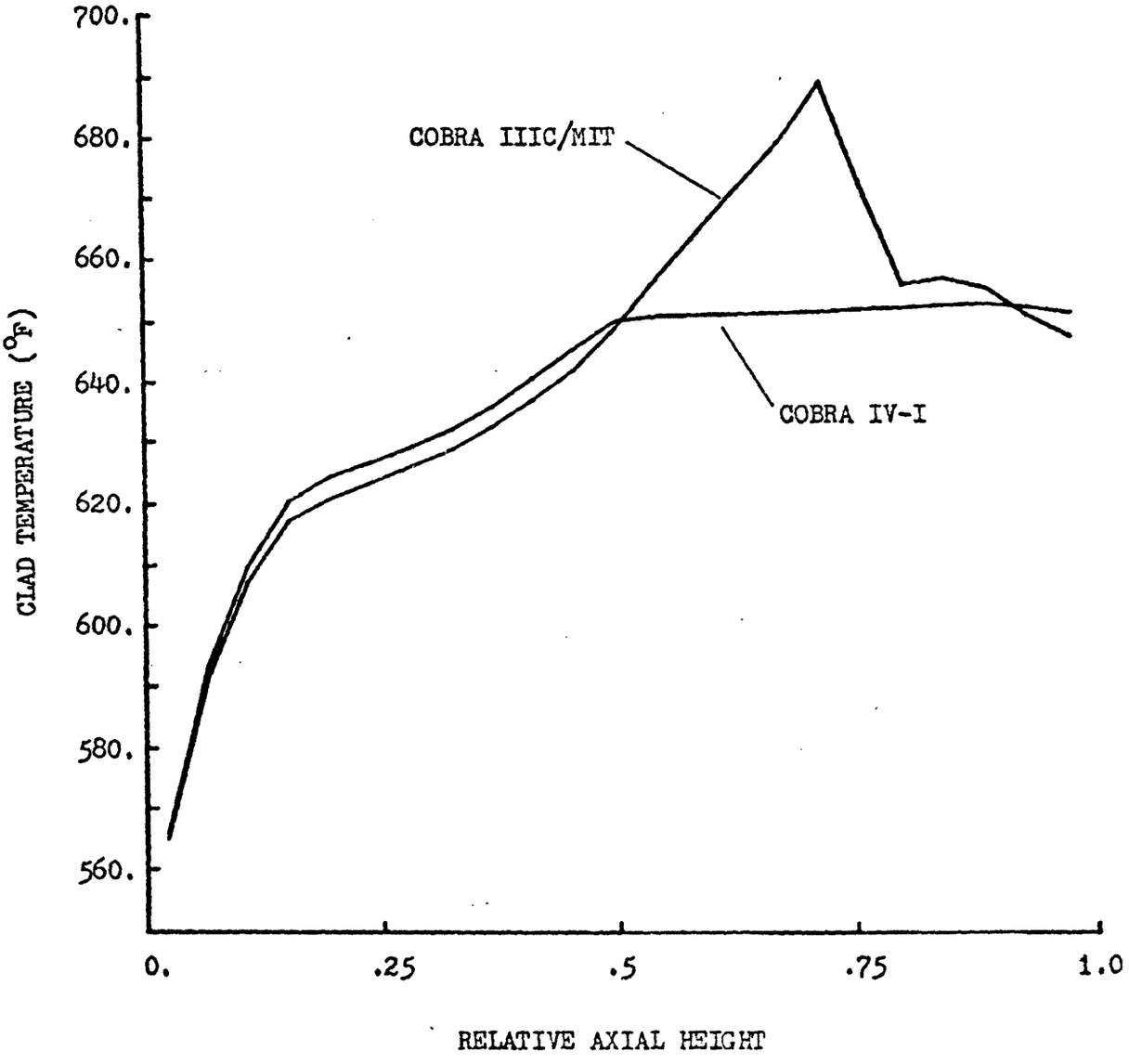

FIGURE 4.4

CLAD TEMPERATURE VERSUS AXIAL HEIGHT

STEADY-STATE RESULTS FOR CASE 2, ROD 9

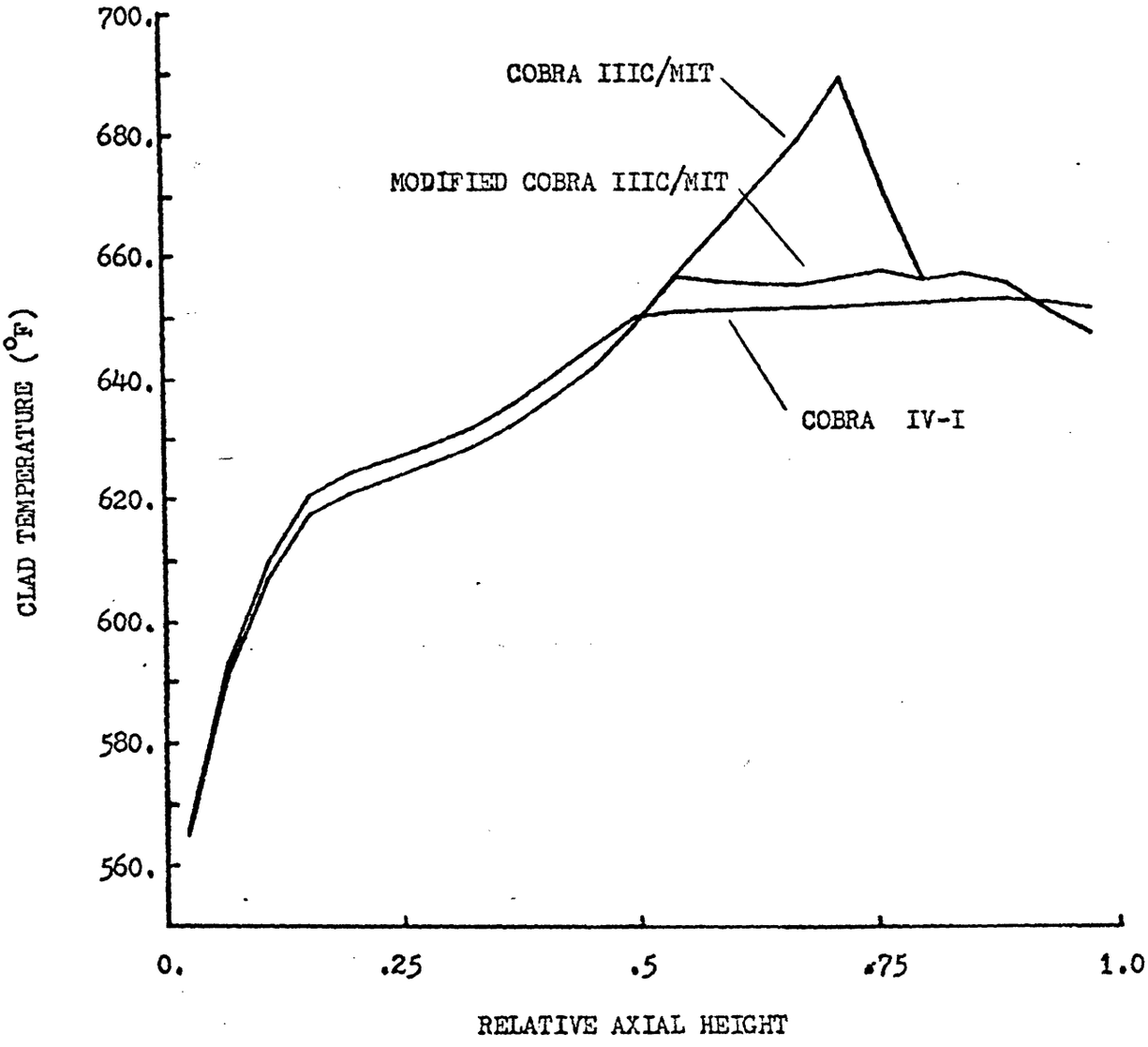

FIGURE 4.5

CLAD TEMPERATURE VERSUS AXIAL HEIGHT

STEADY-STATE RESULTS FOR CASE 2, ROD 9

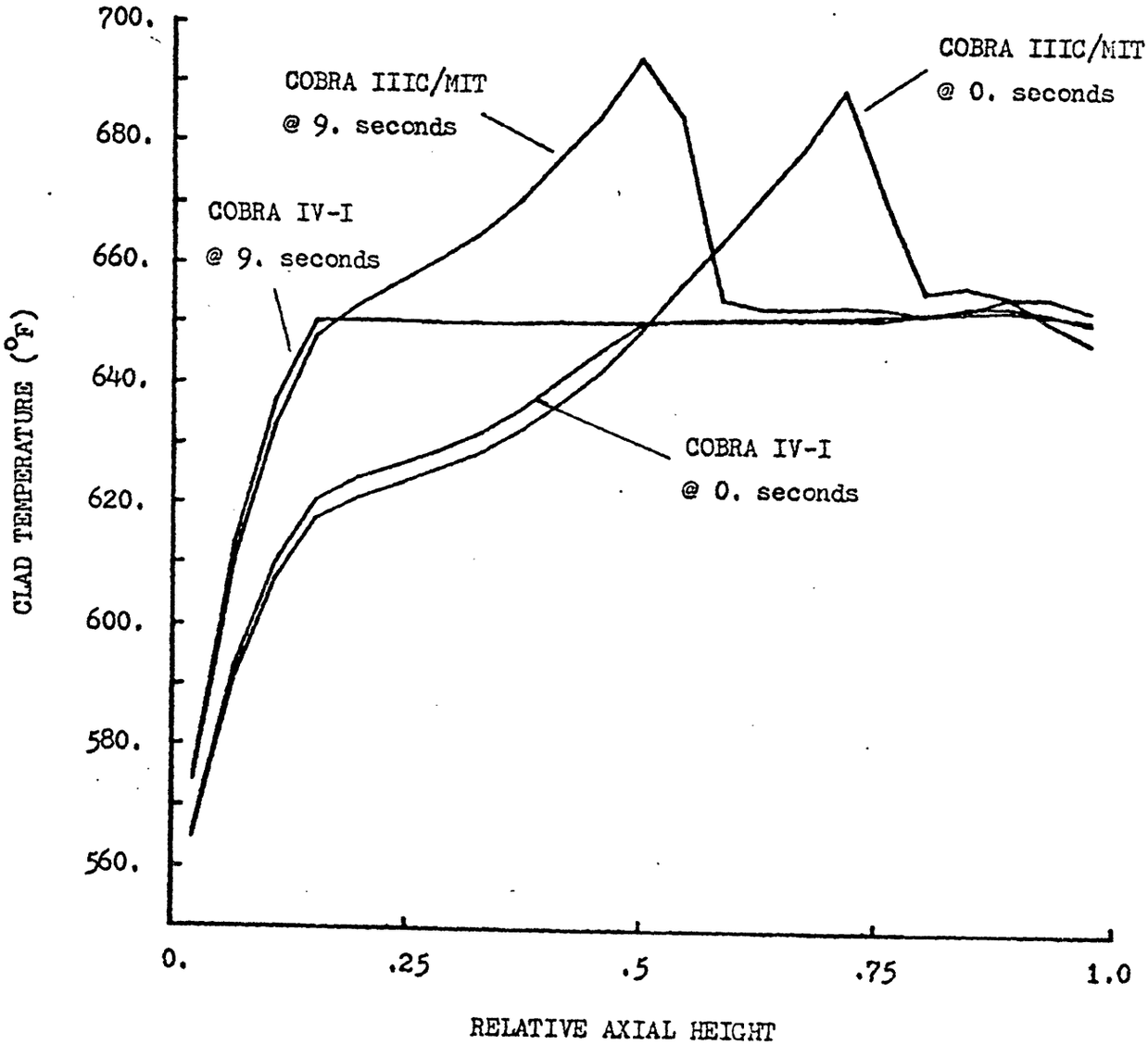

FIGURE 4.6

CLAD TEMPERATURE VERSUS AXIAL HEIGHT
RESULTS FOR CASE 2, ROD 9

never exceed approximately 650 °F. As is described above, the dependence of the COBRA IIIC/MIT heat transfer logic on boiling leads to these temperature peaks.

Another interesting effect of the COBRA IIIC/MIT logic is the shifting of the maximum temperature during the transient. The peak of the temperature distribution follows the shift in the boiling front. As the transient proceeds, boiling occurs earlier along the channel. Consequently, the nucleate boiling correlation is used earlier and the temperature distribution peaks earlier. This result also shows the strong influence which boiling has on the COBRA IIIC/MIT clad temperature predictions.

4.4.2 Summary

In spite of these differences in the clad temperature predictions, COBRA IIIC/MIT and COBRA IV-I agree rather well on most of their predictions for this loss of flow transient. The DNBR, density, and enthalpy predictions are all in very good agreement both in steady-state and during the transient. Only the clad temperatures differ, but these could be brought into better agreement by changing the COBRA IIIC/MIT heat transfer logic. Therefore, it can be concluded that, with the exception of its clad temperature predictions, COBRA IIIC/MIT is predicting very reliable results for this case.

4.5 Case 3 Results

In order to gain additional insight into the applicability of these two codes for loss of flow analyses, a third transient is analyzed. This transient has typical values for the steady-state solution, but then uses a rate of flow decrease which is much greater than that used

in the first case. The higher loss rate makes this transient more severe than in the first case and qualities of up to 6% are present at 8.0 seconds into the transient. Therefore, this case allows comparisons of the two codes for both boiling and non-boiling conditions.

4.5.1 Discussion

Once again the DNBR predictions of the two codes are compared. Although the DNBR predictions do not agree as well as they had in the second case, the results are still in good agreement. For example, the maximum difference in the MDNBR at any time during the transient is approximately 2.6%. As seen in Table 4.5, most MDNBR predictions are within 1% of each other. The location of the MDNBR is also predicted to be the same by both codes. In addition to these comparisons, the DNBR predictions for rod 9 are also compared. As illustrated in Table 4.6, these predictions agree rather well up to a certain axial height at both times. For example, the predictions at 8.0 seconds are within 0.2% of one another up to 62.4 inches. After this point, the predictions are still within 5% of one another, but the extremely good agreement is lost. Hence, the degree of agreement between the DNBR predictions varies along the rod.

The larger differences in the DNBR predictions above 62.4 inches at 8.0 seconds are a result of different heat flux predictions. An examination of the heat flux predictions reveals that the COBRA IV-I predictions are higher than those of COBRA IIIC/MIT. These higher heat fluxes lead to the observed lower DNBR predictions. The prediction of different heat fluxes results from different clad temperature predictions. As illustrated in Figure 4.7, the clad temperature predictions at 8.0

TABLE 4.5

MDNBR VERSUS TIME DATA

RESULTS FOR CASE 3

TIME	COBRA IIIC/MIT		COBRA IV-I	
(sec)	MDNBR	ROD	MDNBR	ROD
0.	3.293	9	3.286	9
1.	3.159	9	3.125	9
2.	3.005	9	2.958	9
3.	2.833	9	2.775	9
4.	2.649	9	2.581	9
5.	2.377	9	2.384	9
6.	2.135	9	2.157	9
7.	1.933	9	1.939	9
8.	1.698	9	1.731	9

TABLE 4.6

DNBR COMPARISONS

RESULTS FOR CASE 3, ROD 9

	t = 0.0 SECONDS		t = 8.0 SECONDS	
HEIGHT (in.)	COBRA IIIC/MIT	COBRA IV-I	COBRA IIIC/MIT	COBRA IV-I
3.0	10	10	10	10
8.9	10	10	7.088	7.088
14.8	8.015	8.001	5.454	5.456
20.8	7.109	7.095	4.830	4.837
26.7	7.017	7.003	4.745	4.750
32.7	7.048	7.035	4.730	4.731
38.6	7.036	7.024	4.701	4.704
44.5	7.014	7.003	4.667	4.669
50.5	6.918	6.906	4.562	4.561
56.4	6.695	6.685	4.392	4.394
62.4	6.495	6.486	4.239	4.240
68.3	6.144	6.134	3.989	3.857
74.3	5.741	5.733	3.710	3.566
80.6	5.422	5.414	3.475	3.319
86.2	5.157	5.147	3.260	3.098
92.2	4.885	4.879	3.055	2.896
98.1	4.538	4.531	2.722	2.656
104.0	4.149	4.140	2.336	2.379
110.0	3.856	3.850	2.111	2.161
115.9	3.507	3.501	1.912	1.935
121.8	3.293	3.286	1.749	1.761
127.8	3.512	3.436	1.698	1.731
133.7	4.076	3.989	1.862	1.891

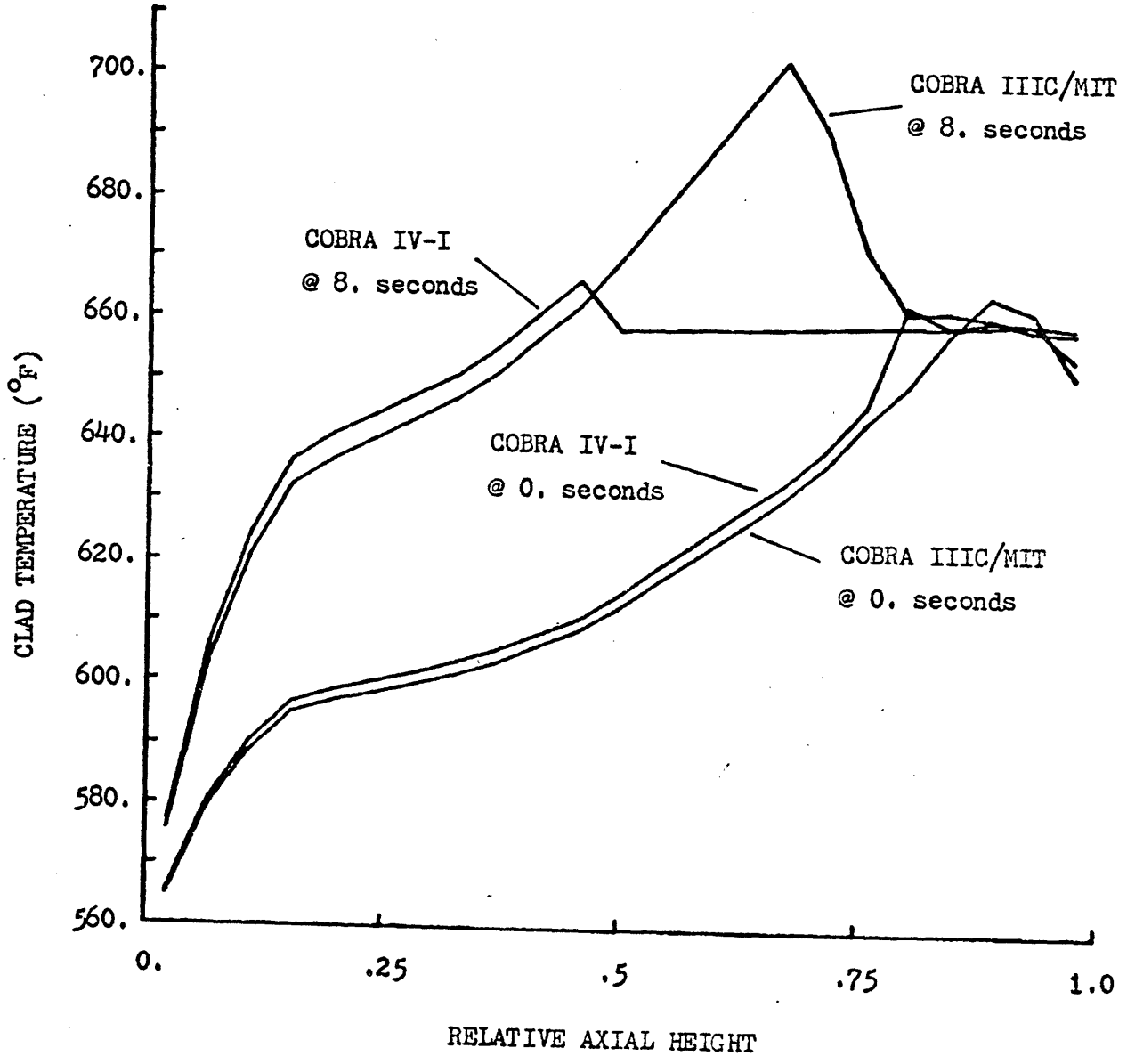

FIGURE 4.7

CLAD TEMPERATURE VERSUS AXIAL HEIGHT
RESULTS FOR CASE 3, ROD 9

seconds are significantly different from one another along the same length where the DNBR predictions are in poorer agreement. Evidently, these different clad temperatures, which result from the differences in the heat transfer logic in the two codes, combine with different heat transfer coefficients to yield dissimilar heat flux predictions. Therefore, the dissimilar heat transfer logic indirectly leads to the different DNBR predictions.

Other variables, such as the density and enthalpy, are also compared for this third case. The density and enthalpy predictions are found to be in good agreement during the transient. All predictions agree to within 2% of one another and most agree even better. This good correspondence indicates that differences in clad temperatures has little effect on these fluid variables.

4.5.2 Summary

The comparisons of the various parameters for this third case show that the two codes do not agree as well as they had in the first two cases. This poorer agreement is caused by dissimilar heat flux predictions. The clad temperature predictions are significantly different and, as a consequence, differences in the heat flux predictions occur. With different heat fluxes, the DNBR predictions of the two codes show poorer agreement. However, this poorer agreement is limited to positions where the large discrepancies in the clad temperature predictions exist. At other axial locations, the two codes agree fairly well. Hence, although the discrepancies in the clad temperature predictions lead to poorer agreement between the codes in certain locations, overall, the two codes are in fairly good agreement.

4.6 Case 4 Results

A final case was run in order to make further comparisons of COBRA IIIC/MIT and COBRA IV-I. This case uses both a higher inlet temperature and a higher power than does the first case. Consequently, boiling occurs even in steady-state and qualities of up to 19% are present at 7.0 seconds into the transient. This transient is the most severe case analyzed and, as with the other cases, is used to compare the predictions of the two codes.

4.6.1 Discussion

Comparisons of the DNBR predictions reveal very good agreement between the two codes. Both the MDNBR values and the locations of the MDNBR are predicted to be nearly the same by each code. As seen in Table 4.7, the MDNBR predictions differ by a maximum of 1.5%, even though the MDNBR values are very low. The DNBR predictions for rod 9 are also in good agreement. As seen in Table 4.8, the DNBR predictions agree to within 2% of each other at both 0.0 seconds and 7.0 seconds. These results do not show the slight differences which are observed in the third case. Hence, even for this severe case, the DNBR predictions are in very good agreement.

However, as seen in Figure 4.8, the clad temperature predictions of the two codes differ significantly. The COBRA IIIC/MIT predictions exhibit peaks which are indicative of the position of the boiling front. As the boiling front moves toward the channel inlet during the transient, the peak temperature also shifts toward the inlet. Again the strong dependence of the heat transfer logic on boiling cause these predictions to peak as they do. On the other hand, the COBRA IV-I

TABLE 4.7

MDNBR VERSUS TIME DATA

RESULTS FOR CASE 4

TIME	COBRA IIIC/MIT		COBRA IV-I	
(sec)	MDNBR	ROD	MDNBR	ROD
0.	1.065	9	1.062	9
1.	1.024	9	1.022	9
2.	0.972	9	0.970	9
3.	0.904	7	0.899	7
4.	0.828	7	0.827	7
5.	0.752	9	0.748	7
6.	0.677	9	0.671	7
7.	0.596	14	0.587	14

TABLE 4.8

DNBR COMPARISONS

RESULTS FOR CASE 4, ROD 9

	t = 0.0 SECONDS		t = 7.0 SECONDS	
HEIGHT (in.)	COBRA IIIC/MIT	COBRA IV-I	COBRA IIIC/MIT	COBRA IV-I
3.0	10	10	10	10
8.9	5.008	4.997	4.239	4.232
14.8	3.841	3.831	3.244	3.213
20.8	3.394	3.383	2.844	2.810
26.7	3.328	3.319	2.768	2.732
32.7	3.312	3.296	2.719	2.679
38.6	3.285	3.268	2.670	2.630
44.5	3.241	3.233	2.619	2.577
50.5	3.153	3.145	2.538	2.493
56.4	3.031	3.026	2.425	2.381
62.4	2.906	2.901	2.309	2.264
68.3	2.725	2.718	2.145	2.100
74.3	2.523	2.519	1.914	1.917
80.6	2.340	2.336	1.740	1.748
86.2	2.168	2.161	1.588	1.593
92.2	2.004	1.997	1.449	1.453
98.1	1.823	1.812	1.309	1.315
104.0	1.618	1.606	1.161	1.163
110.0	1.437	1.431	1.010	1.010
115.9	1.264	1.259	0.855	0.856
121.8	1.122	1.123	0.721	0.722
127.8	1.062	1.065	0.633	0.634
133.7	1.097	1.104	0.597	0.600

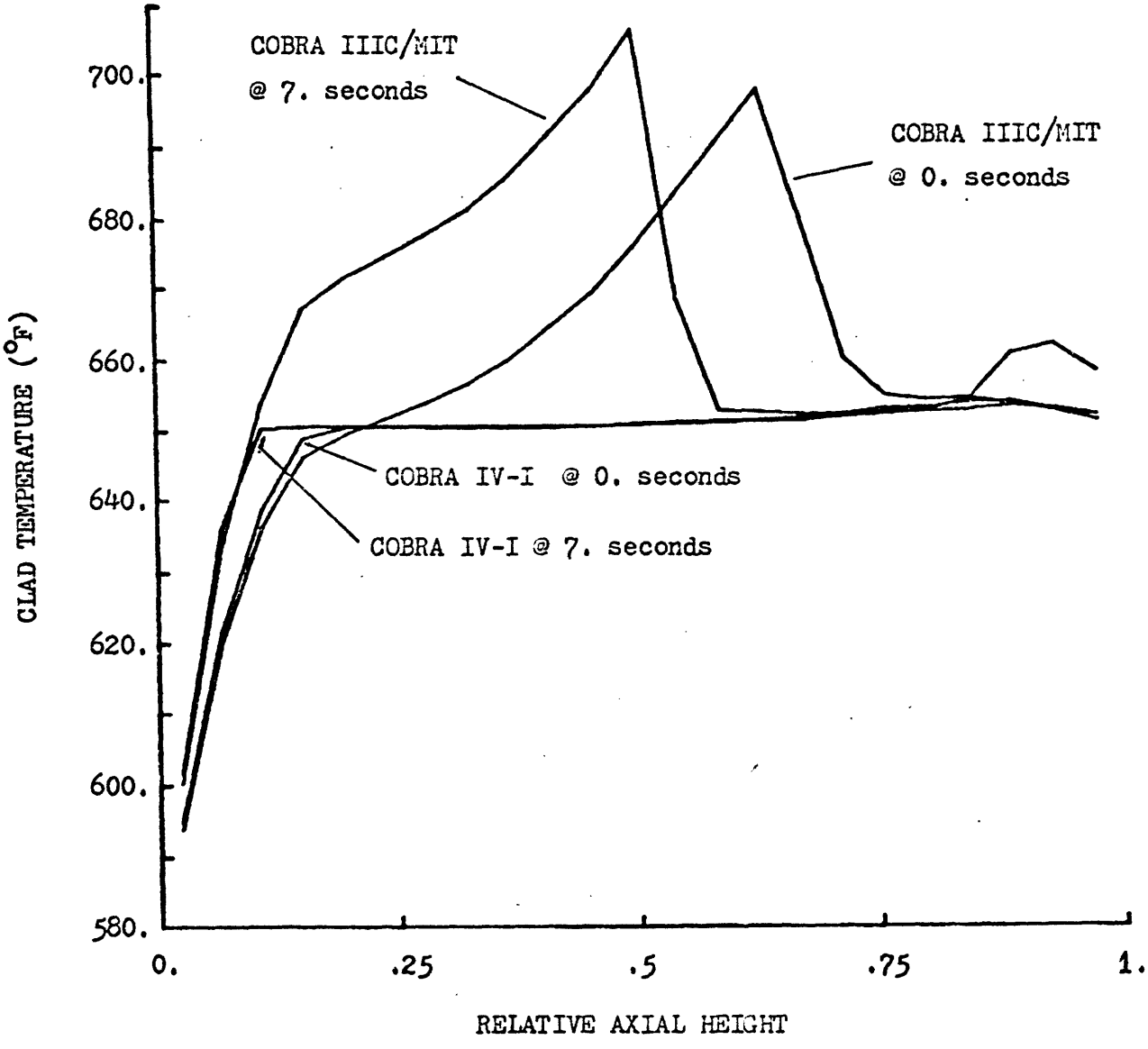

FIGURE 4.8

CLAD TEMPERATURE VERSUS AXIAL HEIGHT

RESULTS FOR CASE 4, ROD 9

predictions never exceed the fluid saturation temperature by more than a few degrees. The use of the nucleate boiling correlation along most of the channel prevents the clad temperature from peaking. Once again, the dissimilarity of the heat transfer logic in the two codes results in the different clad temperature predictions.

Nevertheless, the density and enthalpy predictions of the two codes are in good agreement. The density predictions are within 0.5% of one another throughout the transient. Similarily, the enthalpy predictions agree to within 0.1% during the transient. Apparently, the differences in clad temperature do not significantly affect either the enthalpy or the density predictions.

4.6.2 Summary

The comparisons made for this fourth case reveal surprisingly good agreement between the two codes. Although this transient is very severe, the DNBR, enthalpy, and density predictions of the two codes compare very well to one another. Only the clad temperature predictions show any significant differences. As long as the clad temperature is below the fluid saturation temperature, the two codes agree rather well. The predictions diverge above this temperature due to the different heat transfer logic. Furthermore, the COBRA IIIC/MIT predictions exhibit large peaks in the clad temperature distribution which result from this code's dependence on boiling. In spite of these different clad temperature predictions, the two codes still agree extremely well as evidenced by their DNBR, density, and enthalpy predictions.

4.7 Conclusions

Four loss of flow transients are analyzed in this chapter in order to assess the predictive capabilities of COBRA IIIC/MIT. These transients represent a wide range of possible loss of flow transients. For example, the first case represents a conventional transient while the fourth case represents a very severe, but unrealistic transient. The second and third cases are more severe versions of the first transient. These four transients also produce a wide variety of fluid conditions. The first case, which is the least severe, has no boiling occur at any time during the transient. On the other hand, the second and fourth cases have boiling occur in steady-state and throughout the transient. The third case is similar to the first in that no boiling occurs in steady-state, but boiling does occur as the transient progresses. Hence, these four transients cover a variety of fluid conditions and possible loss of flow transients and should constitute an envelope of possible cases.

Both COBRA IIIC/MIT and COBRA IV-I are used to analyze these transients in order that their results might be compared. Although the investigation of these transients is approached in a manner normally used for DNBR analysis, the main intent of these investigations is not to determine the DNBR for design purposes. Instead, these investigations allow the two codes to be assessed by comparing their predictions. Since COBRA IV-I should be a better tool than COBRA IIIC/MIT, these comparisons would indicate whether or not COBRA IIIC/MIT is performing satisfactorily. Consequently, the results from these four transients are compared and the following four conclusions can be made.

First of all, it is found that, throughout these comparisons, the clad temperature predictions of the two codes are significantly different.

These differences increase both as the power is increased and as the transient progresses. In fact, the only time the clad temperature predictions are similar is in steady-state for cases 1 and 3. The differences in the heat transfer packages of the two codes lead to the dissimilar clad temperatures. However, these differences are not due to different heat transfer correlations being available, since both codes have the same correlations in their heat transfer packages for the range of interest in these transients. Rather, the reason for the differences is the way in which the heat transfer coefficients are used. The COBRA IV-I heat transfer logic dictates that the nucleate boiling correlation be employed once the clad temperature exceeds the fluid saturation temperature. Alternatively, the COBRA IIIC/MIT heat transfer logic dictates that the nucleate boiling correlation be used only if the quality were greater than zero (ie. boiling occurs). The result of using these different logic systems is that the clad temperature predictions diverge once the fluid saturation temperature is exceeded. The COBRA IIIC/MIT predictions do not appear to be correct and, hence, it is recommended that a COBRA IV-I heat transfer logic system be implemented in COBRA IIIC/MIT.

A second conclusion would be that, in spite of the discrepancies in the clad temperature predictions, the DNBR predictions are in very good agreement. This good agreement is a result of the fact that, even though different clad temperatures are predicted, the heat flux predictions of the two codes are very similar. Consequently, the DNBR predictions of each code are very similar for each case. In fact, the higher power cases (2 or 4) have better agreement than do the other cases. The only case which is even slightly affected by the different

clad temperature predictions is the third case. In this case, different heat fluxes are predicted and, consequently, the DNBR predictions are in poorer agreement. However, on the whole, the DNBR predictions of the two codes agree extremely well with one another.

A third conclusion would be that fluid variables such as density and enthalpy, are predicted to be nearly the same by each code. This good agreement between the two codes indicates that the improved energy equation in COBRA IV-I has no significant effect on the predictions of these variables during the transients. Furthermore, these predictions are very similar even though a wide range of fluid conditions are considered. Therefore, the COBRA IIIC/MIT density and enthalpy predictions appear to be quite adequate, since they agree so well with the COBRA IV-I predictions.

Finally, it can be concluded that COBRA IIIC/MIT performs very well for the DNBR analysis of the loss of flow transients. Based on the comparisons with COBRA IV-I, it is found that the two codes predict essentially the same DNBR results. The good correspondence of these results proves that COBRA IIIC/MIT could predict results which are nearly identical to those of the improved code, COBRA IV-I. Therefore, the use of COBRA IIIC/MIT for DNBR analysis should be quite satisfactory.

CHAPTER 5

COMPARISONS WITH EXPERIMENTAL DATA

5.1 Introduction

The ideal method for verifying the predictions of any subchannel code is by comparison with experimental measurements. As part of this investigation, two different sets of experimental data are compared to the calculated results of both COBRA IIIC/MIT and COBRA IV-I. The first data set was obtained from incore measurements of the Maine Yankee Reactor (28). These measurements consist of the reactor coolant temperatures at the core exit. By modeling both the reactor core geometry and operating conditions as designed and using the measured inlet temperature as input, the predicted exit temperatures of both codes are compared to the measured values at the same radial locations. The second data set was obtained from the isothermal two-bundle crossflow tests performed at B & W (29). These tests measured the axial pressure distribution and the flow distribution was calculated based on the measured pressures. Both codes are used to model the test apparatus and the calculated results are compared to the B & W data. The results of the comparisons from both of the two data sets are discussed below.

5.2 Maine Yankee Exit Temperature Comparisons

An analysis of the Maine Yankee reactor's coolant temperatures at the core exit was performed using both COBRA IIIC/MIT and COBRA IV-I. This analysis is used to compare the predictions of these two codes with the incore thermocouple data. This data consists of exit temperature measurements at various radial locations throughout the core. Using this

data, the predicted values from the two codes are compared to measured values and the results of these comparisons are discussed below.

5.2.1 Thermocouple Locations

A total of 23 temperature measurements were taken at various radial locations in the core. As can be seen in the 1/4 core schematic, which is illustrated in Figure 5.1, the thermocouples are distributed throughout the core. Specifically, there are 7 locations in the first quadrant, 6 locations in the third quadrant, and 5 locations in the second and fourth quadrants. Each thermocouple is positioned at the exit of an assembly and its measured value represents the assembly averaged exit coolant temperature. Since these measurements are assembly averaged values, they are well suited to be compared with assembly averaged predictions of either COBRA IIIC/MIT or COBRA IV-I. Consequently, comparisons of these measured values with the predictions of the two codes are performed.

5.2.2 Comparisons with COBRA IIIC/MIT

The first comparisons are made using COBRA IIIC/MIT. A 1/4 core analysis using COBRA IIIC/MIT was performed in order to make these comparisons. This analysis uses 62 channels with each channel representing one assembly. Using symmetry, the exit temperature predictions for the 1/4 core can be compared with the measured values in each quadrant, thereby producing a whole core analysis. Hence, comparisons are made with all of the 23 measured values.

The results of these comparisons indicate that the COBRA IIIC/MIT predictions are very good. As illustrated in Table 5.1, the differences between the measured and predicted values are usually very small. Out

FIGURE 5.1

QUARTER-CORE SCHEMATIC

LOCATIONS OF THERMOCOUPLES

a – QUADRANT I
b – QUADRANT II
c – QUADRANT III
d – QUADRANT IV

						1 b d	2
			3 b d	4	5	6	7
		8	9	10 c	11	12 c	13
	14 c	15	16	17	18 c	19	20 c
21	22	23 a d	24	25 b	26	27	28
29	30 a	31	32 d	33	34	35	36 c
37 a	38	39	40	41 b	42	43 a	44
45	46	47	48	49	50	51 d	52	53
54	55 a	56	57 a	58	59	60	61 a b	62

TABLE 5.1

COMPARISON BETWEEN MEASURED AND

COBRA IIIC/MIT PREDICTED EXIT TEMPERATURES

QUADRANT I

Bundle	Measured - Predicted Temperature Difference (°F)
23	-2.5
30	-7.0
37	-4.1
43	-1.9
55	-10.8
57	+2.5
61	+1.3

QUADRANT II

Bundle	Measured - Predicted Temperature Difference (°F)
1	-24.0
3	-2.8
25	-3.2
41	-9.6
61	-4.0

QUADRANT III

Bundle	Measured - Predicted Temperature Difference (°F)
10	-1.5
12	-22.5
14	-0.3
18	-1.7
20	-0.1
36	-1.9

QUADRANT IV

Bundle	Measured - Predicted Temperature Difference (°F)
1	+4.2
3	-12.1
23	-4.4
32	-4.8
51	-5.1

Total Number of Measurements = 23

Number of Predictions $\pm$ 2 °F = 7

Number of Predictions $\pm$ 5 °F = 16

Number of Predictions $\pm$ 10 °F = 19

Number of Predictions > 10 °F = 4

of the 23 measured values, 17 of the predicted values are within 5 °F of their corresponding measured value. Another interesting observation is that the predicted values are nearly always greater than the measured values. This result indicates that the predictions of COBRA IIIC/MIT can be considered as being usually conservative. Therefore, the predicted values of COBRA IIIC/MIT are found to agree quite satisfactorily with the measured values.

5.2.3 Comparisons with COBRA IV-I

Having completed the COBRA IIIC/MIT comparisons, further comparisons are made using COBRA IV-I. Since COBRA IV-I must use a large amount of computer storage, only a 1/8 core analysis was performed. Even this size problem requires 650K bytes of computer storage, while the COBRA IIIC/MIT 1/4 core case uses only 400K bytes. However, the symmetry of the core allows the COBRA IV-I 1/8 core analysis to be valid for making comparisons with the measured exit temperatures. Therefore, comparisons are made between the 23 measured values and the corresponding predictions of COBRA IV-I.

These comparisons show that COBRA IV-I also predicts the exit temperatures very well. As seen in Table 5.2, the differences between the measured and predicted values are essentially the same as those calculated for the COBRA IIIC/MIT comparisons. This good agreement occurs because the COBRA IIIC/MIT and COBRA IV-I predictions are usually within 0.1 °F of one another. Furthermore, a total of 16 of the COBRA IV-I predictions are within 5 °F of their corresponding measured value. This good agreement between the measured and predicted values indicates that COBRA IV-I is also able to adequately predict the exit temperatures.